Sferic Propagation in the Cutoff Region of the

Earth-Ionosphere Waveguide

by

Kunal K. Surana

Submitted to the Department of Electrical Engineering and Computer Science

in Partial Fulfillment of the Requirements for the Degrees of

Bachelor of Science in Electrical Engineering

and Master of Engineering in Electrical Engineering and Computer Science

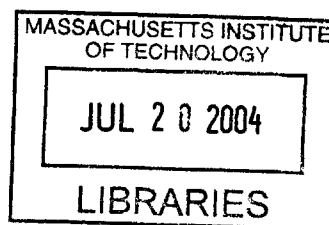at the Massachusetts Institute of Technology

May 28, 2004

Author_____
                    Department of Electrical Engineering and Computer Science
                                                          May 25, 2004

Certified by_____
                                                          Dr. Earle Williams
                                                          Thesis Supervisor

Accepted by_____
                                                          Arthur C. Smith
                    Chairman, Department Committee on Graduate Theses

BARKER

Sferic Propagation in the Cutoff Region of the Earth-Ionosphere Waveguide
by
Kunal K. Surana

Submitted to the
Department of Electrical Engineering and Computer Science

May 28, 2004

In Partial Fulfillment of the Requirements for the Degree of
Bachelor of Science in Electrical Engineering
and Master of Engineering in Electrical Engineering and Computer Science

ABSTRACT

The waveguide cutoff phenomenon provides information about the height of a waveguide. This cutoff for the earth-ionosphere waveguide is illuminated by lightning sferics and is used to monitor the change in ionosphere height through the day-night boundary. The observed ionospheric heights are found to be dependent on the three kinds of source-receiver paths: daytime, nighttime and mixed. Accurate locations for individual events are obtained from the National Lightning Detection Network (NLDN) to enable the analysis. Tweek sferics, which asymptote towards the transverse resonance frequency of the waveguide, predominate in the night path giving the most precise information about ionospheric heights. Weak dispersion and steep transitions in one-dimensional spectra provide information about daytime heights. Propagation over mixed paths reveals both daytime and nighttime signatures. Nighttime observations are also compared against theoretical predictions (Porrat et al, 2001). Agreement is best for large peak current events (>100 kA). Some indication of a residual daytime effect in a nighttime ionosphere is also observed.

Thesis Supervisor: Dr. Earle Williams
Title: Research Scientist, Parsons Laboratory

Acknowledgements

TABLE OF CONTENTS

4

1   Introduction

Atmospherics (electro-magnetic (EM) radiation from lightning strokes, or sferics) occur in the earth-ionosphere cavity and can be modeled as dipoles that exist as an impulse in time. Dipoles radiate EM waves; needless to say, sferics also radiate EM waves. For low frequencies, certainly for frequencies below 10 KHz, these EM waves propagate within the earth-ionosphere cavity as guided waves; waves guided by the earth-ionosphere cavity (the earth-ionosphere waveguide or simply, the EI waveguide).

In 2-dimensions, waveguide propagation can essentially be understood as EM waves bouncing between two parallel plates in a standing wave pattern in one direction while propagating in a perpendicular direction. (This analogy can easily be extended to 3-dimensions as well as circular waveguides.) It is clear that as the wave propagates through a waveguide, it "samples" the waveguide between the source and the observer.

Therefore, the observed EM radiation can be presumed to contain important information about the earth-ionosphere cavity. That, in fact, is true. The observed waveform can be used to obtain a number of parameters related to the ionosphere as well as the source-observer distance. One such extremely useful parameter is the cutoff frequency of the ionosphere. The cutoff frequency is the frequency below which EM waves do not satisfy the boundary conditions given by Maxwell's equations. EM waves that have frequencies less than that of the waveguide cutoff frequency are heavily attenuated within the waveguide. Thus, one expects there to be a sharp increase in the energy content at the waveguide cutoff.

A wealth of information can be gleaned directly or indirectly from the cutoff frequency: (i) The cutoff frequency can be directly used to estimate the height of the ionosphere [Hayakawa et al, 1994; Rafalsky et al, 1995]; (ii) Under suitable meteorological or ionosphere conditions, we are be able to track the change in the ionosphere height through the day-night boundary.[1] (iii) Obtaining ionosphere height estimates (from the cutoff frequency using basic EM concepts) can enable us to

---

[1] The lower ionosphere starts at an altitude of about 60 Km during the day and is at a height of about 85 Km at night. The rate of change of ionosphere height from day to night with the cutoff technique has yet to be studied in detail. Smith et al (2004) have studied it, but from a statistical standpoint only.

understand what meteorological and ionosphere conditions lead to the various kinds of observed sferics such as tweeks and whistlers [Helliwell, 1965].

Dispersion in the EI waveguide in the frequency range from the cutoff upwards into the VLF range gives rise to tweek sferics. The higher frequencies from a lightning discharge arrive first, followed by lower frequencies, and if listened to with an audio amplifier, make a 'tweek' sound. The waveguide dispersion in a frequency-time spectrogram (STFT) asymptotes to the tranverse resonance frequency of the waveguide, which is equal to the cutoff frequency (Nickolaenko and Hayakawa, 2002). Tweek sferics have been studied by Reeve and Rycroft (1972), Yamashita (1978), Hayakawa et al (1994), Rafalsky et al (1995), Shvets et al (1996), and Shvets (2004). Rafalsky et al (1995) suggested that the modal interference in the interval between the first and second cutoff frequencies [Section 3.1.3] could be used to determine the source-receiver distance. Previous studies of tweek sferics did not benefit from a detailed knowledge of the locations of lightning sources, a notable advance in the present study.

1.1 Historical Background

Waveguide mode theory has its roots in research in the early twentieth century. Heaviside and Kennelly (1902) postulated the existence of an atmospheric "conducting" layer in order to explain the observed reflection of radiowaves. Appleton and Barnett (1925) first verified the existence of such a conducting layer, the ionosphere.

Since then, a number of papers have attempted to characterize and explain the received time-domain electrical signals from individual lightning flashes (e.g., Laby et al. 1937, 1940; Watson-Watt et al. 1937). However, the study of the propagation of sferics in the EI cavity reached its peak in the mid-twentieth century. Two different but equivalent theoretical approaches have been primarily used to describe the propagation of sferics in the EI cavity.

The first theoretical approach, or the ray or reflection theory approach, is easier to understand physically. Expressions for deriving ionospheric reflecting height using the spherical geometry of the earth were derived by Laby et al. (1940) and Kessler and Hersperger (1952). Kinzer (1974) and earlier researchers have also derived equations to determine the lightning range and the ionospheric height, for the planar case; the planar

7

model of the EI cavity is reasonable for ranges up to a few hundred kilometers only. Beyond that, effects due to the spherical geometry of the earth must be taken into consideration.

The second theoretical approach involves viewing the EI cavity as a waveguide and solving Maxwell's equations for the allowed modes of propagation. The general theory has been discussed in great detail in Wait (1962), Galejs (1972) and more recently, reviewed in Cummer (2002). In recent years, the VLF region, with particular emphasis on the EI waveguide cutoff region has been studied in great detail by Barr (1966, 1970) and Challinor (1967) with analog electronics. It's interesting to note that before the EI cavity was prevalently modeled as a waveguide, the waveguide cutoff region was also known as the 'absorption band' (Challinor 1966), because of the heavy attenuation in these frequencies as predicted by waveguide theory.

In both of the above approaches, the limitation of the models can be explained in terms of the limited understanding of the boundaries of the waveguide, particularly the ionosphere. In the past, the ionosphere was modeled either as a sharp boundary (for VLF frequencies), or as a number of sharply bounded slabs of constant characteristics (Johler and Harper 1962; Wait 1962). Today, the exponential, scale height model, proposed by the Greifinger couple (1978-1979) is considered the most representative analytical model and is widely used.

1.2   Methods

This section contains an overview of the methods used in this thesis. A wideband antenna provides the ability to study the frequency content of sferics data up to 10 KHz. Discrete-time Signal Processing techniques are used to collect, store and analyze the data. Finally, Fourier Transform, Short-Time Fourier Transform (STFT, or frequency-time spectrogram) and Wavelet techniques are used to determine cutoff frequencies, and the asymptotic transverse resonances of the earth-ionosphere waveguide

8

2   Apparatus

The atmospheric observation system used to collect the data is located at the Alton Jones Campus, (Greenwich, RI) of the University of Rhode Island (41.8N, 71.4W). The measurement station was originally set up by the late Charles Polk and has been used to measure N-S and E-W horizontal magnetic fields (H_{NS}, H_{EW}) as well as the vertical electric field (E_Z) [Polk, 1982], [Heckman et al., 1998] and [Huang et al, 1999].

2.1   Antenna

The first electric field antenna, installed by Polk in the late 1960s was used until 2002, when a lightning strike shattered the antenna ball. A new E_z antenna was then installed to supersede the old one. The new antenna tower consists of five hollow cylinders of ceramic insulators stacked to form a column 7 meters high [Figure 2-1]. Perched on top of the insulating column are the antenna electrode and within it, a charge pre-amplifier. The insulator column serves two valuable purposes:

a) It provides unprecedented mechanical susceptibility – Polk's old antenna was susceptible to mechanical oscillations caused by the wind; the new antenna is virtually immune to this noise.

b) It isolates, to some extent, the charge amplifier at the top from the space charge noise near the earth's surface.

2.1.1   Wideband Charge Amplifier

The antenna electrode is essentially a hemispherical ball antenna. It sits on top of the insulating ceramic column and is somewhat similar to the system described by Ogawa [Ogawa et al., 1966]. Inside this sealed hemisphere is a custom charge amplifier, designed by Michael Stewart of Thunderstorm Technology Inc. Unlike the typical antennas that pick up electric field, this antenna's preamplifier measures the charge induced by the vertical electric field on the top electrode. The electrical output is found to be linearly proportional to the vertical electric field; its frequency response is plotted in

Figure 2-2. This makes it superior to the traditional ultra-high impedance systems used by Ogawa, Polk, Sentman and others.

2.1.2 Post-amplifier system

The post-amplifier system is enclosed in a metal lock box at the base of the antenna tower. It comprises an amplifier with wideband specifications and a switch-adjustable gain. The system also has a 3 Hz "DC-blocking" high-pass filter, a 20 KHz Butterworth anti-aliasing filter, and 60 Hz, 120 Hz and 180 Hz notch filters. The gain setting on the system is $(\times 5 \times 2) = \times 10$. A 600 ft cable connects the electronics box to the hut which contains the observation and data acquisition equipment.
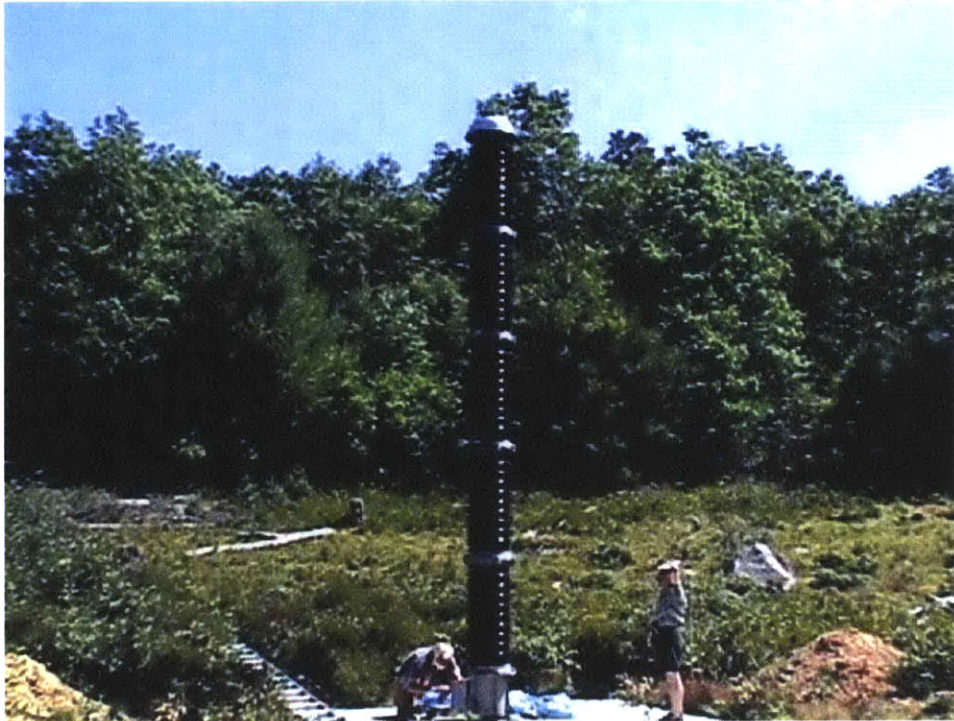
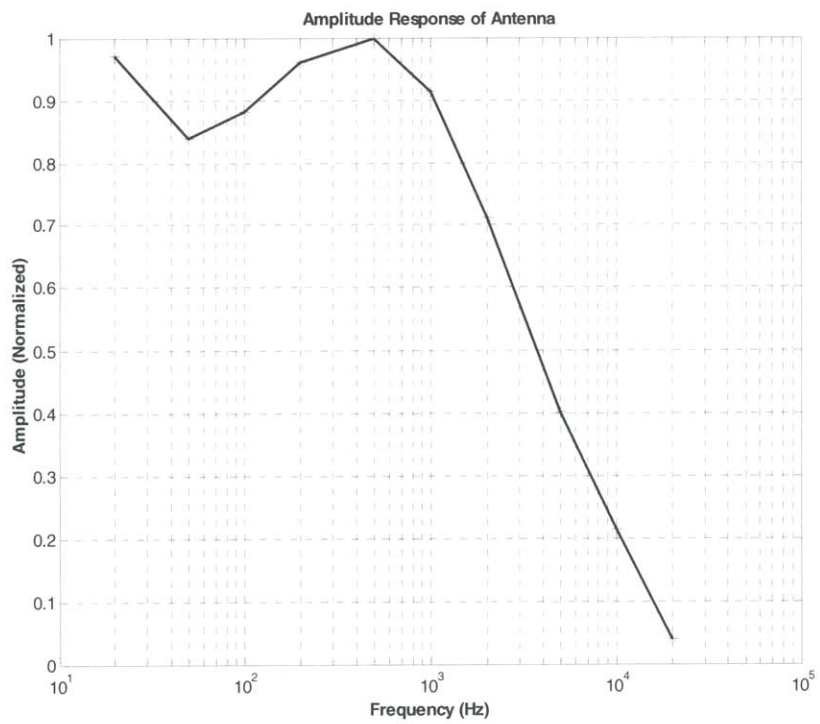**Figure 2-1: Receiving antenna at Rhode Island (41.8N, -71.4E)**

Figure 2-2: Frequency Response of wideband charge amplifier

2.2 Data Acquisition System (DAS)

Data acquisition is accomplished by a Data Translations Board, model DT3005. The DT3005 is a 16-bit converter with a maximum sampling frequency of 200 KHz. The application that controls the board was written in C++ using the Windows Application Programming Interface as a part of this thesis.

2.2.2 Data Acquisition Software

While designing the data acquisition software, two options were considered. The first was to collect a specified interval of data before and after an event. The process of data collection is as follows: An event triggers data collection. The event (trigger), here, occurs when the input voltage exceeds a pre-specified value. With this process, therefore, data is collected discontinuously, or in bursts, and only when the event criterion is satisfied.

The main problem with this method of collecting data in bursts is that it filters signals based on a threshold. The method reduces the ability to do analysis on weak signals – this problem is especially problematic if one wants to study distant signals. Thresholding may implicitly preclude the study of distant signals since they attenuate heavily with distance. A possible solution is to set the threshold to be low, in which case this method, in practice, would effectively be similar to the second method of data collection outlined below.

The second method of data collection is simpler. The idea is to collect a large block of data at once. This large block of data is typically collected over the course of a few hours through the day-night boundary – one of the primary foci of this thesis – although occasionally, we have collected data continuously for a week in an effort to capture interesting events.

The main problem with this second method is the large increase in the volume of data. A system sampling at 50 KHz Hz will have 50,000 samples per second and will require storage requirements of about 20 MB per minute, or 1.2 GB in an hour. Fortunately, since data storage has become less expensive over the years, this is not a prohibitive problem. However, since the system is in a remote location and cannot be frequently maintained, collecting large volumes of data can present difficulties,

12

regardless. Additionally, large amounts of data naturally lead to the proverbial searching for a needle in a haystack.

Ultimately, the second method of continuous data collection - stored, for ease of access, in files containing one-minute of data each - was decided as the method of choice for this thesis. Since large amounts of data were collected, a specialized Matlab application with a user-friendly graphical interface was designed and implemented as part of this thesis to study the data collected.

2.3 Time Stamping

The conclusions of this thesis are heavily dependent on locating lightning strikes accurately, to within a few kilometers. Light travels 300 Km in a millisecond; a lightning occurs every 100ms somewhere in the globe. The ability to accurately (at least better than 1 millisecond) time stamp sferics is thus critical in locating them accurately.

2.3.1 Why Time Stamp Sferics?

Two primary goals of this thesis are to monitor the changes in ionospheric height through the day-night boundary, and to propose an empirical hypothesis regarding the meteorological, ionospheric and distance conditions best conducive to the observation (production) of tweek sferics. To achieve either goal, the ability to accurately determine the location of the sferic is critical. Knowing the location of the sferic, the source-observer distance and path can be deduced. Further, the meteorological conditions at the location of the sferic can be determined as well (if the date and time of the sferic is known). Although the observational system (at Rhode Island) does not provide any means for estimating the location of a sferic, it is possible to estimate the location of events using an indirect method.

There exist lightning detection networks, over the continental United States (CONUS) as well as world-wide, that continuously compile data on the location of every reasonably large sferic along with the time of occurrence, accurate to the tens of microseconds. Two such detection networks are National Lightning Detection Network (NLDN, CONUS) and The Dowden VLF Lightning Detection Network (Dowden, worldwide). In theory, if one were to pick large-amplitude sferics and one knew the time

of their occurrence, one could obtain their location simply, by comparing their time of occurrence against the time of occurrence provided by the networks (adjusted for some value of lag proportional to the distance). That is indeed possible; and in fact is the method used to identify network-located sferics in the Rhode Island data archive.

There is a caveat to using the above-described indirect comparison method. Sferics occur at an average rate of about 100 per second. Empirically, it is observed that for the above method to be effective, that is, to obtain unambiguous matches of sferics with the data provided by the networks, time-stamping of each sferic accurate to better than one millisecond is critical.

2.3.2 Time-Stamping Procedure for Digital Data

The critical time-stamping apparatus consists of a Global Positioning System (GPS) clock and a PC-friendly PCMCIA board by Symmetricom. To obtain accurate time, the board takes the GPS signal as its input and converts it to time. The current time is then read from a C/C++ application using an Application Programming Interface (API) that is sold packaged with the board. The C++ application was written by the author specifically for this thesis.

Unfortunately, the time obtained using the GPS clock and the Symmetricom board does not provide the requisite resolution better than one millisecond accuracy; it is however accurate to better than one-tenth of a second. Furthermore, the time difference between the recorded time and the actual time is observed to be non-deterministic, and cannot be accounted for. The above difficulty in achieving accurate timing can be attributed to a number of sources, or some combination thereof. Some of them may be:

1) The Windows XP OS has its own set of interrupts and queues. Not being designed for timing critical tasks, Windows' assignment of internal priorities may be the source of the inaccuracy.

2) The number of applications and background process vary from one day to the other. This variability may very well be a source for the variability in the deviation of the time difference from the actual time. Since this variability cannot be deterministically characterized, it cannot be accounted for.

14

3) The current system runs on a 1GHz processor. A faster processor may provide more accurate timing by virtue of its speed; an upgrade of the current system is likely to produce an improvement of performance.

A hack was therefore devised to circumvent this problem. The GPS clock outputs a 1-Hz pulse of duration 20 microseconds and of amplitude 5V, on the second, every second. Introducing this pulse, after amplification, into the signal received from the antenna would provide a fiducial mark for every second (accurate to at least 20 microseconds) thus resolving any uncertainties related to the time of a sferic (to a resolution far greater than one millisecond). The hack was in fact successful. A high-level schematic of the circuitry[2] for introducing the fiducial 1-Hz mark (on the second every second) can be found in Figure 2-3. V_{input} is the signal sampled and collected by the data acquisition system.
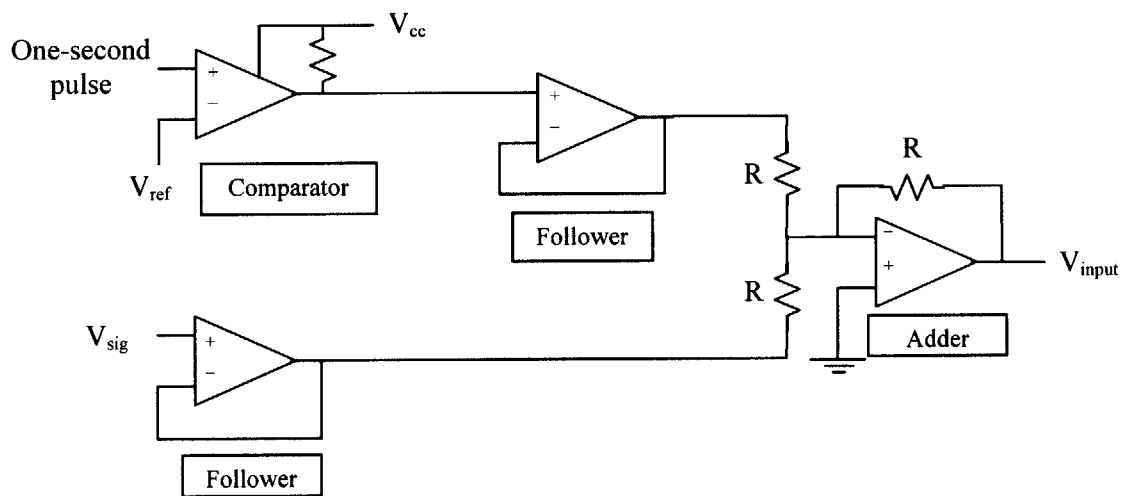
Figure 2-3: Circuit to add a 1 Hz pulse from the GPS clock to the antenna signal as a fiducial mark for accurate time-stamping of sferics

2.4   Data Processing

The acquired data is processed using MATLAB. Matlab is an intuitive technical computing environment. It provides core mathematics and advanced graphical tools for data analysis, visualization, and algorithm and application development. Matlab was favored mainly because of quick development time and also because Matlab is a de facto standard of technical computing.

Matlab provides toolboxes which are collections of highly-optimized, application-specific functions built in the Matlab language. The Matlab toolboxes essential for data processing in this thesis are:

- Signal Processing Toolbox
- Wavelet Toolbox
- Mapping Toolbox

Matlab also offers users a simple and convenient way of creating Graphical User Interfaces (GUIs). The use of GUIs was extremely helpful in gaining a better understanding of the sferics. The Sferic Processing System (SPS) implemented in Matlab as part of this thesis, forms the cornerstone for the analysis.

3   Theory

3.1   Waveguide Propagation

This section deals with waveguides with particular reference to the behavior of the earth-ionosphere cavity. It first describes the basic concept behind waveguide theory in Section 3.1.1, which is followed by a brief outline of the earth-ionosphere waveguide model in Section 3.1.2, described in detail in Porrat et al (2001).

3.1.1   Basic Theory

Electromagnetic Wave (EMW) propagation within a waveguide can be understood relatively easily in the context of guidance of EMW by a pair of perfectly conducting plates [Figure 3-1]. The medium between the plates is considered homogeneous and isotropic. We assume for the sake of simplicity that $\partial/\partial y = 0$. (The wave is propagating in the $\bar{z}$ direction.)
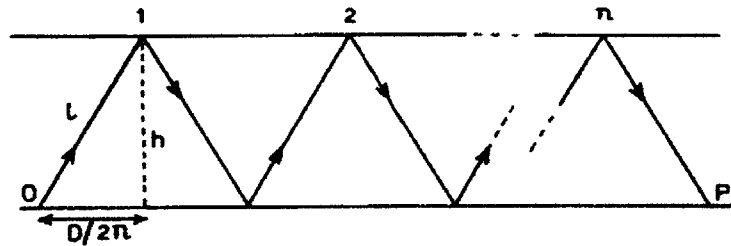
Figure 3-1: Waveguide propagation (Malan, Physics of Lightning)

Using Maxwell's Equations (and their corresponding boundary conditions), it can be shown [Kong, 2000] that for the wave to be guided, the bouncing waves must interfere constructively for $k_x d = m\pi$. Substituting the above guidance condition [Figure 3-2] in the dispersion relation, it is seen that for

$$k_{cm} = \frac{m\pi}{d}$$

$k_z = 0$. It is seen that for $k < k_{cm}$, k_z becomes imaginary resulting in the guided wave attenuating in the $\bar{z}$ direction. This frequency, k_{cm}, is called the cutoff spatial frequency.

Substituting,

$$k = \frac{\omega}{c}$$

where,

c is the speed of light in free space

$\omega = 2\pi f$ is the angular frequency

f is the frequency of the electro-magnetic wave

the guidance condition can also be stated as follows:

$$f_{cm} = \frac{mc}{2d}$$
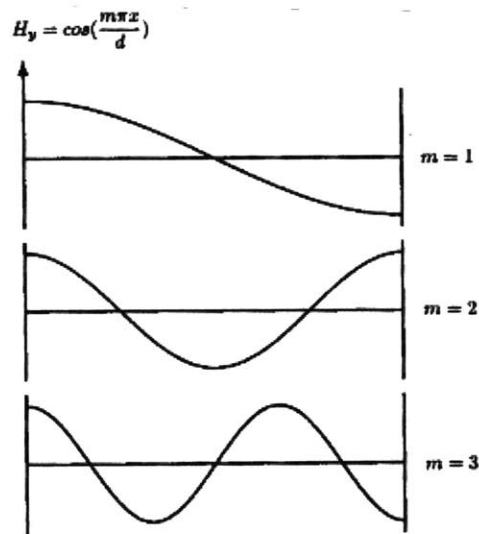
Figure 3-2: Modes in a Waveguide (Kong, Electromagnetic Wave Theory)

Here, f_{cm} is the cutoff frequency of the electro-magnetic wave. The above result suggests that only frequencies above f_{cm} can propagate in a waveguide while frequencies $f < f_{cm}$ attenuate.

3.1.2 Propagation in the Earth-Ionosphere Cavity

G.N. Watson [1919] was the first person to employ a formal waveguide approach for the propagation of EM waves in the EI cavity. The largest analytical contribution to the currently accepted mode theory of waveguide propagation appears to have been made by Wait who has single-handedly written many hundreds of papers on this subject.

3.1.2.1 Propagation in a Lossless Waveguide

The simplest model of the earth-ionosphere waveguide consists of a planar waveguide with infinitely conducting walls; the effects of both the earth's curvature and its magnetic field are neglected. In the model it is also assumed that both the height of the source and the receiver are close to the ground compared to the wavelength λ. The vertical component of the electric field generated in this waveguide by a vertical electric dipole was described by [Wait, 1962]:

$$E_z = \frac{\mu_0 \omega I ds}{4h} \sum_{n=0}^{\alpha} \delta_n S_n^2 H_0^{(2)}(kS_n \rho) \tag{1}$$

where a cylindrical system (ρ, ϕ, z) is used [Figure 3-3].

$\mu_0 = 4\pi \times 10^{-7}$ is the permeability of free space;

$\omega = 2\pi f$ is the radial frequency;

I is the source current (assumed uniform over the source length);

ds is the source length;

h is the waveguide height;

$\delta_0 = 1; \delta_n = 2$ for n > 0;

$H_0^{(2)}(\cdot)$ the Hankel function of the second kind of the 0th order;

$k = \dfrac{\omega}{c}$ is the wavenumber in free space;

$c = 3 \times 10^8 \, ms^{-1}$ is the speed of light;

$C_n = \cos(\theta_n)$ is the cosine of the eigenangle for the nth mode;

θ_n is the eigenangle of the nth mode, shown in Figure 3-2;

$S_n \sin(\theta_n) = \sqrt{1 - C_n^2}$ is the sine of the eigenangle for the nth mode;

In the far field for $\rho > 3h$ and $\rho > 2\lambda$ [Porrat et al, 2001], the above expression after further approximation becomes:

$$E_z = \frac{E_0 (\rho/\lambda)^{1/2}}{2(h/\lambda)} e^{i[k\rho - \pi/4]} \sum_{n=0}^{\alpha} \delta_n S_n^{3/2} e^{-ikS_n\rho} \tag{2}$$

Similarly, the magnetic field is described by:

$$H_\phi = \frac{E_0 (\rho/\lambda)^{1/2}}{2\eta(h/\lambda)} e^{i[k\rho - \pi/4]} \sum_{n=0}^{\alpha} \delta_n S_n^{1/2} e^{-ikS_n\rho} \tag{3}$$

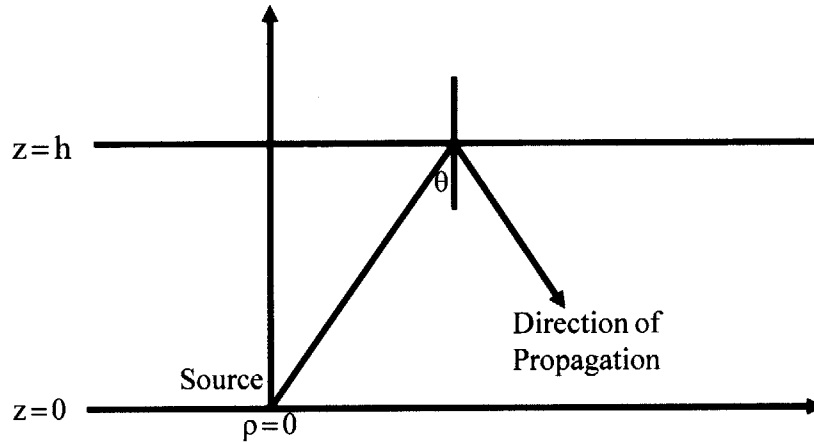Figure 3-3: Propagation in a planar waveguide with cylindrical geometry (ρ, ϕ, z)

3.1.2.2 Propagation with a Lossy Ionosphere

A more realistic model of the EI waveguide extends the lossless model described above by considering a finitely conducting ionosphere. The prevalent model of the ionosphere for ELF/VLF propagation is described by the single scale height exponential profile of

conductivity [Wait and Spies, 1964]. This model was further extended by Greifinger and Greifinger [1978, 1979].

Using such a profile of the ionosphere, for frequencies below the second mode (the first harmonic of the waveguide frequency), Equation 3 can be written as [Porrat et al, 2001]:

$$H_\phi = -\frac{E_0(\rho\lambda)^{1/2}}{2\eta} e^{i[k\rho-\pi/4]} \left[\frac{\delta_0 S_0^{1/2}}{h_0} e^{-ikS_0\rho} e^{-\alpha_0\rho} + \sum_{n=1}^{2} \frac{\delta_n S_n^{1/2}}{h_1} e^{-ikS_n\rho} e^{-\alpha_n\rho} \right] \quad (4)$$

Similarly, the electric field can be described by:

$$E_z = -\frac{E_0(\rho\lambda)^{1/2}}{2} e^{i[k\rho-\pi/4]} \left[\frac{\delta_0 S_0^{3/2}}{h_0} e^{-ikS_0\rho} e^{-\alpha_0\rho} + \sum_{n=1}^{2} \frac{\delta_n S_n^{3/2}}{h_1} e^{-ikS_n\rho} e^{-\alpha_n\rho} \right] \quad (5)$$

In the foregoing equations, the following conditions pertain:

(1) The altitudes h_0 and h_1 are [Greifinger and Greifinger, 1978 and 1979]:

$$h_0 = H - \zeta_0 \ln\left(\frac{2.5 \times 10^5}{2\pi f} \right)$$

$$h_1 = h_0 + 2\zeta_0 \ln\left(\frac{2.39 \times 10^4}{2\zeta_0} \right)$$

where,

$\zeta_0 = \dfrac{1}{\beta_0}$ is the G&G scale height in Km

Further, h_0, h_1 and H are also in Km and f is in Hz.

(2) The modal eigenvalues are approximated by [Sukhorukov et al, 1992]:

$$C_n = \frac{n\pi}{kh_1}$$

$$S_n = \sqrt{1 - C_n^2}$$

(3) The attenuation rates α_0 and α_n are given by [Porrat at el, 2001]:

$$\alpha_0 \approx \frac{0.286 f}{\beta h_0} \left[\frac{dB}{Mm} \right]$$

For $f > \sqrt{2} f_n$ (where f_n is the cutoff frequency of mode n)

$$\alpha_n \approx \frac{0.286 f}{\beta h_1} \left| \frac{C_n^2}{S_n} \right| \left[\frac{dB}{Mm} \right]$$

For $f_n + m \times 60 < f < \sqrt{2} f_n$,

$$\alpha_n \approx \frac{0.286 f}{\beta h_1} |S_n| \left[\frac{dB}{Mm} \right]$$

(4) The excitation factors δ_0 and δ_n are given by [Porrat at el, 2001]:

$$\delta_0 \approx 1$$

For $f > \sqrt{2} f_n$ (where f_n is the cutoff frequency of mode n)

$$\delta_n \approx 2 \left| \frac{C_n^2}{S_n} \right|$$

For $f_n + n \times 60 < f < \sqrt{2} f_n$,

$$\delta_n \approx 2 |S_n|$$

3.1.3 Modal Interference Patterns as an Estimate for Ionosphere Height

Apart from the basic rectangular waveguide theory, modal interference patterns can also be used to obtain the height of the ionosphere if the distance of the sferic from the source is known. The procedure for calculating the ionosphere height given a frequency

spectrum of a sferic from a known distance, generously provided by Sasha Shvets (personal communication, 2004), is described below:

1) Determine the cutoff frequency, f_{c1}

2) Select two clearly defined minima between the first cutoff frequency (f_{c1}) and the second cutoff frequency $(2f_{c1})$: Let the first minima be f_1 and the second minima be f_2

3) Use the formula below to obtain the ionosphere height:

$$h = \frac{r}{2n}\left(\sqrt{b^2 - 1} - \sqrt{a^2 - 1} - b + a\right)$$

where,

h is the height of the ionosphere

r is the source-receiver distance

n is the number of oscillations between f_1 and f_2

$$a = \frac{f_1}{f_{c1}}$$

$$b = \frac{f_2}{f_{c1}}$$

and f_1, f_2 and f_{c1} are defined as above

3.2 Wavelets[3]

While the first recorded mention of the term "wavelet" was in 1909, in a thesis by Alfred Haar, the concept of wavelets in its present theoretical form was first proposed by Jean Morlet and the team at the Marseille Theoretical Physics Center working under Alex Grossmann in France. The methods of wavelet analysis have been developed and initially disseminated mainly by Y. Meyer and his colleagues, who have ensured the methods' dissemination. The main algorithm dates back to the work of Stephane Mallat in 1988.

---

[3] Much of the theoretical content and images in this section have been obtained from Misiti M. et. al., Wavelet Toolbox (For use with Matlab) User's Guide (Ver. 1), and are included here for completeness.

3.2.1 Why Wavelet Analysis?

Perhaps the most well-known tool signal analysts have at their disposal is Fourier analysis whose mathematical underpinnings date back to the work of Joseph Fourier in the nineteenth century. Fourier analysis transforms a signal from its time domain[4] representation to its frequency domain representation, [Figure 3-4]. While useful, this technique has some serious drawbacks. A signal whose frequency content changes dramatically with time, speech for example, cannot be usefully analyzed using traditional Fourier analysis techniques. Short-Time Fourier Transforms (STFTs) are the next logical step to correct this deficiency.

Figure 3-4: Frequency Spectrum of a time signal

STFT is a simple extension of a regular Fourier Transform and is most effective for time-signals whose frequency content varies considerably with time – a speech signal for example. It differs from a traditional Fourier transform in that instead of analyzing the frequency spectrum of an entire signal, only a small window of the signal is analyzed at a time, and this window is slid across the entire signal at pre-specified intervals until the "local" frequency spectra of the entire signal is obtained, [Figure 3-5]. The spectra of the signal taken through time are then plotted on time-frequency axes.

STFTs, although more useful than tradition Fourier Transform (FT) analysis (in some instances), have their own set of drawbacks. These drawbacks are, in some sense, an extension of Heisenberg's Uncertainty Principle: The resolution in the time domain is inversely dependent on the resolution in the frequency domain. More precisely, resolution/knowledge in one domain necessarily leads to a lack of resolution/knowledge in the other. Wavelet analysis is the next logical step of representing signals.

---

[4] The discussion in this section assumes a one-dimensional time signal. The discussion is equally valid for any one-dimensional signal. Furthermore, the above discussion on wavelets can be generalized to more than one dimension as well.

Figure 3-5: Visual representation of the process of making STFTs

Instead of the traditional time-frequency representation that the STFT uses, wavelet analysis relies on a time-scale representation, [Figure 3-6, for a contrast of STFT analysis against wavelet analysis]. Additionally, unlike traditional Fourier analysis which uses smooth sinusoids as its basis, wavelets deliberately rely on more abrupt signals as their bases. In fact, it is the abruptness of their bases that make wavelets a superior tool in applications where traditional Fourier analysis falls short.
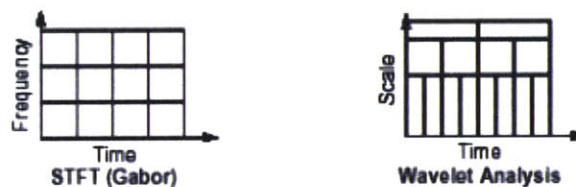
Figure 3-6: Pictorial representation of STFT analysis vs Wavelet Analysis

A major advantage provided by wavelets is the ability to do local signal analysis – that is, to analyze a localized target area within a larger signal. Just looking at pictures of wavelets and sine waves [Figure 3-7], one intuitively expects that signals with sharp changes might be better analyzed with an irregular wavelet than with a smooth sinusoid. Due to the local extent of wavelets – wavelets are non-infinite in duration for all practical purposes - it also makes sense that local features can be described better with wavelets. Wavelet analysis is thus capable of revealing aspects of the data such as trends, breakdown points and discontinuities missed by other signal analysis techniques.

3.2.2 Wavelet Analysis: A Practical Introduction

A wavelet is a waveform of effectively limited duration that has an average value of zero. Compare wavelets with sinusoids. Sine waves do not have limited duration; they extend from minus to plus infinity; they are smooth and predictable. Wavelets, on the other hand, tend to be irregular and asymmetric [Figure 3-7].

Sine Wave   Wavelet (db10)
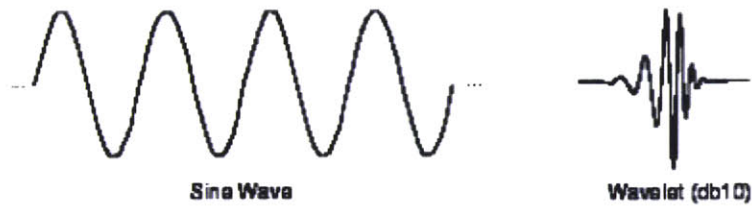
Figure 3-7: A sine wave and a wavelet

Sine waves are the basis of Fourier analysis. Fourier analysis consists of breaking up a signal into sine waves of various frequencies [Figure 3-8]. Similarly, wavelets form the basis of wavelet analysis. Wavelet analysis is the breaking up of a signal into *shifted* and *scaled* versions of the original (or *mother*) wavelet [Figure 3-9].

Fourier

Transform

Signal   Constituent sinusoids of different frequencies

Figure 3-8: A signal as a sum of sinusoids

Wavelet

Transform

Signal   Constituent wavelets of different scales and positions

Figure 3-9: A signal as a sum of shifted and scaled wavelets

Scaling a wavelet simply means stretching (or compressing) it. The scale factor, *a*, quantifies how much the wavelet is stretched or compressed. The smaller the scale factor, the more compressed the wavelet, [Figure 3-10]. In the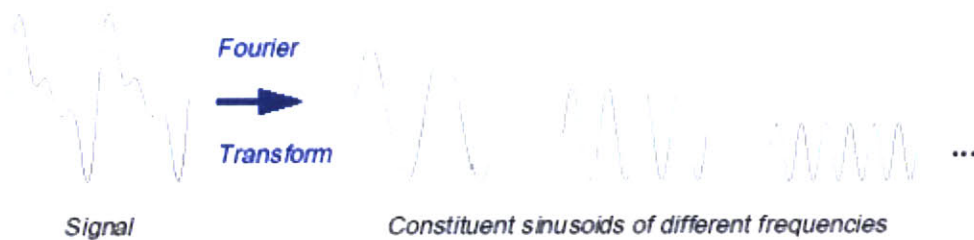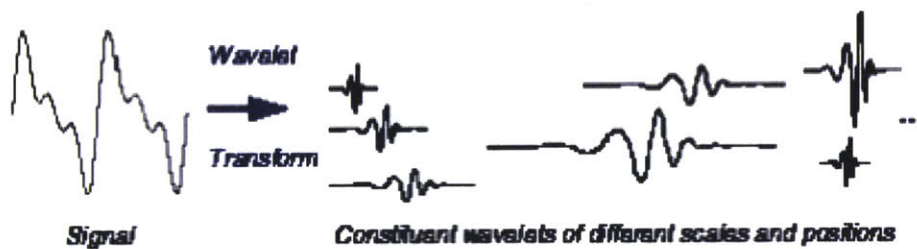 context of the time-scale axes referred to earlier, the scale axis simply refers to the scaling (stretching or compressing) of the wavelet.

$$f(t) = \psi(t) \quad ; \quad a = 1$$

$$f(t) = \psi(2t) \quad ; \quad a = \frac{1}{2}$$

$$f(t) = \psi(4t) \quad ; \quad a = \frac{1}{4}$$
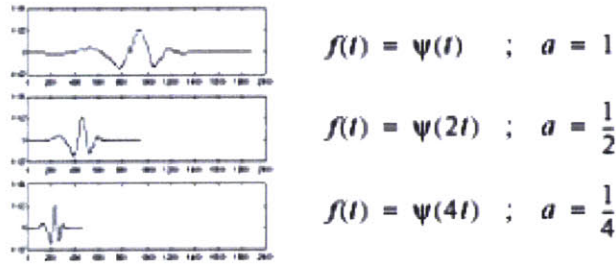
Figure 3-10: Scaled wavelets

Shifting simply implies displacement in time. Shifting a wavelet simply means delaying (or hastening) its onset. Mathematically, delaying a function *f(t)* by *k* is represented by *f(t-k)*, Figure[3-11].

Wavelet function
$\psi(t)$

Shifted wavelet function
$\psi(t-k)$

Figure 3-11: Shifted wavelets

3.2.2.1 Wavelets

Unlike sinusoids which have only one form, there are a number of different families of wavelets: Daubechies, Biorthogonal, and Coiflets to name a few. Figure 3-12 shows a few wavelets. The process of creating useful wavelets is out of the scope of this thesis.

3.2.2.2 Suitability of wavelets – An Empirical Approach

Wavelets measure the correlation between the scaled mother wavelet and the original signal. The choice of wavelet is thus, typically, application dependent. The choice of an appropriate wavelet is found to vary based on the nature of the discontinuity to be detected. While a detailed explanation on the selection procedure is out of the scope of this thesis, following are some rules of thumb, obtained empirically by the author.

The *haar* (*db1*) wavelet works well for detecting abrupt discontinuities. For the purposes of this thesis, the author used either the *haar* or the *db2* wavelets to obtain cutoff estimates. To detect ramps, the higher order wavelets from the Daubechies family were used.

3.2.2.3 Example: Detecting a discontinuity in a sine wave

The following contrived example attempts to demonstrate how wavelets can be used to precisely detect discontinuities in a signal. This example will also be used to demonstrate the superiority of wavelets as compared to regular Fourier transforms and even STFTs in certain applications.
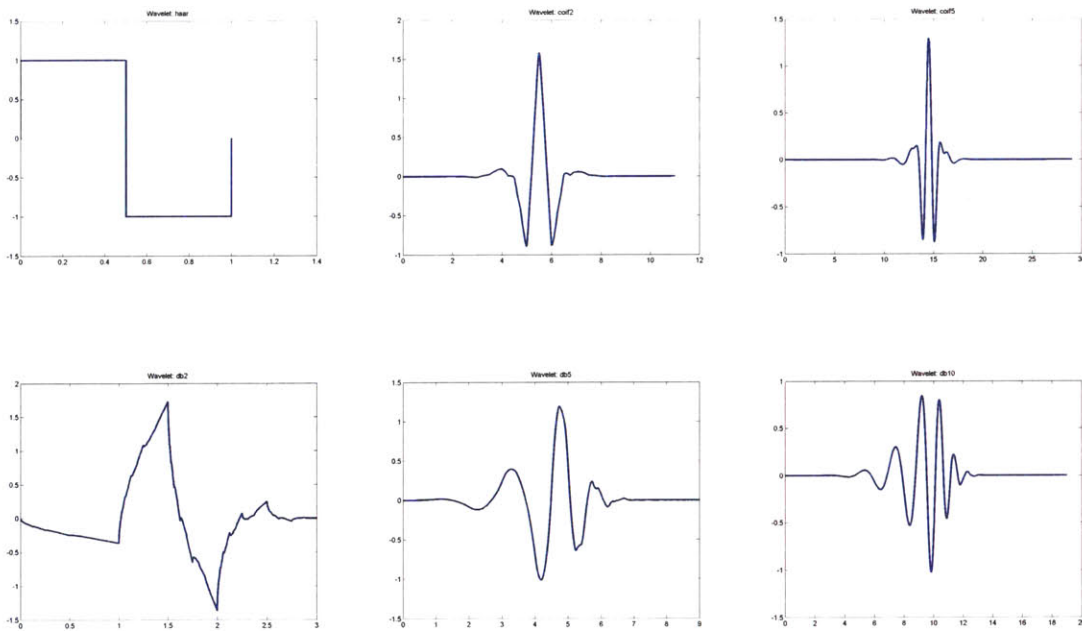

Figure 3-12: Wavelets – haar, coif2, coif5, db2, db5, db10 (from left to right, top to bottom)

The time signal is a pure sinusoid with a discontinuity, artificially inserted around time t=10s, [Figure 3-13 a and b]. The goal is to detect, as closely as possible, the time of the discontinuity. As expected, the Fourier spectrum [Figure 3-14] does not give us any information about the time of the discontinuity. The STFT [Figure 3-15] does slightly better. Temporal and Spectral smearing, however, prevent us from deducing the exact time of the discontinuity. The wavelet transform [Figure 3-16], on the other hand, accurately shows precisely where the discontinuity is located.

3.2.2.4 Discrete Wavelet Transform – Approximations and Details

While the wavelet transform contains all the relevant information, there is a property of wavelet analysis that can facilitate the process of inferring the location of the discontinuity.
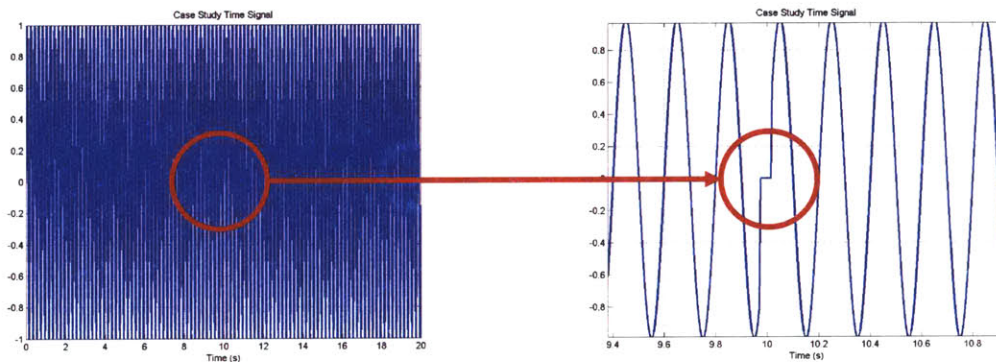
Figure 3-13 a and b: Original Sine wave, f = 5 Hz, with a tiny discontinuity around t = 10s

For many signals, the low-frequency content is the most important part. It is what gives the signal its identity. The high-frequency content, on the other hand, imparts flavor or nuance. Consider the human voice. If one removes the high-frequency components, the voice sounds different, but remains intelligible However, if one removes enough of the low-frequency components, one hears only gibberish. Wavelet analysis allows the separation of a signal into two components, broadly speaking, the *approximations* (low frequency) and the *details* (high frequency). In the context of the example of the sine wave with a discontinuity, the *detail* signal [Figure 3-17] gives the location of the discontinuity precisely. We know that the *detail* contain the high frequency components;

the discontinuity is obviously a high-frequency component. As expected, the *detail* signal registers the discontinuity.

Furthermore, the *detail* signal is a one-dimensional signal. Locating the discontinuity, whether manually or algorithmically now becomes substantially easier than in the time-frequency space. (In this example, the location of the discontinuity is simply the location of the spike – the maximum of the 'detail' signal.)

3.2.3   Estimating the EI Waveguide Cutoff Frequency Using Wavelets

We can use wavelets to detect sharp discontinuities. From waveguide theory, one expects a sharp rise in EM radiation at the waveguide cutoff region, [Figure 3-18]. Thus, wavelets can be used to detect a sharply discontinuous cutoff frequency precisely. An approximate value for the cutoff frequency is provided by the details signal, [Figure 3-18].

From the EI waveguide theory [Section 3.1.2.2; Porrat, 2001] one expects to see a ramp in the energy starting from frequencies of $\sqrt{2}f_{cutoff}$. Another way of deducing the cutoff may be to deduce the location of the ramp and estimate the cutoff by dividing the frequency by $\sqrt{2}$. While the accuracy of the above is unknown, and the error not well understood, deducing the location of the ramp does provide a reinforcing estimate of the cutoff frequency. As mentioned earlier, the author recommends either the *haar*, or the *db1* and *db2* wavelets for detecting a sharp cutoff; a higher order wavelet, *db3-db6* is believed to be better suited for detecting ramps.

Note: The presence of sharp peaks due to the noise in the background spectrum can lead to discontinuities producing unexpected results. When estimating the cutoff frequency, care should be taken to ensure that the estimated frequency is actually a fair estimate of the waveguide cutoff frequency, and not an estimate of a high frequency 60 Hz harmonic.
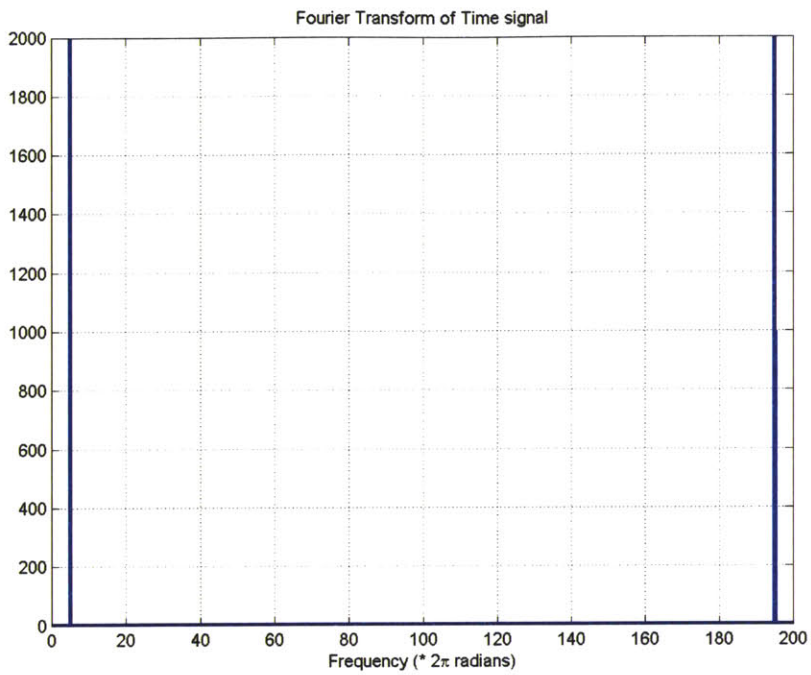
Figure 3-14: A simple Fourier transform of the sine wave shows
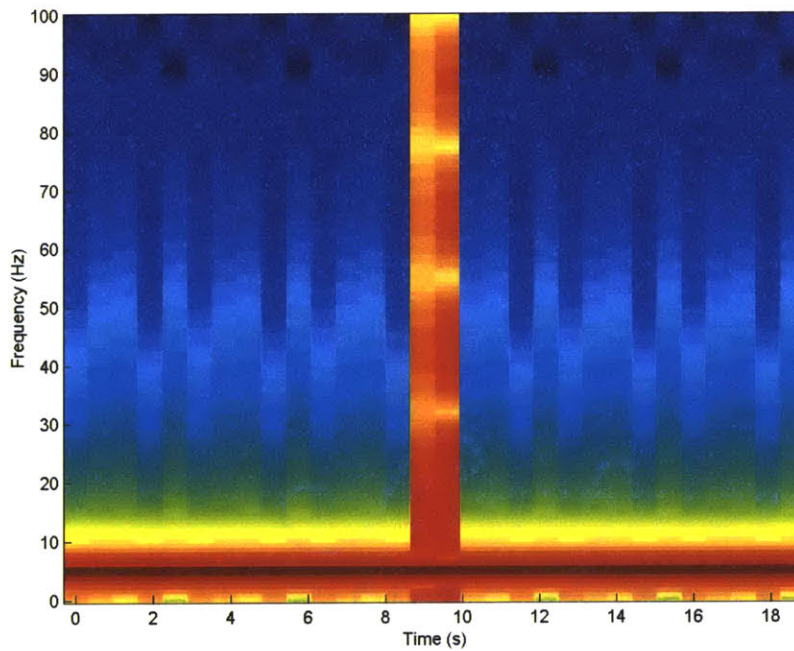the presence of 5 Hz; it contains no information about the noise.

Figure 3-15: STFT – shows the presence of noise but does
not reveal the precise time of the discontinuity
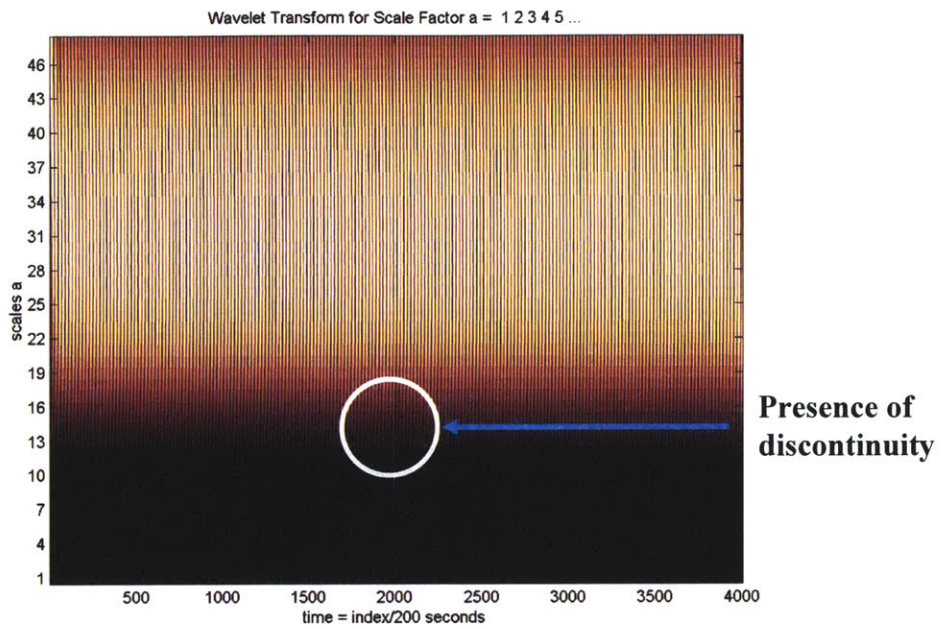
Figure 3-16: Wavelet transform of a sine wave with a discontinuity
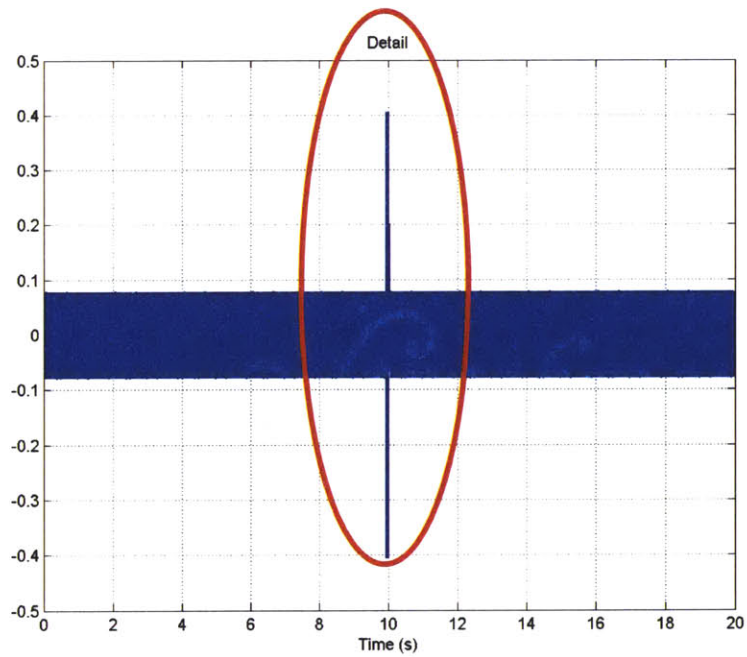
Figure 3-17: Details (displays presence of discontinuity precisely)
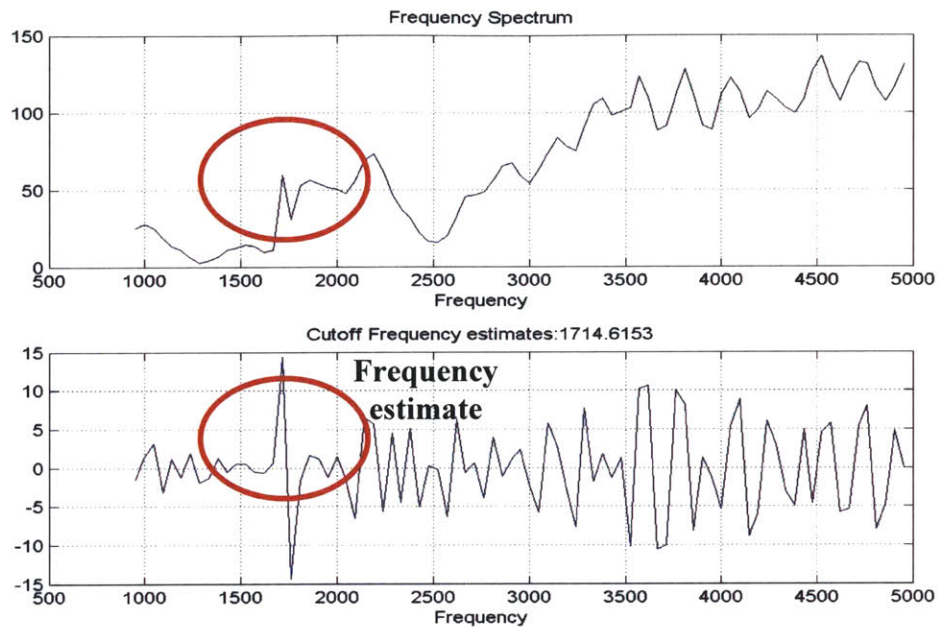
Figure 3-18: Waveguide Cutoff frequency and Wavelet estimate of the cutoff

3.2.3.1 Error in Frequency Estimate

This thesis merely proposes the use of wavelets as a black box to estimate a waveguide cutoff; the aim is to produce a consistent estimate based on some factor. Quantifying the error in the frequency estimate is beyond the scope of this thesis.

However, a lower bound on the error can be obtained based on a basic understanding of DSP. The lower bound of the error is exactly equal to the amount of spectral smearing; spectral smearing is equivalent to the effective resolution of a frequency spectrum and is inversely related to the window length by the following equation:

$$R = \frac{CF_s}{N}$$

where,

R is the frequency resolution

C is a pre-determined constant for the window (2 for rectangular windows; in this thesis, we are concerned with rectangular windows only.)

F_s is the sampling frequency

33

N is the window length

For a typical 25 ms window sampled at 50 KHz, as is common in this thesis,

$R = 80 \, \text{Hz}$

3.2.4   Limitations and Future Work

Despite the advantages, estimating the cutoff frequency by wavelets is not without limitations: Not all frequency spectra lend themselves to analysis by wavelet as tractably as the one in Figure 3-18. For example, Figure 3-19 displays a distinct waveguide cutoff; yet, due to the jaggedness of the frequency spectrum, wavelet analysis is unable to produce a clear frequency maximum in the right region. In such cases, it is recommended that a peak corresponding to a frequency estimate that best represents the cutoff frequency (height of the ionosphere) be selected, 1700 Hz in this example. The analysis of frequency spectrum similar to the one in Figure 3-12 may be improved by selecting more appropriate wavelets, or by designing smarter algorithms to estimate the cutoff frequency from the *detail*.
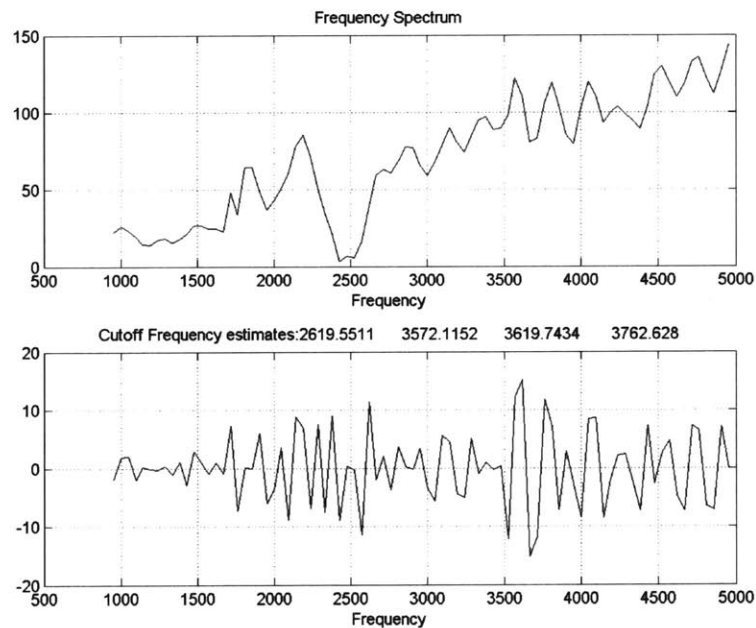

Figure 3-19: Jagged frequency spectrum (not well-analyzed by wavelets)

Additionally, as mentioned earlier, the error of the estimate is not well quantified. Further study or research in wavelets may be needed to obtain more accurate error estimates than the lower bound provided by using the spectral smearing rationale.

4   Noise – Its Characterization and Removal

The presence of noise is a major problem associated with analyzing sferics. The noise invariably compels analysts to focus on large amplitude events which occur relatively close to the receiver, since these events are expected to have a higher signal-to-noise Ratio (SNR). The presence of noise thus precludes the analysis of a large percentage of events; as a corollary, however, if the noise were better understood, a much larger percentage of events would lend themselves to analysis. While a thorough treatment of the noise is beyond the scope of this thesis, this section attempts to provide a basic understanding of the noise, the methods used in this thesis to limit its effects. This section also lists further avenues of exploration.

4.1   Sources

The sources of noise can broadly be sub-divided into two categories – the *background spectrum* and *anthroprogenic noise*.

4.1.1   Background Spectrum

Sferics occur at the rate of 100 per second, globally. In a localized storm, the rate of occurrence can be much greater. Any antenna system receives EM radiation from all the lightning strikes that occur anywhere in the world. The integrated EM radiation that an antenna receives at any point in time is termed the *background spectrum*. Fortunately, the lossy EI waveguide causes most sferics to undergo a high attenuation with distance. The background spectrum is rarely a big problem.

4.1.2   Anthroprogenic Noise

Anthroprogenic noise literally means man-made noise. The biggest offenders are EM contamination from power lines, as well as military RF transmissions and electric trains [Figure 4-1].

In North America, the energy from the electromagnetic fields of the power lines is present at 60 Hz (and its harmonics), while overseas it is usually present at 50 Hz. The power line noise present at the Rhode Island station contains harmonics beyond 10 kHz;

for low-amplitude distant sferics, this noise tends to obscure the atmospheric data in the ELF/VLF band selected for this study.

There are other sources of noise present in the electric spectrum, observed as peaks of energy concentrated at particular frequencies. While the exact source of these peaks is unknown, they are likely caused by radio frequency (RF) communication stations. Since both the noise due to the power lines (at frequencies of 60Hz and its harmonics), as well as the noise due to the RF stations are relatively slowly varying, it is often convenient and sometimes useful to lump these anthropogenic sources with the background EM radiation due to the sferics, and call the combination, the *background spectrum*.

4.2 Noise Removal

Anthroprogenic noise drowns out most distant events. Noise removal is thus integral to estimating the waveguide cutoff frequency, especially for low-amplitude distant sferics.

4.2.1 Removal of 60-cycle Harmonics

The noise due to the power lines - at frequencies of 60Hz and its multiples – can be removed using basic discrete-time signal processing (DSP) filtering techniques in a number of ways.

One way is to use a set of notch/comb filters to remove the 60 Hz noise and its harmonics. The drawback of this method, however, is that a notch filter tends to remove all the energy present at a particular frequency introducing artificialities in the frequency spectrum. Thus, with notch filters, the initial problem of discerning the cutoff frequency through the 60 Hz harmonic peaks is merely translated to discerning the cutoff frequency through 60 Hz harmonic "gorges" or notches. For this thesis, a non-linear filter that preserves some of the background information is used to reduce the effects of power lines' noise. The primary of advantage of such a filter is that the output retains at least some degree of faithfulness to the original background spectrum.
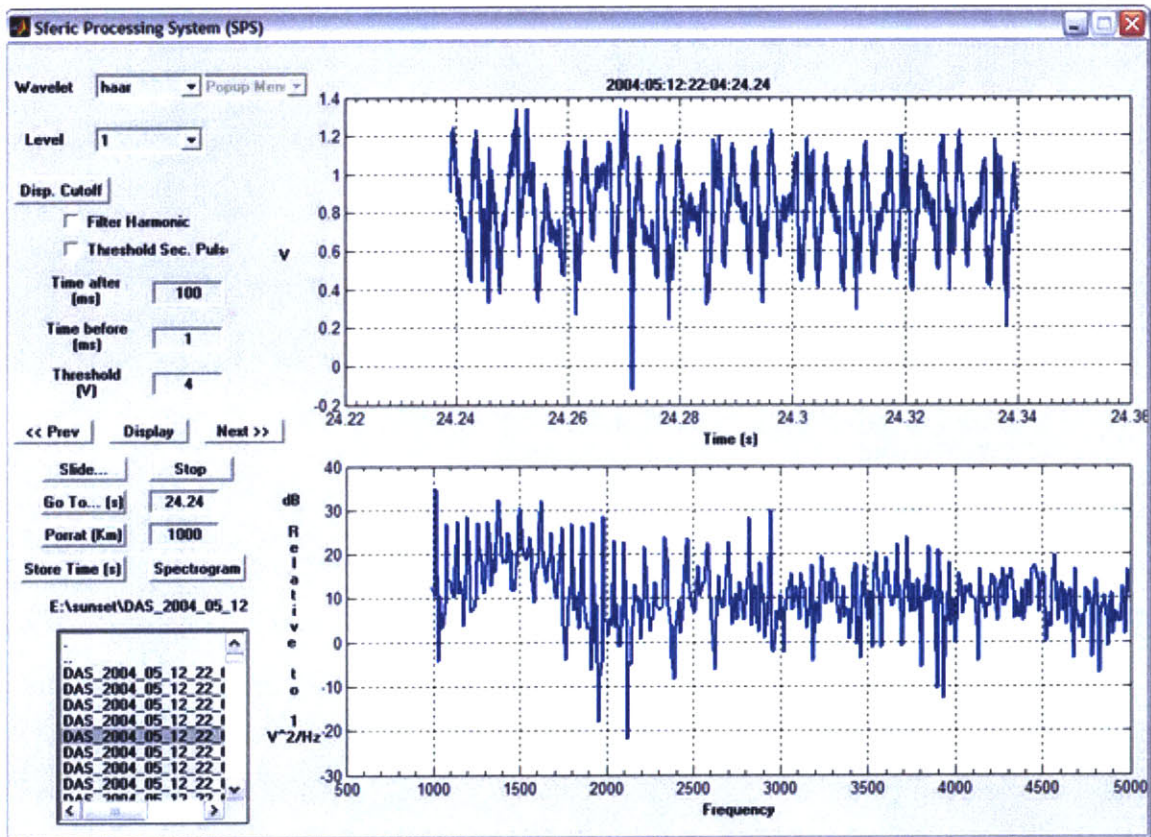
Figure 4-1: The background spectrum clearly shows anthropogenic noise in the form of sharp peaks. Analysis of sferic amidst this background noise is virtually impossible.

The non-linear method of filtering is as follows: The frequency spectrum of any window contains 60 Hz harmonics rising above the background spectra. To remove the power lines harmonics, a frequency range around the noise peak is selected such that the energy present at both limits of the frequency range is at the background spectrum level, to be determined empirically. The frequencies between the two frequency ends are then filled with values such that the slope between the two ends is constant. In fact, the frequency values between the ends of the frequency range are filled so that the result is an up-sampled version of linear interpolation between the frequency ends. An important fact to keep in mind while using this method is that to reconstruct a time-domain signal from the filtered frequency domain signal, one must make sure that the Fourier transform after filtering satisfies all the symmetrical properties of real signals.

Figures 4-2 and 4-3 visually demonstrate the process of noise-removal using the above filter, in a contrived example. In this example, the noise peak and the signal are symmetric, hence the plateau-like structure of the resultant filtered signal. In asymmetric signals, the result is a straight line with a non-zero slope that connects the two ends of the signals, instead of a flat top as in the case of the example.

It should be noted that the determination of the local energy level of the background spectrum in the vicinity of a 60Hz harmonic peak is somewhat arbitrary. It is best obtained empirically, by trial and error. It should be further noted that the frequency range over which the 60 Hz harmonic needs be linearized is dependent on the length of the window – a result of spectral smearing. For this thesis, a 1 minute window length was filtered using a range of 3 Hz on each side of the 60 Hz harmonics; these numbers were obtained empirically. Also, power lines harmonics were removed all the way up to the Nyquist rate (here, 25 KHz).

4.2.2 Results

The results of noise removal are displayed in Figures 4-4 and 4-7. The first pair is the Fourier Transforms of an event before and after noise removal; Figures 4-6 and 4-7 are two spectrograms of an event before and after noise removal. An approximate waveguide cutoff frequency is readily visible in the spectrogram of the signal from which noise has

39

been removed. It is clear that the importance of noise removal cannot be over-emphasized, even if it be only the removal of the noise due to power-lines.

4.2.3   An Alternative Method of Noise Removal: Wiener Filtering

A potentially more effective technique would be to use Wiener filtering techniques to filter the *background spectrum* (EM radiation due to the sferics along with the anthropogenic noise).

Wiener filtering methods essentially assume that the noise source is uncorrelated with the signal source. Fortunately in our case, the background spectrum is uncorrelated with the signal source. The power lines and RF communication noise are obviously independent of a lightning strike; the background spectrum which is an integration of all the lightning events around the globe can be assumed uncorrelated to a good approximation.

While the details of Wiener filtering are beyond the scope of this book, the author believes that a well implemented Wiener filter would do a better job of removing the noise than the techniques outlined above.

Contrived Example: Noise peak to be removed
(from indices -1 to 1.5)
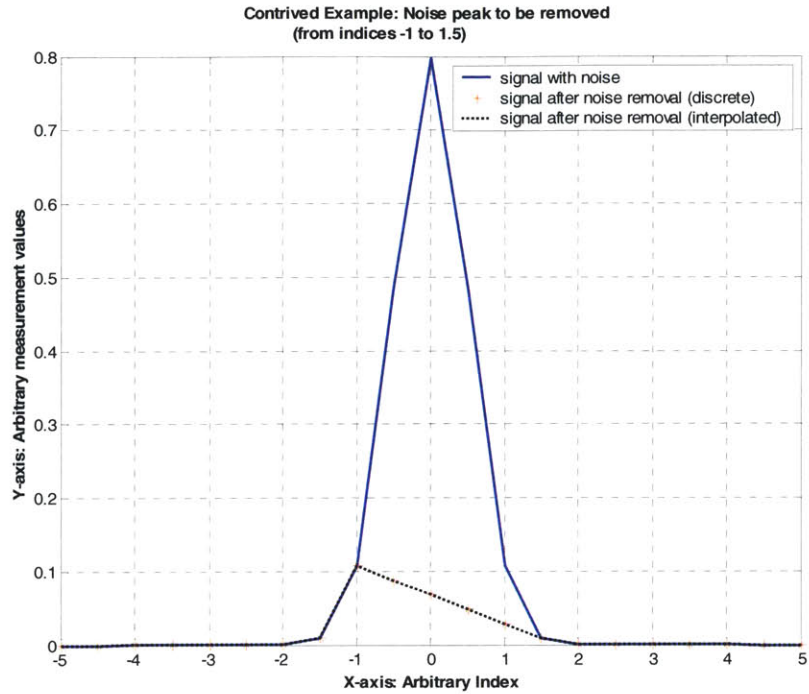
**Figure 4-2: A contrived example to visually demonstrate the process by which
the non-linear filter removes the power lines spike from the signal
(Before)**

Contrived Example: After noise removal
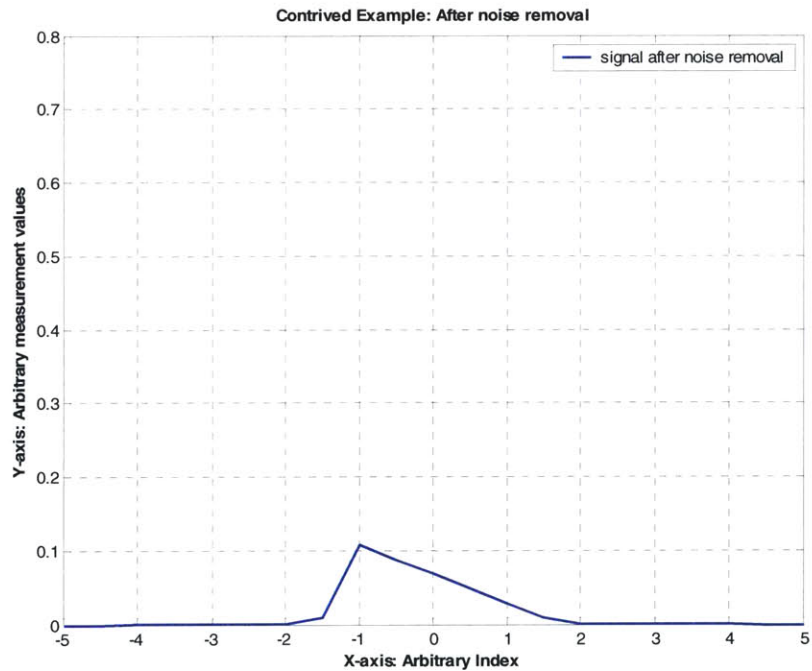
**Figure 4-2: After noise removal; note how the non-linear filter "linearly"
interpolates between two specified points around the center frequency to remove
the offending noise while preserving (somewhat) the background spectrum**
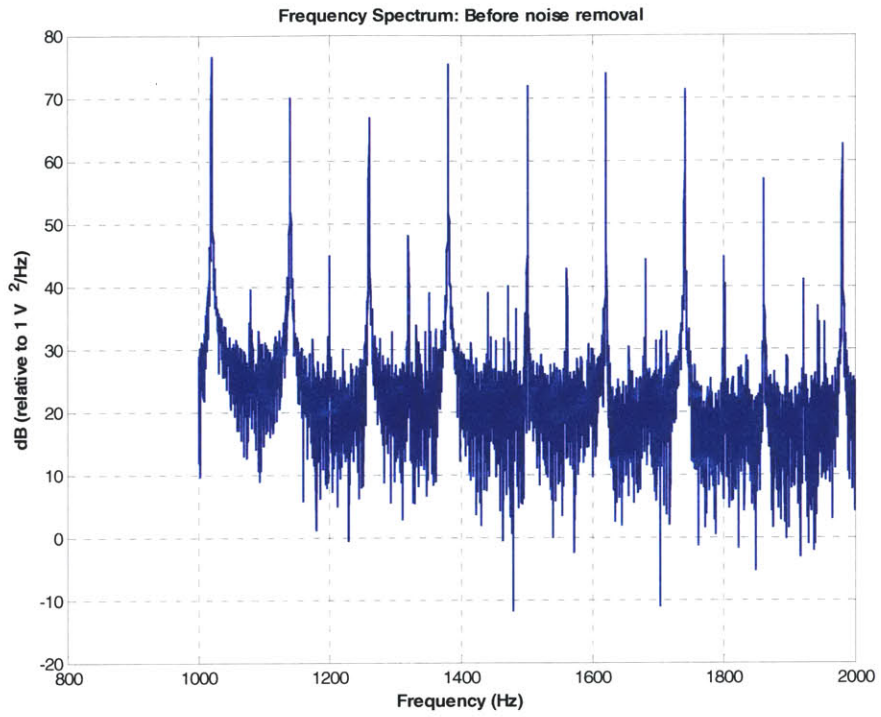
Figure 4-4: Fourier Transform of an event with noise (before noise removal)
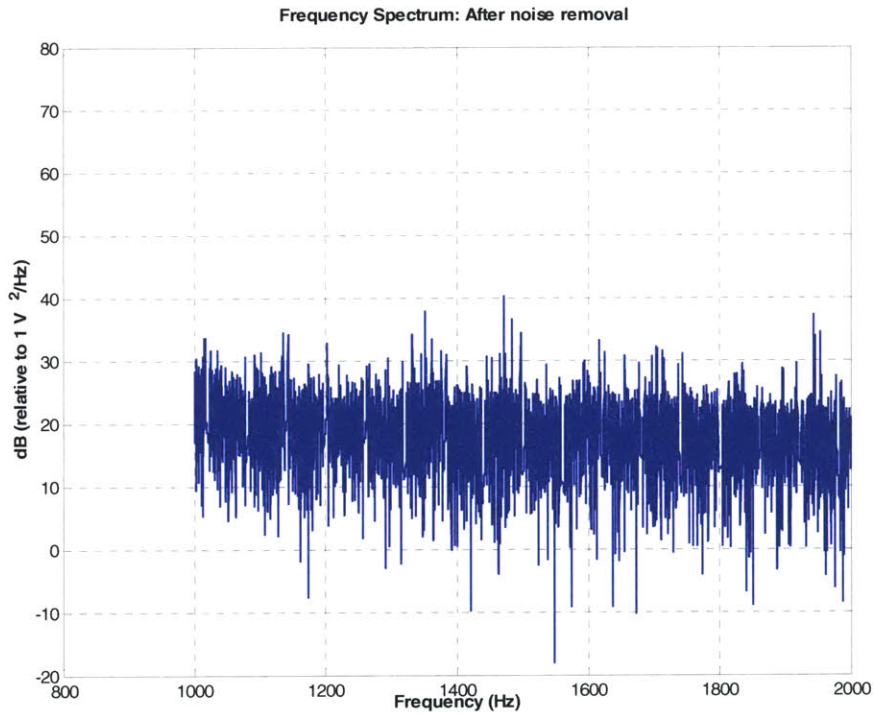
Figure 4-5: Fourier Transform of an event after noise removal

2003:8:10:1:59:23:135:471.3013

Figure 4-6: STFT of an event with the background spectrum (before noise removal)

2003:8:10:1:59:23:135:471.3013

Figure 4-7: STFT of the event in Figure 4-6 after noise removal

43

5 Data Processing Methods

The applications that process the acquired (digital) data have been developed by the author in Matlab's programming environment [Section 2.4]. Given the visual nature of spreadsheets, Microsoft Excel was also used occasionally, for deducing possible rules of thumb before verifying their veracity through rigorous statistical tests.
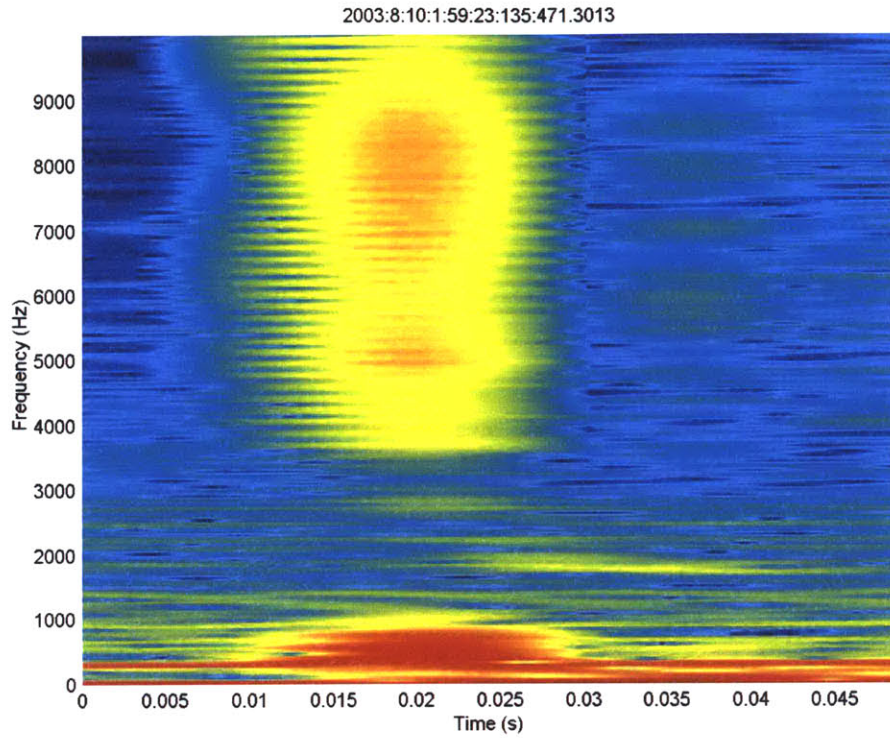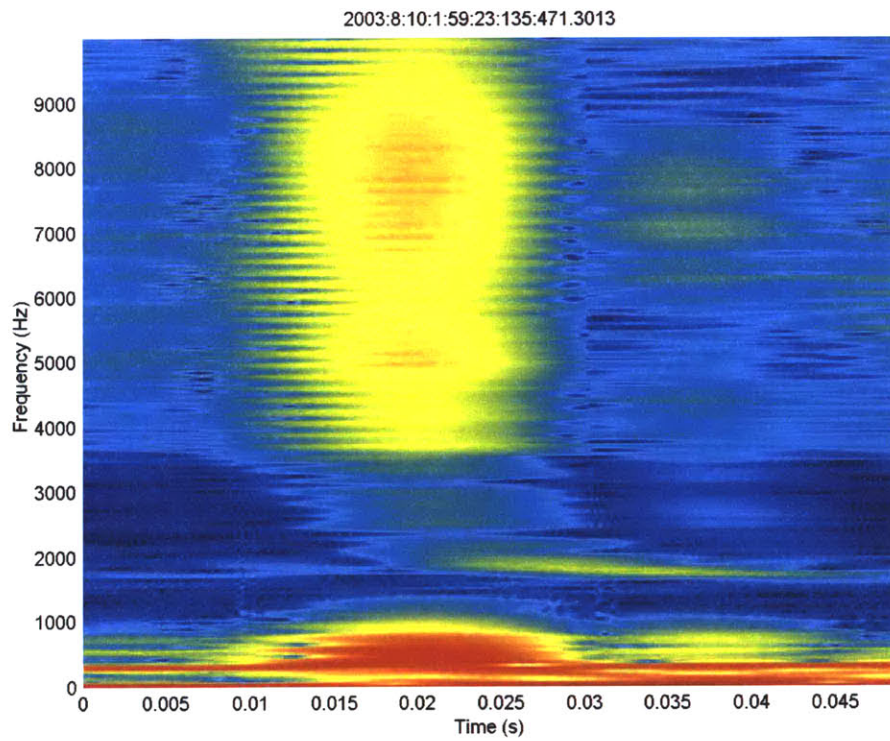
5.1 Sferic Processing System (SPS)

Sferic Processing System (SPS) is designed to allow users to "playback" the continuously recorded data in a continuous fashion. SPS is a GUI based application developed by the author and written in Matlab. Data are continuously collected for a few hours, frequently through the time of the day-night boundary [Section 2.4]. SPS facilitates the easy visualization of the large amounts of collected data. The frequency spectrum of the window is also simultaneously displayed. Figure 5-1 displays a screenshot of the user interface.

5.1.1 A Brief Description

The salient features of SPS are as follows:

1) A **list menu** on the main page allows the user convenient access to all the files in the current directory. It also allows the user to traverse through the entire windows directory structure on the local machine. All the files (and directories) in the current directory are visible to the user in the menu. Double-clicking a data-file (created by the DAS) displays the 60-second length of data as a plot along with the corresponding DFT in one figure; double-clicking on a sub-directory displays the contents of the sub-directory; double-clocking on the super-directory symbol '..' displays the contents of the parent directory of the current directory; finally, double clicking on any other file opens the file in a default application.

2) A '**threshold**' field that allows the user to specify a threshold voltage for sferic display. Internally, the threshold generates a list of sferics within the data file whose values are greater than the threshold. One can traverse through this list of sferics

44

using the '**<<Prev**', '**Display**' and '**>>Next**' buttons. All displays have the plot of the window at the top and a plot of the window's DFT at the bottom.

3) Two fields '**Time before**' and '**Time after**' which can effectively be used to specify the window length in milliseconds. They are also used to specify the length of the window to be displayed before and after the onset of a sferic. This is especially useful while creating spectrograms described next.

4) Clicking on the '**Spectrogram**' button displays a 512-point windowed frequency-time spectrogram or, Short Time Fourier Spectrum (STFS) of the current window in a separate figure.

5) The '**Go To...**' field along with the 'Time before' and 'Time after' fields provide another way of displaying a particular section of a data file.

6) Finally, the '**Store Time**' button provides users with the ability to bookmark a particular time section and store it in a Data Information File (DIF)– a file of the same name as its source data file but with a '.dif' extension.

5.1.1.1 Estimating the Cutoff Frequency

SPS allows one to easily identify a sferic and display it in a window of arbitrary user-specified size (in milliseconds). Simultaneously, SPS also displays the frequency spectrum of the time domain waveform. The cutoff frequency is estimated from this frequency spectrum.

Note: All sferics do not have frequency spectra that display a readily-estimable cutoff. This may be due to a number of factors including high attenuation due to a large source-receiver separation or due to a low-amplitude sferic, with a small signal-to-noise ratio.
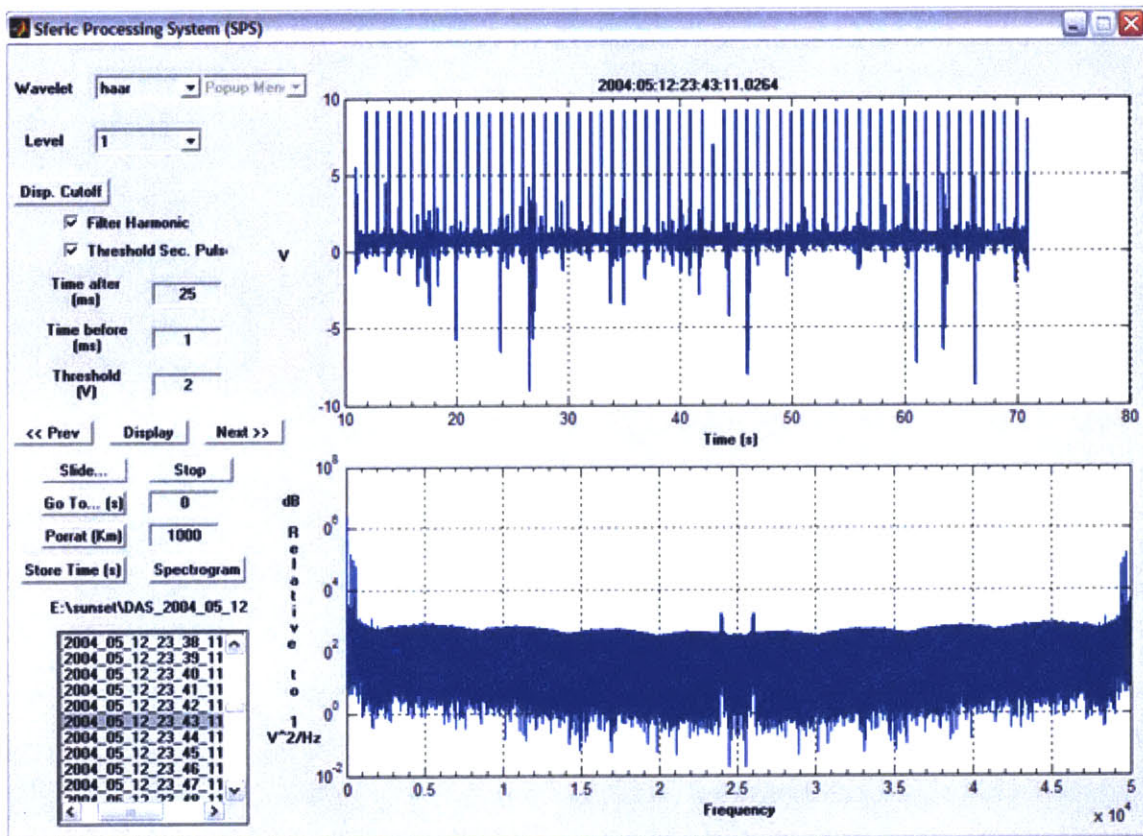
Figure 5-1: A screenshot of Sferic Processing System (SPS), implemented with Matlab, showing a 1-min data file with the sferic signal, along with the GPS 1-Hz pulse required for accurate time-stamping of lightning events for comparison with NLDN and Dowden.

Obtaining a manual cutoff estimate

Obtaining an estimate for the cutoff frequency manually is a somewhat arbitrary process. The first step is to find a sferic which has a readily-visible cutoff in its frequency spectrum. Once a cutoff is found, depending on the time of day, one selects the frequency that provides the best estimate of the cutoff in line with a value that produces a reasonable estimate for the ionospheric for the time of occurrence of the sferic [Smith et al, 2004].

The arbitrariness in the cutoff selection process stems from the fact that it the decision to select the frequency that maximizes the local magnitude as opposed to the frequency that maximizes the local slope, or even the frequency where the rise in the amplitude actually begins is somewhat arbitrary. The presence of local "peaks" due to anthroprogenic noise sources sometimes complicates the analysis further. It is the presence of these sources of arbitrariness in this situation that motivated the development of an automatic procedure.

Obtaining cutoff estimates using wavelets

Wavelets provide an efficient and even more importantly, a consistent method of "black-boxing" the cutoff selection procedure [Section 3.4]. This section merely provides an overview of how one can use the wavelet functionality within SPS to obtain an estimate for the waveguide cutoff frequency. While this thesis does not pretend to quantify or even understand, except at a superficial level, the error of the estimate, the advantage of using wavelets (or any other black-box approach, for that matter) as opposed to using eyeball estimates, lies in that one is assured that the estimates produced are at least always consistent with some criteria; errors inherent in the eye-balling method, described above, due to pre-conceived biases are minimized.

Obtaining a cutoff estimate using wavelets is a semi-autonomous process. The first step in the process is to display a time waveform along with its corresponding frequency spectrum on the main screen. Needless to say, the time waveform must be such that its frequency spectrum allows for approximating the cutoff by 'eyeballing.' Once such a screen is displayed, the next step is to select the wavelet most suitable for the application [Section 3.4]. For the purposes of this thesis, since the error in cutoff

47

frequency estimation by the wavelet technique has not been well-quantified, the author recommends using the same wavelet to determine cutoff estimates through a particular study.

The third and final step is to display the cutoff estimate. This is done by pressing the 'Disp. Cutoff' button. A new figure with two plots are displayed – one of the original Fourier spectrum, and the other which contains the "details" signal deconstructed from the original spectrum using wavelets. The cutoff frequency can now be estimated by first narrowing the region of interest by eyeballing and then selecting the frequency of local maxima present in the narrowed region of interest in the "detail" signal.

5.2   Locating Sferics

While SPS is a useful tool for studying the data files and for obtaining useful estimates of cutoff frequencies, it does not provide users with the location of the sferics. Two separate applications, one each for the National Lightning Detection Network (NLDN) and the Dowden VLF Detection Network (Dowden), written by the author provide location information for observed sferics.

The process of deducing the location of a sferic, described as the indirect comparison method in Section 2.4.1 is, as follows: A list of all sferics whose times are greater than a specified threshold is made using an application in Matlab, and stored in a file. Once such a list is compiled, the time of occurrence of each sferic in the list is matched against the time of occurrence[5] of sferics in the NLDN dataset (and separately, for the Dowden dataset) and a new list which contains the matched sferics along with their actual times and locations is created.

The time, location and peak current[6] of sferics thus identified any number of hypotheses regarding the effects of distance and other ionosphere and meteorological phenomena on the observation of sferics can be drawn.

---

[5] The time of occurrence is adjusted for the distance-lag between the source lightning and the receiver station at RI.
[6] NLDN can provide an estimate of the peak current along with the location of the event.

6   Results and Discussion

The salient results pertaining to this thesis along with a complete discussion are presented in this section. The section is divided into two sub-sections. The first sub-section presents the analysis of the change in ionospheric height through the day-night boundary for a specific day; as part of the analysis, it contains discussions about sferic propagation in the day, at night and through the day-night transition with particular emphasis on tweek sferics. The second sub-section compares a theoretical model of sferic propagation at night, against empirically observed sferics within the 500 Hz and 5 KHz frequency band for a range of distances.

Before proceeding to a discussion of the observations, however, it is important to note and understand the distinction between sunset at the ground and sunset at the ionosphere. The ionosphere lies ~100 Km above the earth. Basic intuition tells us that a person standing on a tower 100Km high would see the sun even after the sun has set on the ground. A simple geometric calculation can be used to estimate approximately how long it takes for the sun to set over the ionosphere and is given approximately[7] by the equation below:

$$t = \frac{\sqrt{R_e h}}{v_e}$$

where,

R_e is the radius of the earth

h is the height of the ionosphere

v_e is the velocity of the earth's rotation

Plugging the numbers, the sun sets at the ionosphere approximately 30 minutes after sunset on the ground. For the purposes of this thesis, the time of the end of civil

---

[7] The calculation does not take into account the coordinates of the location.

twilight[8] which occurs about 25 minutes after sunset over the ground, was judged a good enough approximation of sunset at the ionosphere.

The attenuation in sferic propagation is largely a function of the ionization of the ionosphere. In the daytime (when the ionosphere over the path of the sferic is exposed to the sun), there is high ionization evidenced by the lowering of the ionosphere height to ~60 Km; the attenuation for VLF radiation is also extremely high. Conversely, at night, the ionosphere does not undergo any ionization; the attenuation is also much lower than in the daytime. It is expected that the ionosphere transitions from daytime to nighttime abruptly {Smith et al, 2004]. Accounting for this distinction between sunset on the ground and sunset at the ionosphere is therefore an important element of monitoring ionosphere height through the day-night boundary.

6.1   Sferics and the Transitioning Ionosphere

This section presents the analysis of monitoring ionosphere height for a transitioning ionosphere (through the day-night boundary) for specific days. The section first presents the observations, which are then followed by a brief discussion, in the context of the specific meteorological conditions over the CONUS at the time of monitoring. This section also presents examples of lightning flashes processed with the tools described earlier in the thesis.

6.1.1   Monitoring the Transition of the Ionosphere

Recall that the cutoff frequency for the first mode can be used to estimate the height of a waveguide (in this case, the ionosphere) [Section 3.1.1] using the following equation given by waveguide theory:

$$h = \frac{\lambda}{2} = \frac{c}{2f_c}$$

---

[8] Civil twilight is defined as the time when the center of the Sun is geometrically 6 degrees below the horizon.

where,

h is the height of the waveguide (ionosphere)

c is the speed of light

f_c is the cutoff frequency of the waveguide

λ is the wavelength

The ionosphere varies from a height of 60 Km in the day to 90 Km at night [Smith et al, 2004]. Figure 6-1 plots the cutoff frequency against the height of the ionosphere.

6.1.1.1 Initial Approach

The initial approach in monitoring the EI waveguide was as follows: Sferic-related high-bandwidth data (10 KHz) were collected for about 4 hours for each of two days of August 21 and September 15. The start-time of data collection was two hours before sunset and the stop-time, two hours after. The collected data were then analyzed using Sferic Processing System [Section 5.1.1] to obtain cutoff frequency estimates. Finally, the ionosphere height was obtained from the cutoff frequencies using the formula given above.
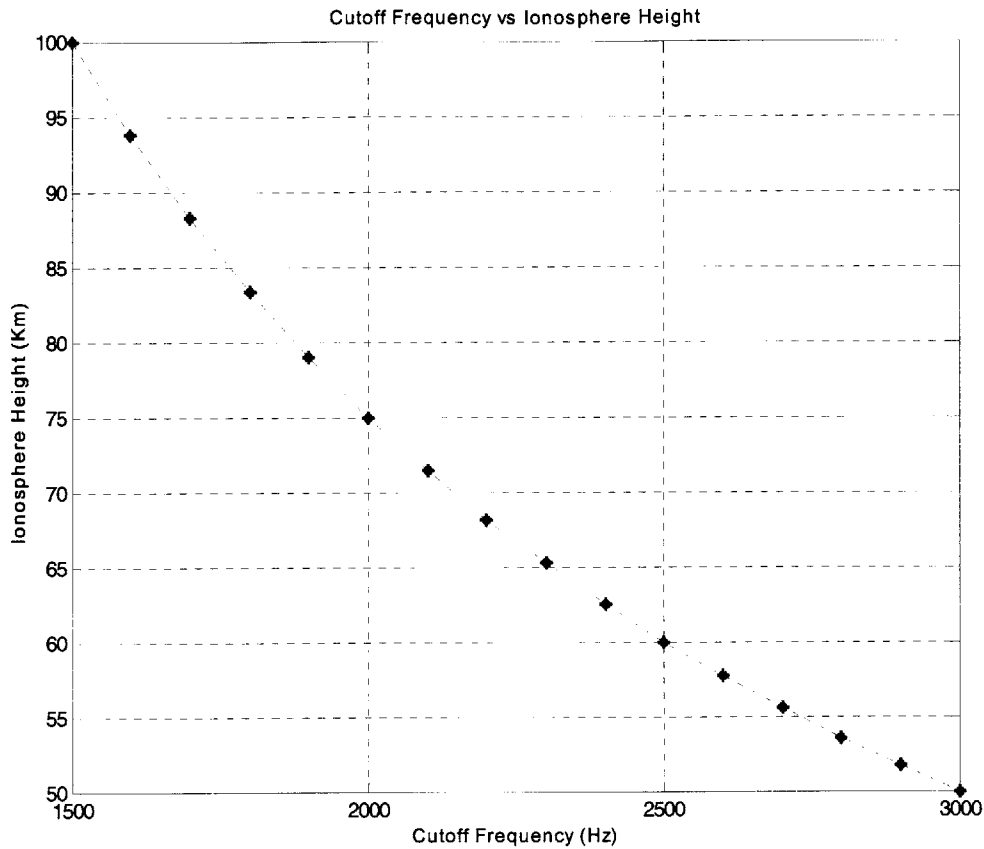
Cutoff Frequency vs Ionosphere Height

Figure 6-1: Ionosphere height as a measure of the cutoff frequency

Observations

For the data collected on August 21, 2003, Figure 6-2 plots the variation in the estimated ionosphere height against time (in minutes relative to the local sunset at Rhode Island at 2337 UT. Figure 6-3 is a plot of the lightning activity on the in the Continental United States (CONUS) for August 21 between 2200 UT and 0200 UT. Ionosphere height estimates through the dusk terminator for September 15, 2003 (local sunset at 2256 UT), are plotted in Figure 6-4. Figure 6-5 is a plot of lightning activity for September 15 similar to Figure 6-3. All lightning data used in the analyses of this thesis have been obtained from NLDN.

In general, both sets of observations show that the daytime height is low and the nighttime height is high in accordance with independent observations [Smith et al, 2004]. The two days do differ, however, in the manner in which the transition occurs.

52

For August 21, It is clear from Figure 6-2 that complete stabilization in the ionosphere height is not evidenced even as late as 60 minutes after local sunset at RI; however, a cluster of observations in the figure do show signs of ionosphere height stabilization about 40 minutes after sunset (t = 0 on Figure 6-2). A second important observation was made regarding lightning activity for the above time period: It shows clearly that while the ionosphere was being monitored for the day (2200UT to 0200 UT), lightning activity, as opposed to being clustered in a particular location, was scattered throughout the CONUS.

On the other hand, for September 15, stabilization in the ionosphere height is clearly evidenced 35 minutes after sunset on the ground on RI [Figure 6-4]. Additionally, the map of lightning activity on the CONUS for this day [Figure 6-5] clearly shows concentrated areas of lightning activity on the CONUS. Contrast this map with the map of August 21 [Figure 6-3] in which lightning activity is clearly scattered. Another point to note from Figure 6-5 is that a good percentage of the lightning on September 15, for the period of monitoring, was concentrated in a storm near Rhode Island and to the south.

Discussion

The first pass approach raises an interesting question: It is unlikely that the ionosphere would exhibit such radically different behavior while transitioning from one day to another. Then, what is it that causes the discrepancy in the observed behavior of the way the ionosphere transitions from day to night?

The answer to that question lies in the fundamentals of waveguide theory. Sferic radiation does not sample the ionosphere directly over the receiver; rather, they sample the source-receiver path, a discussion of which is covered in detail in Section 6.2. On August 21, the map of lightning activity over the CONUS [Figure 6-2] clearly shows a lack of concentrated thunderstorm activity; the lightning activity is scattered all over the CONUS. Hence, observations of the scattered sferics naturally provide information about scattered source-receiver paths and not any particular ionosphere path, let alone the ionosphere at the receiver. (Different lightning events from different locations sample a different source-receiver path.) Some of the paths are in the night, some in the day. That a

53

stabilization of the ionosphere height was not observed is therefore hardly a surprising result.

As luck would have it, the meteorological conditions of September 15 were different than those present on August 8. There were three major clusters of thunderstorms [Figure 6-5]; and, each was localized, the largest source being very close (< 300 Km) to the receiver at Rhode Island. Even more conveniently, an active sferic source was also present in the Atlantic to the east of Rhode Island, in the form of Hurricane Isabel.

The unusual weather conditions of September 15 (unusual because lightning tends to be prevalent on the CONUS landmass as compared to the Atlantic Ocean) thus provided a different sample of the ionosphere than the one on August 21. The ionosphere was being sampled by events that were either close by, or from the south; the sun set over the path at approximately the same time as the receiver implying that the sun set over the entire source-receiver path at approximately the same time, further implying that the source-receiver path was likely uniform through the transition. It is therefore, also likely that the conditions were ideal to gaining as close a measure of the actual time it takes for the ionosphere to stabilize. Contrast this with the case of August 21, where the sources were located as much as 3 hours away from sunset. On August 21, with the sun ionizing many of the source-receiver paths which may have been as much as two or three hours distant from the receiver at Rhode Island, it seems natural in hindsight that evidence of the ionosphere stabilizing to its nighttime height would be obtained later on August 21 than on September 15.

The above observations lead naturally, to taking a more refined approach to monitoring the ionosphere through the day-night boundary; to study the ionosphere in conditions in which the source-receiver distances and paths are exactly identified. This refined analysis is the subject of the next section and will clarify the reasons for the different behaviors shown in Figures 6-1 and 6-3.
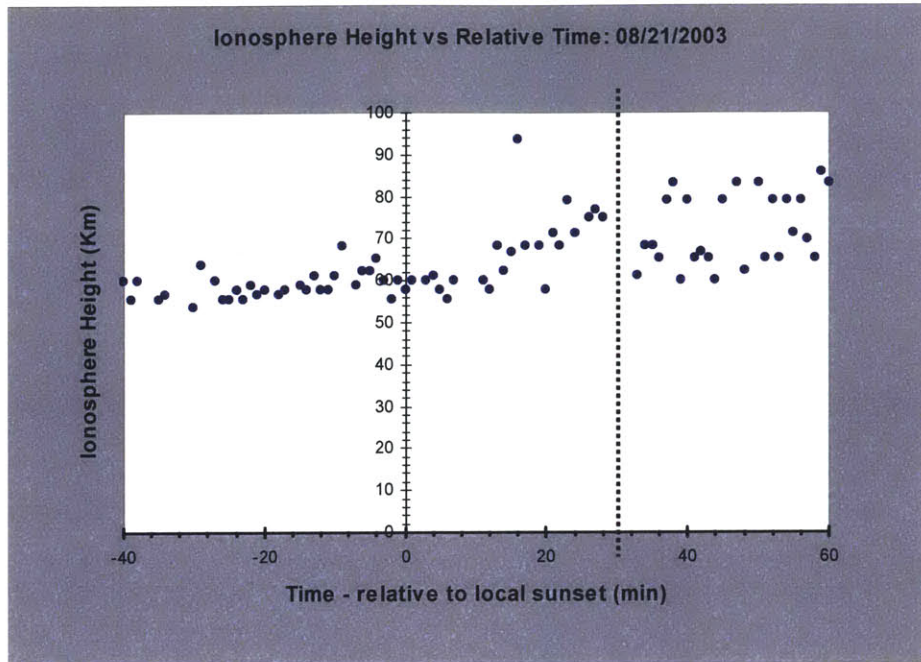
Figure 6-2: Monitoring Ionosphere Height through the day-to-night boundary
Sunset on the ground: 2337UT (t = 0)
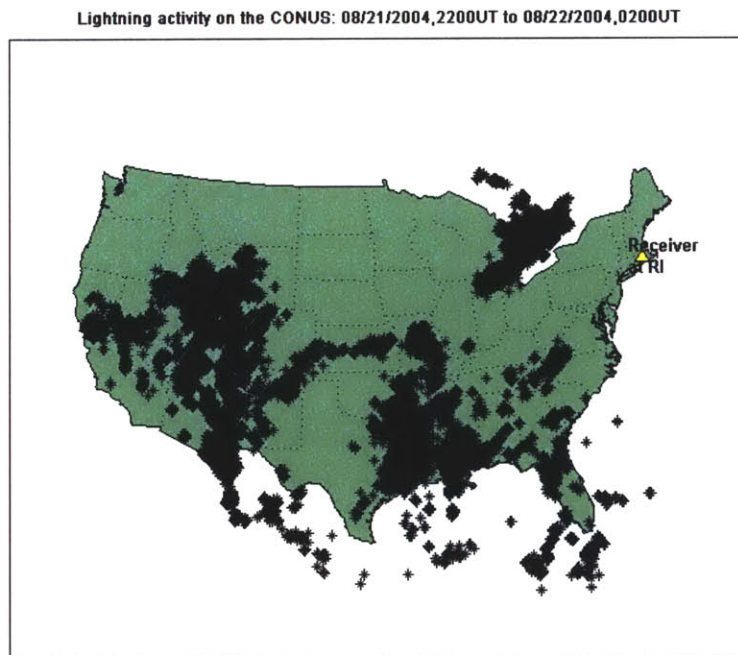**End of civil twilight: 0007UT (t=30) - dotted line**

Figure 6-3: Lightning Activity scattered throughout the CONUS
Sunset (ground) over RI: 2337UT
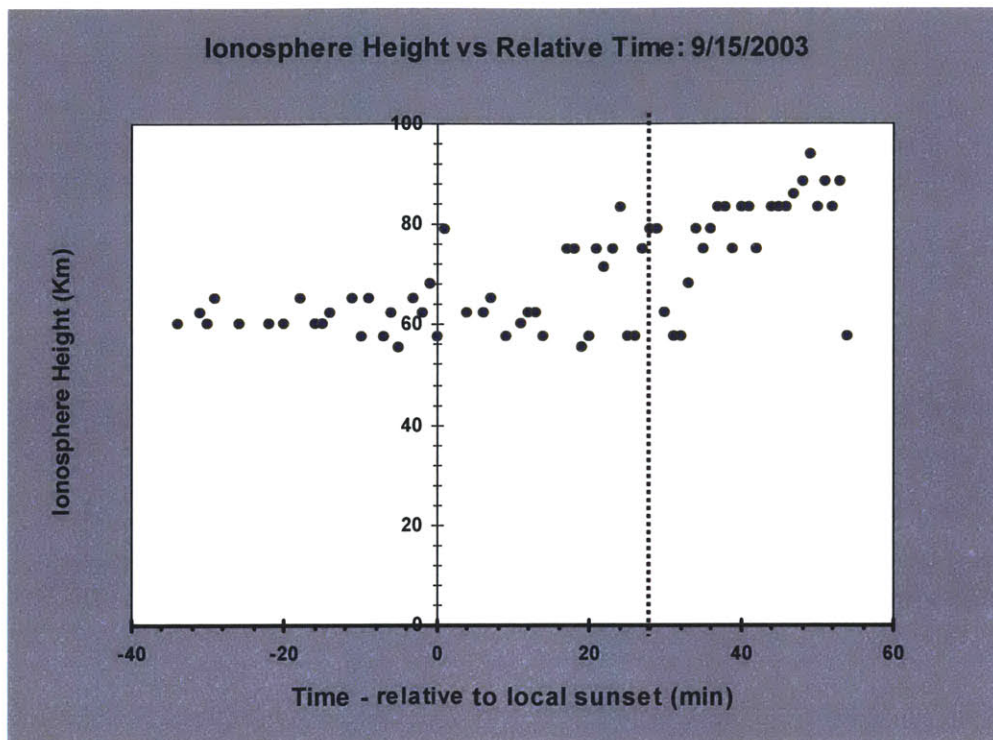**End civil twilight over RI: 0007UT**

Figure 6-4: Monitoring Ionosphere Height through the day-to-night boundary
Sunset on the ground: 2256UT (t = 0)
End of civil twilight: 2324UT (t=28) – dotted line on the plot
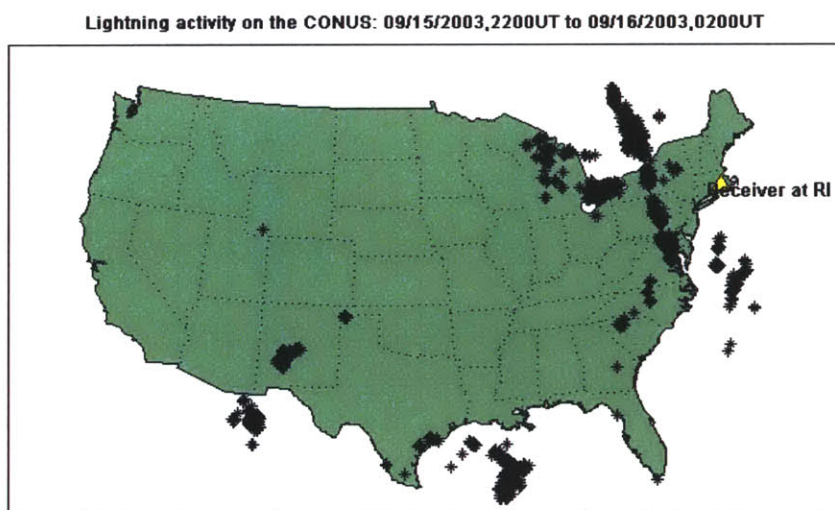

Figure 6-5: Lightning activity on the CONUS clustered through the
day-to-night boundary approx. < 500 Km from the receiver at RI
Sunset (ground) over RI: 2256UT
End civil twilight over RI: 2324UT

6.1.1.2 Refined Approach

Building on the observations of the initial approach, the refined approach emphasizes monitoring the change in ionospheric height for particular source-receiver pairs. The refined approach consists of obtaining ionosphere height estimates for a particular location – hence, a "particular" source-receiver path. Recall, accurate time-stamping of lightning events [Section 2.3], allows us to obtain lightning location information by comparing the Rhode Island times of capture with that provided by NLDN. The main criteria for the validity of this approach is that lightning activity be clustered in a particular region making the source-receiver path essentially constant.

Such a condition was in fact achieved on May 12, 2004. Figure 6-6 plots the thunderstorm activity over the CONUS for May 12. From the figure, it is clear that there were three large clusters of storms active on the CONUS. The refined analysis was therefore carried out for data collected on this date, since the meteorological conditions were ideal for sampling three ranges of source-receiver paths at once. We were assured that the paths would be sampled frequently, thereby allowing a virtually continuous monitoring of the transitioning ionosphere.

The analysis for this date is organized around source-receiver distance. Distances are defined as short-range (<300 Km), mid-range (300 Km to 1000 Km) and long-range (> 1000 Km). The three major clusters of thunderstorm activity over the CONUS align with the above definitions for distances. The table below is a legend for 6 points labeled (1) thru (6) on Figure 6-6; it is provided to give a sense of distance in relation to the co-ordinates of a location as well as a sense of the distance of the main clusters of thunderstorm activity from the source.

Legend	Latitude	Longitude	Ground Sunset (UT)	Distance (Km)
(1)	41.0N	-74.7E	5/13/2004 0:06	280
(2)	39.5N	-81.4E	5/14/2004 0:30	885
(3)	50.4N	-86.8E	5/15/2004 1:24	1506
(4)	41.3N	-90.5E	5/16/2004 1:13	1580
(5)	30.2N	-92.7E	5/17/2004 0:57	2300
(6)	38.9N	-103.3E	5/18/2004 1:56	2700

The procedure used was as follows: The ionosphere height was calculated for many events through the day-night boundary using largely the approach outlined initially

[Section 6.1.1.1], but with one difference. Cutoffs of only those events whose locations were unambiguously known were used in the final analysis. Contrast this with the initial approach [Section 6.1.1.1] where the location of events was immaterial. The events were then segmented based on the distance from the source and the ionosphere heights plotted.

Observations

Figure 6-7 is a plot of ionosphere height against relative time from sunset for events that are less than 300 Km from the receiver at Rhode Island; figure 6-8 is a plot for ionosphere height estimates for events that are 300 Km to 1000 Km distant; and figure 6-9 plots ionosphere height estimates for events greater than 1000 Km away.

It is evident from Figure 6-7, that lightning events that occurred less than 300 Km show an ionosphere that begins to stabilize in approximately 40 minutes after the sunset on the ground; for thunderstorm activity greater than 300 Km but less than 1000 Km away, the ionosphere takes slightly longer to show signs of stabilizing; however, for lightning events that occur greater than 1000 Km, the ionosphere shows, at best, only faint signs of moving towards a nighttime height even 60 minutes after sunset on the ground at Rhode Island (2356UT).

Discussion

The observations from the more refined approach ratify the observations made earlier. The actual location of lightning events is an important aspect to consider while monitoring a transitioning ionosphere. It is important to note here that the result is limited by the time it takes for the sun to set over the ionosphere of the source-receiver path.

An important hypothesis that this thesis would like to propose, made as a result of the above observations, is that it is likely that the meteorological condition best suited to monitoring the local ionosphere height is a source-receiver path that lies along and coincident to the "strike" (the day-to-night boundary), and is within 300 Km of the receiver.

The first part of the hypothesis, that the source lie on the strike, is guided by waveguide theory considerations and observations regarding sferic propagation in the

earth ionosphere waveguide discussed in detail in the following section [Section 6.1.2]. If the source-receiver ionosphere is uniform and changes uniformly, which the above condition practically guarantees, the ionosphere that will be sampled will be one in which the effects of the setting sun will be uniform over the S-R path making it ideal for study. The second part of the hypothesis, that the source be close, is again motivated partly by observations regarding sferic propagation. The observations are also motivated by the empirical evidence of September 15 as discussed in Section 6.1.1.1 with reference to the source cluster in the Atlantic caused by Hurricane Isabel.

Lightning activity on the CONUS: 05/12/2004,2200UT to 05/13/2004,0200UT
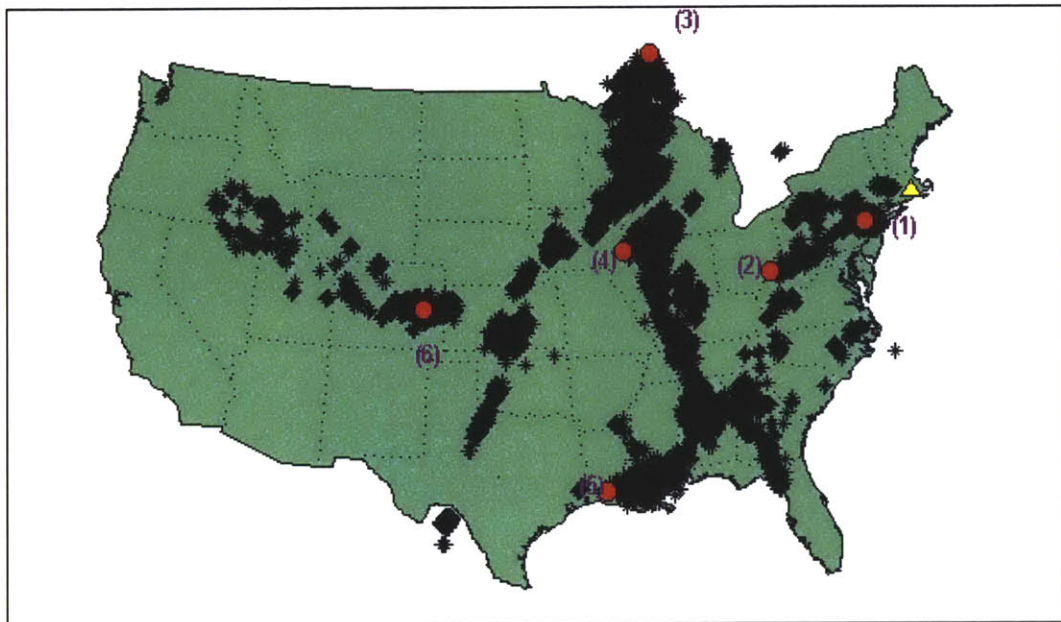
**Figure 6-6: Lightning Activity on the CONUS
located in three main clusters.
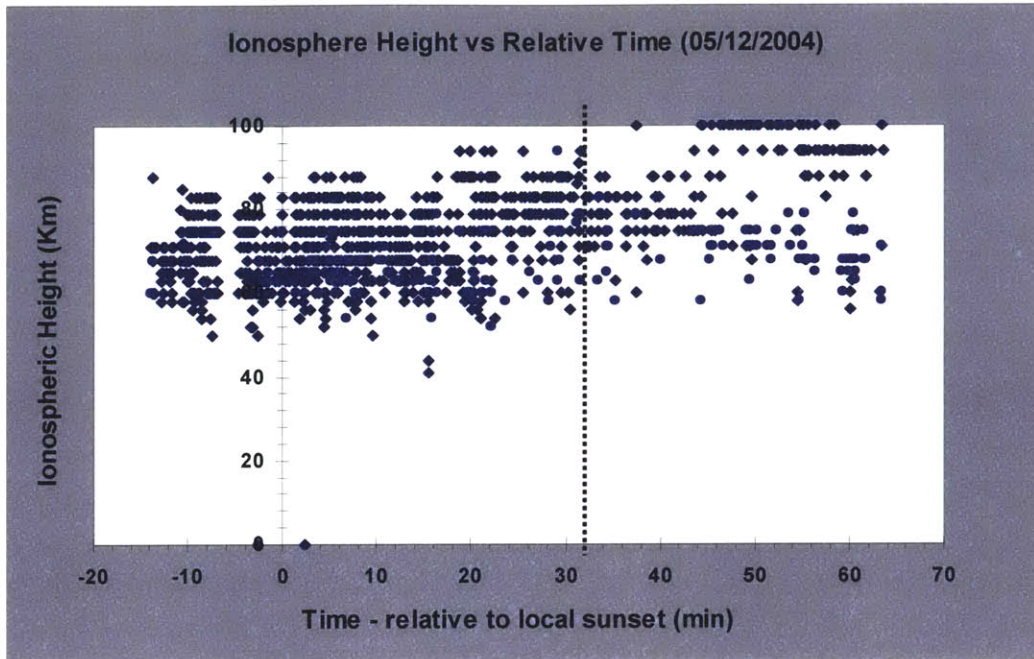Sunset (ground) over RI: 2356UT
End civil twilight over RI: 0028UT**

Figure 6-7: Monitoring ionosphere height through the day-to-night boundary (all events)
Individual data points based on the analysis of individual lightning flashes
Sunset on the ground: 2356UT (t = 0); End of civil twilight: 0028UT (t=32) – dotted line
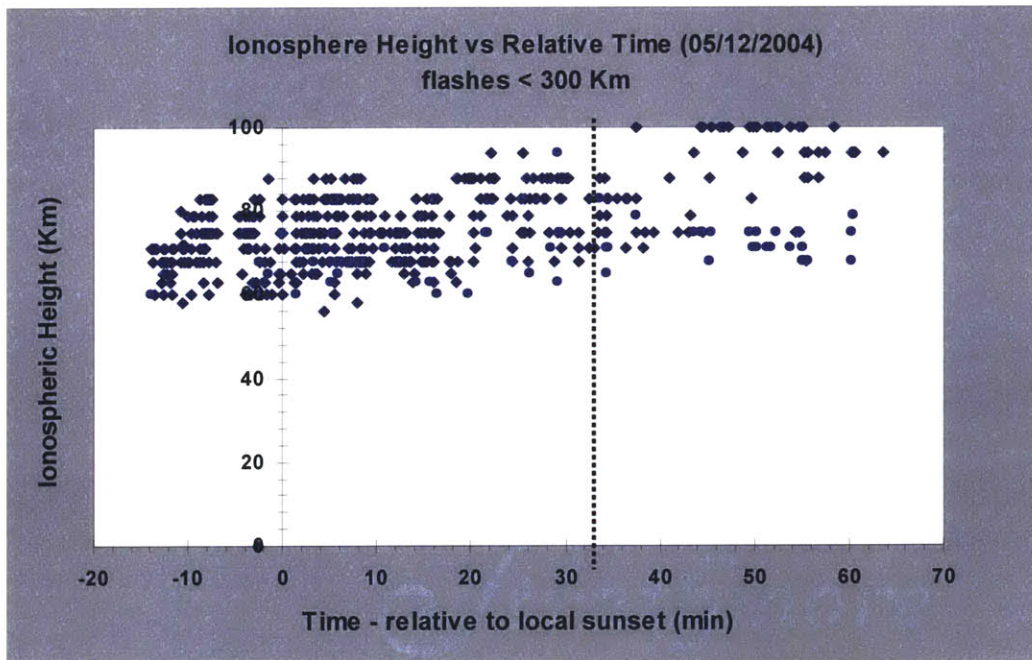

Figure 6-8: Monitoring Ionosphere Height through the day-to-night boundary
Only lightning flashes that occurred < 300 Km from the receiver at RI are plotted.
Individual data points based on the analysis of individual lightning flashes
Sunset on the ground: 2356UT (t = 0)
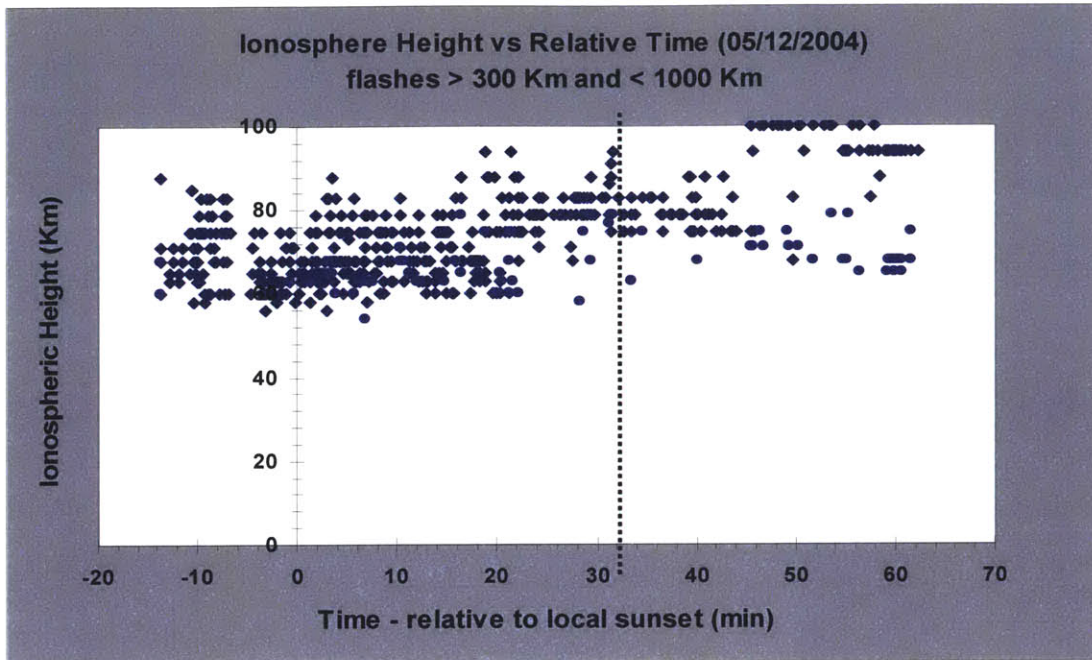**End of civil twilight: 0028UT (t=32) – dotted line**

Figure 6-9: Monitoring Ionosphere Height through the day-to-night boundary
Only lightning flashes that occurred < 300 Km and > 1000 Km from the receiver are plotted.
Sunset on the ground: 2356UT (t = 0)
End of civil twilight: 0028UT (t=32) – dotted line on the plot
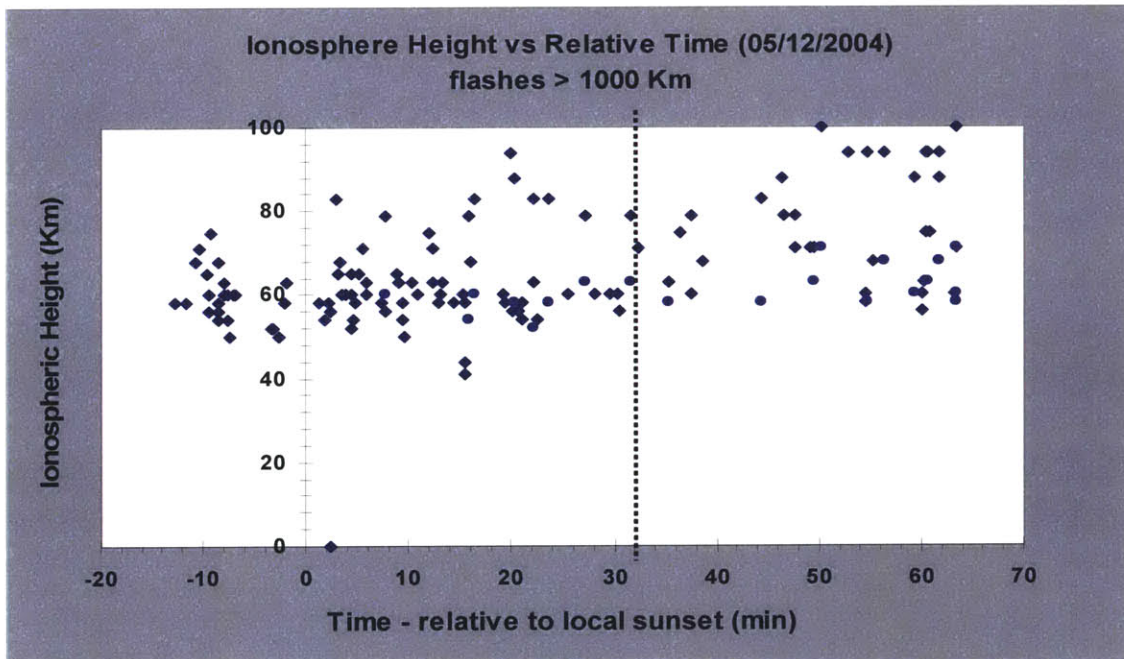

Figure 6-10: Monitoring Ionosphere Height through the day-to-night boundary
Only lightning flashes that occurred >1000 Km from the receiver at RI are plotted.
Sunset on the ground: 2356UT (t = 0)
End of civil twilight: 0028UT (t=32) – dotted line on the plot

6.1.2   Sferic Propagation in the Context of the Transitioning Ionosphere

The analysis of monitoring the ionosphere height as discussed in Section 6.1.1 led to interesting observations regarding the frequency domain behavior of sferics. By its very nature, this study provides a special opportunity to qualitatively compare and contrast sferic propagation through the earth-ionosphere waveguide. The observed effects on sferics traveling through the EI waveguide can be studied in the context of three main variables: (1) Source-receiver path, (2) Amplitude or peak current of the lightning event and (3) Distance of the event from the source. In keeping with the emphasis of this thesis, this section will study sferics in the context of the source-receiver path. However, wherever possible, an effort will be made to relate the observed phenomena to the amplitude of the event and the distance of the event from the receiver.

Based on the source-receiver path of a sferic, observations can be divided into three distinct categories. The first is sferic propagation at **night** (where, by **night,** it is implied that the source-to-receiver path lies entirely in the nighttime ionosphere); sferic propagation during the day (the source-receiver ionosphere is entirely in the daylight); and, sferic propagation during the transition (a part of the source-receiver ionosphere is in daytime and a part is in the nighttime) or propagation in a mixed path.

6.1.2.1 Sferic Propagation on the Night Side

Sferics propagation in the VLF regime is best understood the nighttime ionosphere. This is largely due to the fact that the nighttime ionosphere is at least an order of magnitude less lossy than the ionosphere of the day. Thus, the VLF radiation attenuates an order of magnitude less; and the observations are more faithful to the underlying waveguide model. Night, as mentioned earlier, is defined as the time when the sun has set over at least a large part of the source-receiver path. Note that it is important to distinguish between sunset on the ground and sunset over the ionosphere. This distinction is discussed in detail earlier in this chapter [Section 6.1.1].

The observed waveforms display a fairly consistent low waveguide cutoff frequency ranging from 1500 Hz to 1800 Hz corresponding to an ionosphere height of 100 Km to 83 Km respectively [Figure 6-1]. The frequency-time spectrograms (or Short Time Fourier Transforms, STFT) clearly display dispersion which asymptotes towards

the waveguide cutoff frequency [Figure 6-11] corresponding to well-defined "tweek-train" waveform almost 25 msec long, in the time domain [Figure 6-11].

Multi-modal (3 or more modes) phenomena: An Associated Phenomena

An interesting aspect of nighttime sferics is the presence of higher order modes in some of their STFTs. Recall that the modes of an ideal waveguide, with sharply defined walls, occur at frequencies which are integer multiples of the cutoff frequency [Section 3.1.1]. The indistinct ionosphere boundary of the earth-ionosphere waveguide causes some departure from this simplified model in the sense that modes do not occur exactly at integer multiples of the fundamental cutoff frequency, but are close to them. STFTs of some tweeks [Figures 6-14 thru 6-17] clearly show the presence of three to five [Figure 6-14] modes. Multi-mode sferics are comparatively rare, and have been observed primarily for large-amplitude sferics that propagate to the receiver over a stabilized nighttime ionosphere. Nicholaenko and Hayakawa (2002) have also shown multi-modal spectra in the STFT format in nighttime conditions.

Figure	Description	T_s	T_t	T_{tr}	Distance (Km)	Current (KA)	Cutoff (Hz)
6-11 (&6-12)	Distant event with a single asymptote	40	14	91	1585	-34	1700
6-13 (&6-14)	Time domain shows a long tweek-train; STFT shows 3 modes	Unknown					2200
6-15	STFT of sferic with 4 modes	Unknown (not found in NLDN data)					1600/2100
6-16	STFT of sferic with 5 modes	102	70	82	300	-14.3	1600
6-17	STFT of sferic with 3 modes	62	25	131	1550	-32.7	1700

T_s (min): Time of occurrence of lightning event relative to sunset on the ground at the source

T_t (min): Time of occurrence of lightning event relative to end of civil twilight at the source

T_{tr} (min): Time of occurrence of lightning event relative to end of civil twilight at the receiver

Discussion

A large body of the literature [Hayakawa et al, 1994; Nicholaenko and Hayakawa, 2002; Shvets, 2004] deals with atmospherics that propagate through the nighttime ionosphere. That is understandable since the low-attenuation property of the nighttime ionosphere preserves the details of lightning events for large distance.

The only significant observation regarding the nighttime sferic that this thesis seeks to discuss is what conditions lead to the observance of multiple modes in nighttime sferics. Empirically, multi-modal phenomenon seems to occur only when the entire source-receiver ionosphere has stabilized to a nighttime height. Additionally, it seems that an optimum combination of peak-current (amplitude) and distance leads to observations of multi-modal structure. For example, Figure 6-16 shows the STFT of an event 300 Km away with 5 modes but a low peak current (-14.3 kA); Figure 6-17 shows multiple modes for a distant event with a larger NLDN peak current (-32.7 kA). Contrast the two figures: a close event with a low peak current shows more modes than a distant event with a higher peak current.

This is likely due to that fact that a close event with a high peak current tends to saturate the receiver; on the other hand, low-amplitude, distant events tend to display an asymptote towards the fundamental mode only, as the higher frequencies get attenuated with distance.

6.1.2.2 Sferic Propagation on the Day Side

The daytime ionosphere is extremely lossy causing high attenuation in the cutoff frequency regime; its properties are more difficult to study.

Sferics observed during the daytime seem to display a wide range of cutoff frequencies, from 1700 Hz to 3400 Hz, which if true, correspond to ionosphere height estimates ranging from 88Km to 44 Km, the latter is too low to be correct. Sferics demonstrating cutoff frequencies of 2200 Hz and 3200 Hz in their frequency spectra are shown in Figures 6-18 and 6-19 respectively. Surprisingly, daytime sferics are observed to occasionally exhibit dispersive behavior [Figure 6-20].
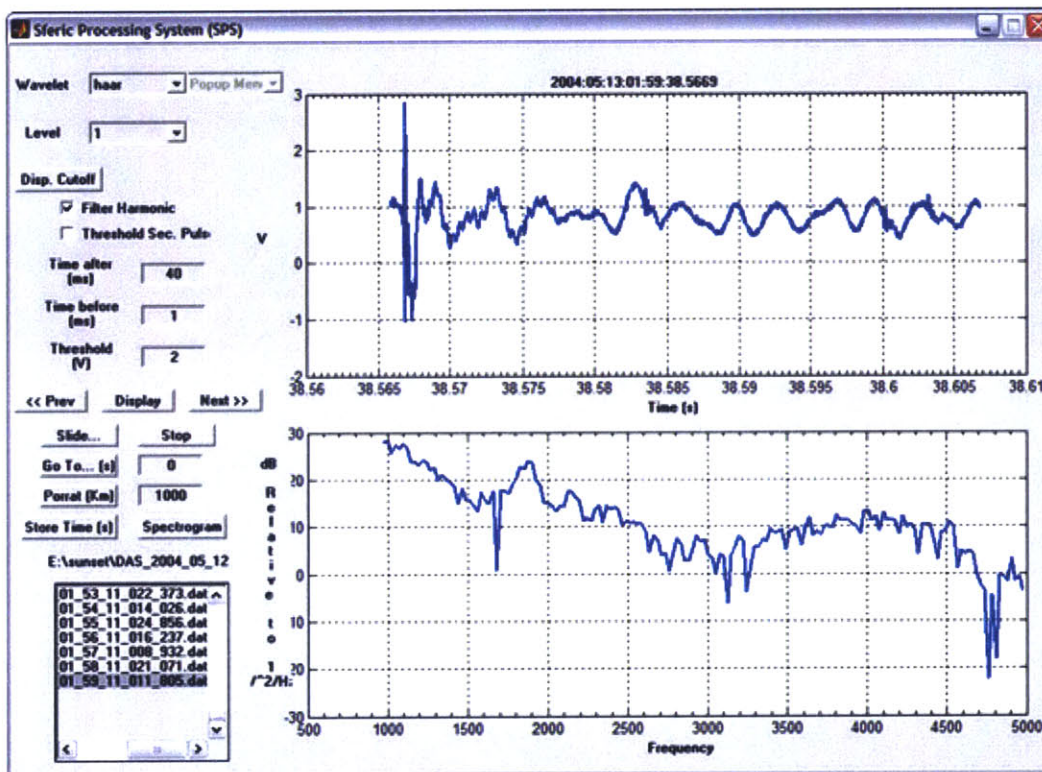
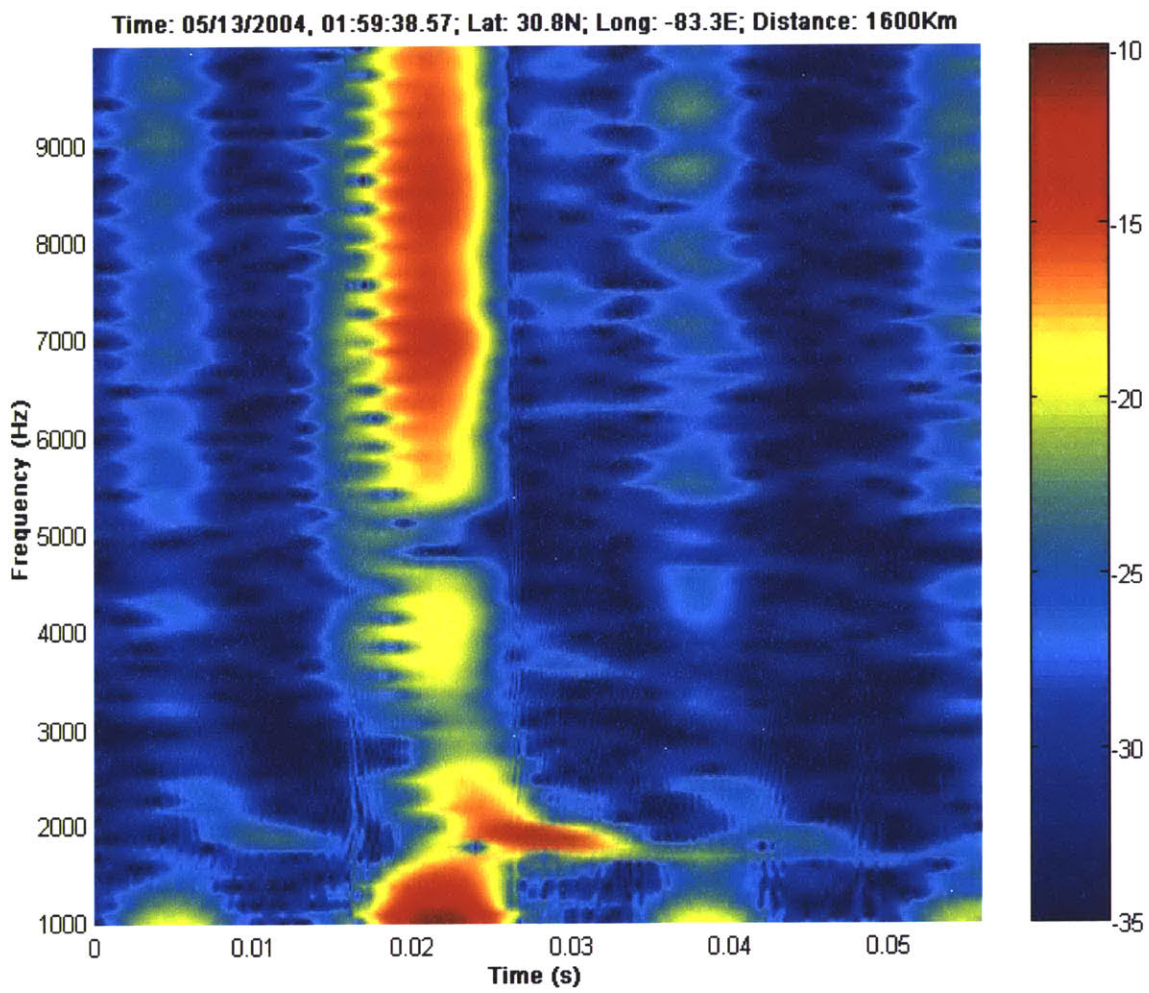**Figure 6-11: A sferic producing a tweek-train 25ms long.**

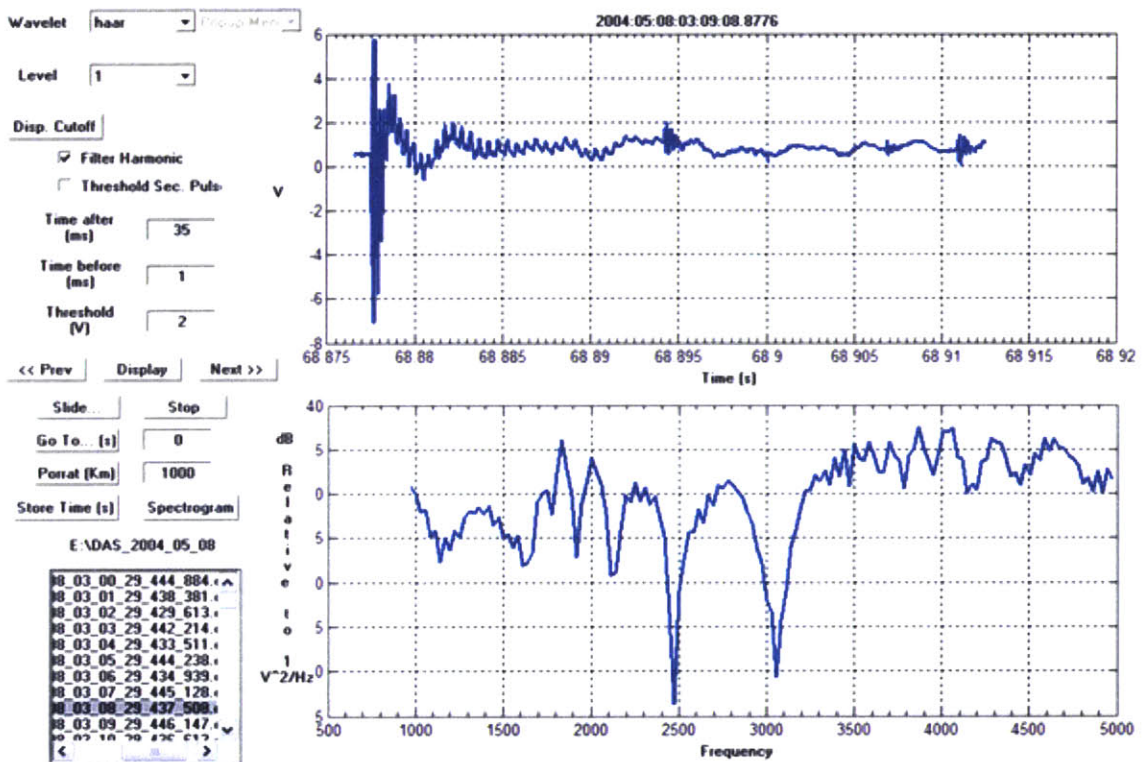**Figure 6-12: STFT the sferic in Figure 6-10 (with a 30 ms tweek train dispersion)**
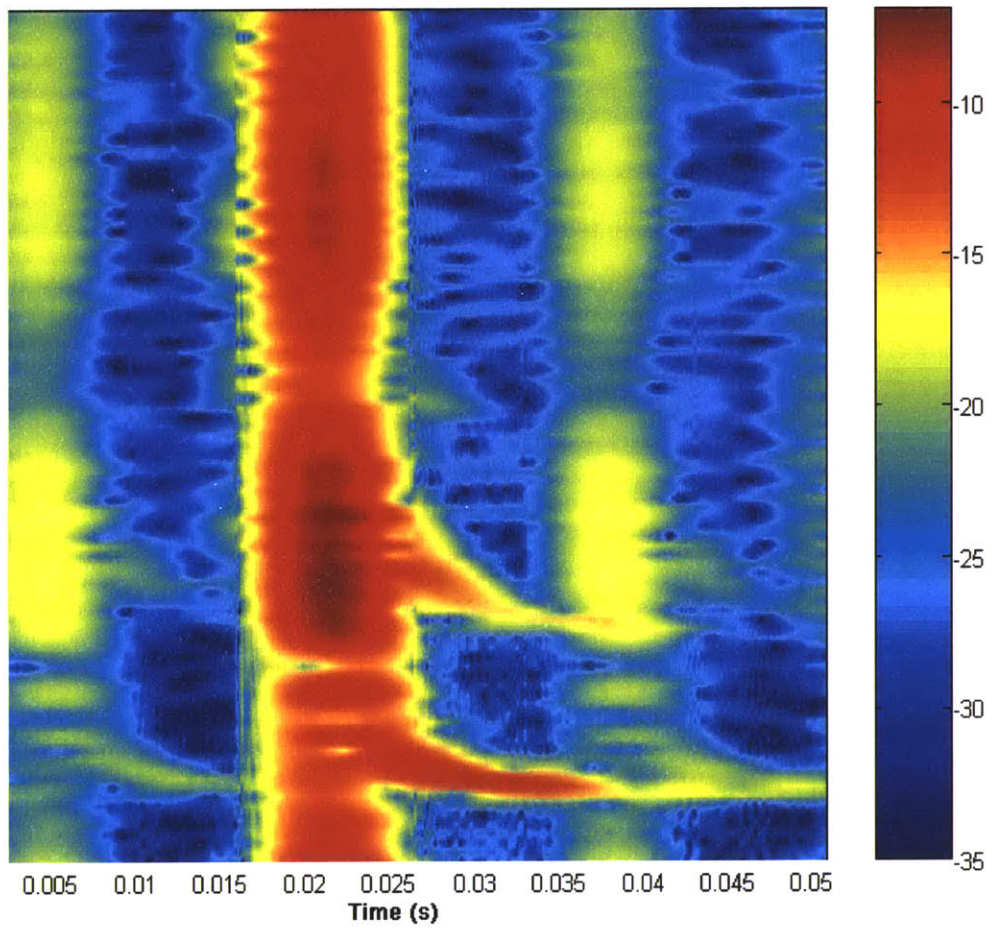
Figure 6-13: A sferic producing a long 30ms tweek-train

Figure 6-14: STFT of a sferic producing a long 30ms tweek.
Note the presence of 3-modes at multiples of 1700 Hz.

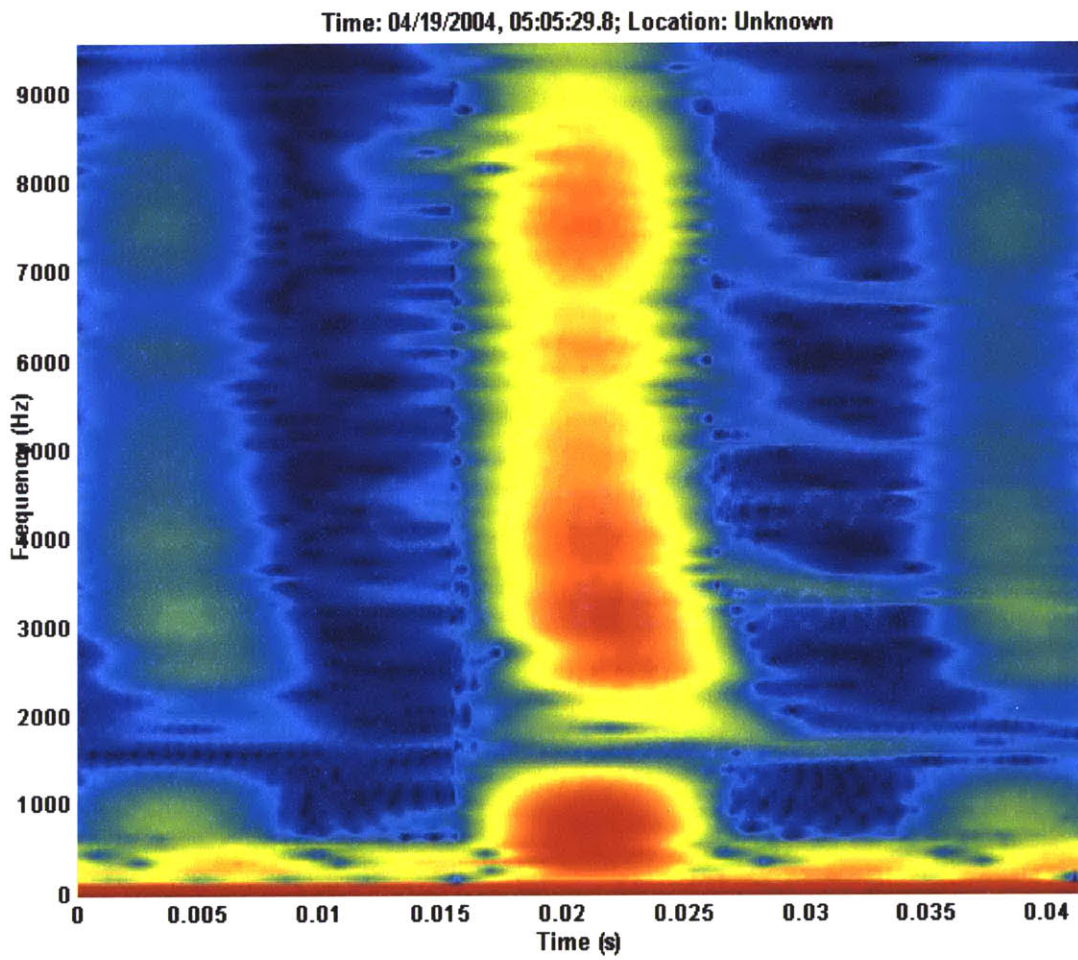**Time: 04/19/2004, 05:05:29.8; Location: Unknown**

Figure 6-15: STFT of a sferic showing 4 distinct modes at multiples of 1700 Hz.
Time: 04/19/2004, 05:05:29; Location: Unknown

70

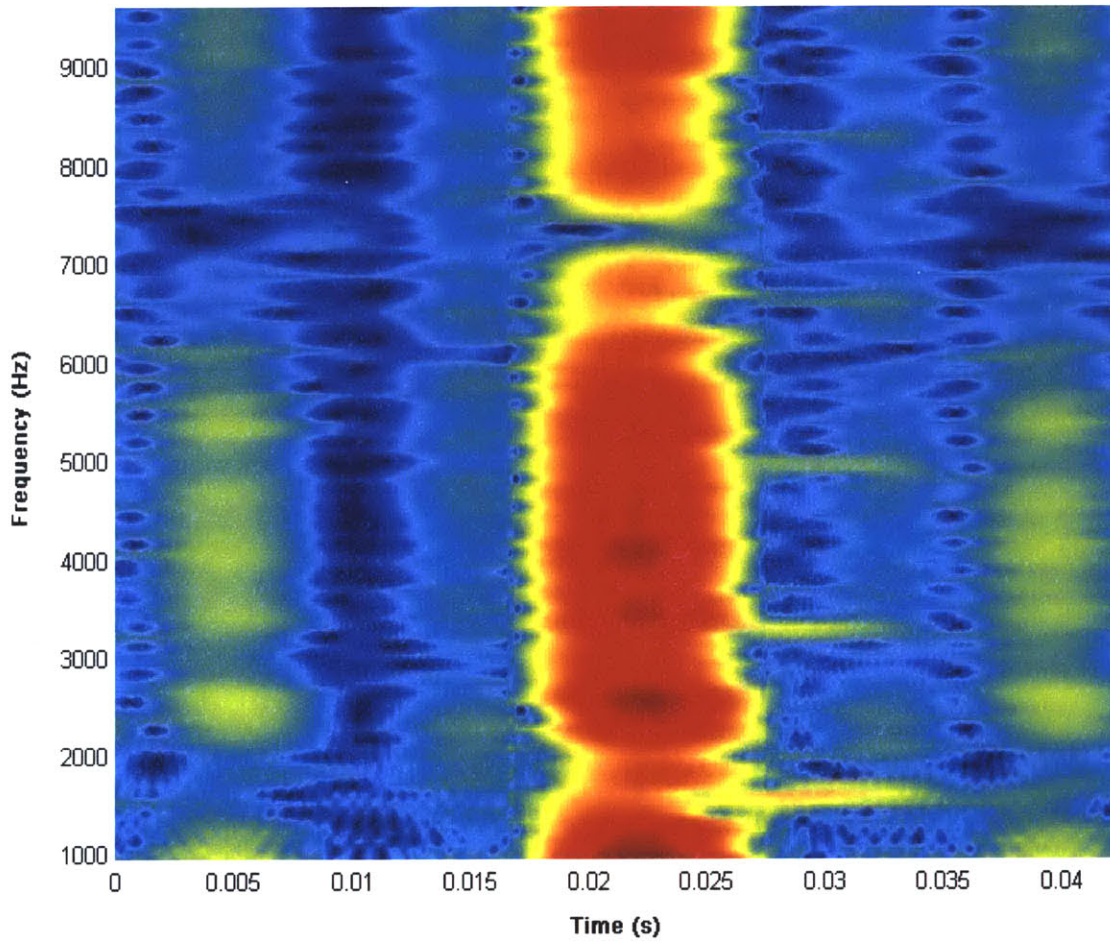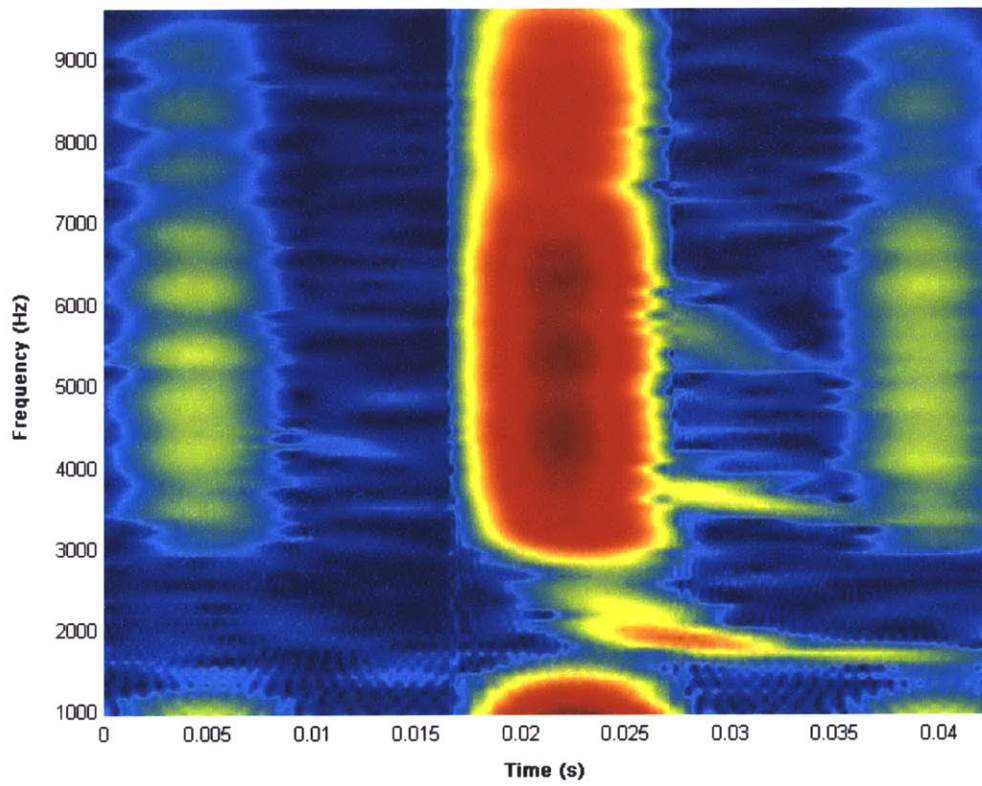Time: 05/13/2004, 01:50:49.0; Lat: 40.8N; Long: -75.2E; Distance: 298.6 Km

Figure 6-16: STFT of sferic showing 5 (4 clearly distinct) modes at multiples of 1700 Hz.

Figure 6-17: STFT of sferic showing 3 modes at multiples of 1700 Hz;
NLDN peak current: -32.7 kA; Distance: 1550 Km

Figure	Description	T_s	T_t	T_{tr}	Distance (Km)	Current (kA)	Cutoff(s) (Hz)
6-18	Clear daytime cutoff frequency	-12	-44	-20	300	-11.8	2200
6-19	Unsupportably high cutoff frequency	-125	-160	-79	1400	-129.6	3100
6-20	Slight dispersion visible in the daytime	-40	-70	-46	650	-18.5	2300

T_s(min): Time of occurrence of lightning event relative to sunset on the ground at the source

T_t (min): Time of occurrence of lightning event relative to end of civil twilight at the source

T_{tr} (min): Time of occurrence of lightning event relative to end of civil twilight at the receiver

Discussion

The daytime ionosphere has a high attenuation. Therefore, reasonable cutoffs in the daytime can only be obtained from nearby sferics, the nearness requirement being conditioned on the peak current of the lightning event. Distant events in the daytime, because of the high attenuation during the daytime, lack information about the ionosphere height as evidenced in figure 6-19.

Figure 6-20 displays the STFT of a sferic showing slight dispersion, occasionally visible in the daytime path. The exact conditions that lead to daytime dispersion are not known; however, we know that a tweek is composed of waves propagating at different angles to the boundary of the waveguide; and, that the best reflection is observed for waves propagating under sliding angles (from personal communication with Alexander Shvets). On the other hand, the highly attenuating daytime ionosphere works against the production since events that are observed after sliding angle reflections tend to be far away. Therefore, the hypothesis is that there is some optimality criterion for which slight evidence of dispersion may be observed in sferics, even in the daytime.

6.1.2.3 Sferic Propagation through a Mixed (Day-Night) Path

A large part of this thesis concerns itself with monitoring the ionosphere through the day-night boundary. Lightning is prevalent in the evening terminator on both the day and

night sides. It therefore follows that the propagation of atmospherics through a mixed day-night path is an important focus of this thesis.

Sferic propagation through a mixed path is a multi-faceted phenomenon. The sferics behave like their daytime counterparts, exhibiting heavy attenuation as observed during the daytime. However, the mixed-path sferics show signature characteristics of both the daytime and the nighttime ionosphere.

The three most interesting observations of their frequency structure are presented in this thesis:

(1) Some sferics display dispersion towards an asymptote that does not coincide with a nighttime ionosphere cutoff frequency of 1600 Hz to 1700 Hz; neither does it coincide with a daytime height; rather, the dispersion tends to asymptotes towards a frequency of 2000 Hz to 2200 Hz, corresponding to an ionosphere height of about 70 Km to 75 Km [Figure 6-21 and 6-22]. Recall that any observed nighttime dispersion always tends to a frequency of 1700Hz in the STFT while daytime sferics display very little dispersion (and only when they are close).

(2) Secondly, certain sferics have spectrograms that show two clear asymptotes instead of one [Figure 6-23].

(3) Finally, some sferics have a clear dispersion in their STFT towards a frequency that corresponds to a nighttime ionosphere as illustrated in Figures 6-24 a and b.

A summary of the sferic observations of the transitioning ionosphere, referencing the figures mentioned above, is tabulated below:

Figure	Description	T_s	T_t	T_{tr}	Distance (Km)	Current (kA)	Cutoff (Hz)
6-21	High frequency dispersion (Dispersion towards 2 asymptotes)	20	-13	75	1630	-94	2200 (2000)
6-22	High frequency dispersion	3	-23	0	1500	-61.8	2200
6-23	Dispersion towards 2 asymptotes	26	-6	17	471	-13.4	1600/2100
6-24a	Dispersion towards nighttime transverse resonance	21	-9	40	2100	+39.8	1700
6-24b	Dispersion towards nighttime transverse resonance	21	-9	40	2100	-50.5	1700

T_s (min): Time of occurrence of lightning event relative to sunset on the ground at the source

T_t (min): Time of occurrence of lightning event relative to end of civil twilight at the source

T_{tr} (min): Time of occurrence of lightning event relative to end of civil twilight at the receiver

Discussion

All the events illustrated in the mixed-path regime in this study have their origins in the daytime ionosphere. (Daytime ionosphere is the ionosphere over which the sun has not set.) Recall from waveguide theory, that cutoff frequencies and ionospheric heights are inversely related [Section 3.1.1; Figure 6-1]. Also recall that the cutoff frequency is defined to be the frequency below which a wave cannot propagate in the waveguide in any other mode except the TEM mode; and that the lower the height of the waveguide, the higher the cutoff frequency. Based on waveguide theory, how then does one reconcile observations of dispersion towards frequencies not supported by a nighttime ionosphere?

Unlike the cases where the source receiver path is exclusively a daytime or a nighttime ionosphere with a single stable height [Sections 6.1.2.1 and 6.1.2.2], sferic observations in a mixed path ionosphere can be best explained in terms of a waveguide or a source-receiver path that has not one, but a range of heights from the source to the receiver corresponding to a range of cutoff frequencies. A simplified illustration of a sferic with a mixed path from source to receiver is shown in Figure 6-26. The true ionosphere obviously does not show a single step change in height; Smith et al (2004), however, show that it may well be a good approximation.
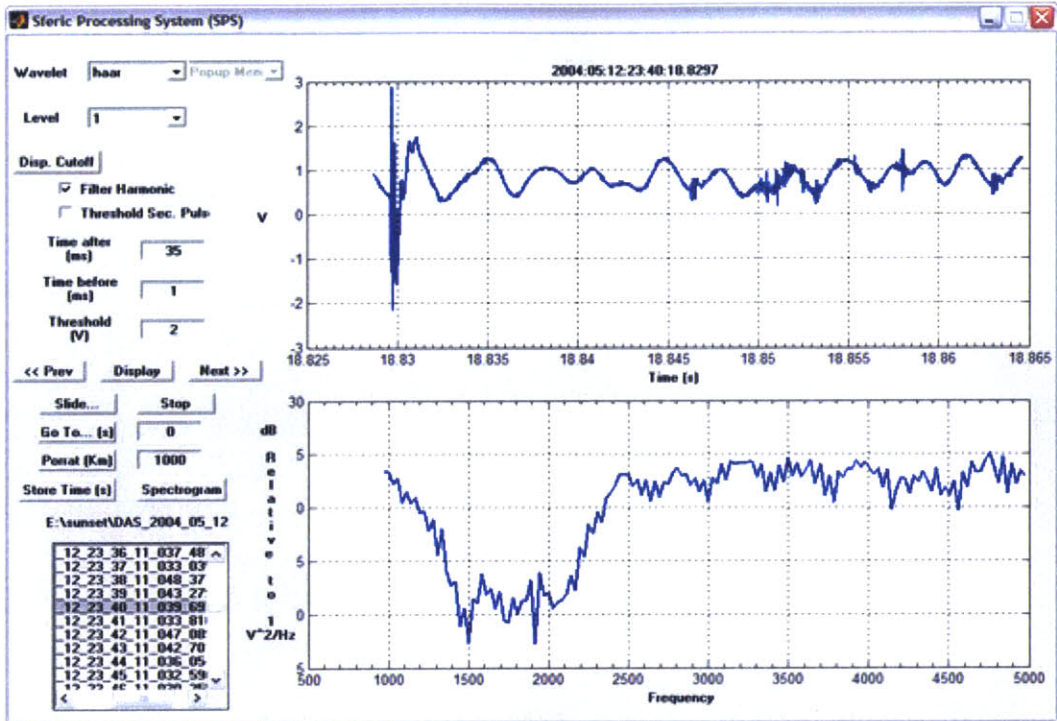
75

Figure 6-18: Daytime sferic showing a clear cutoff at 2200 Hz
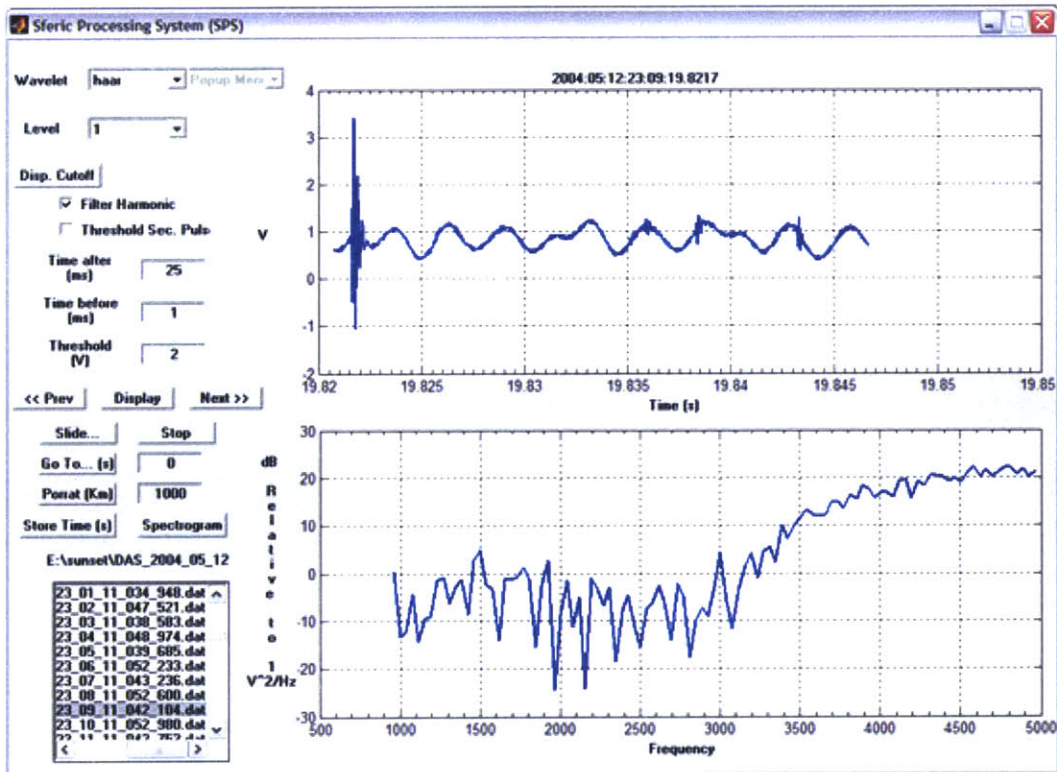**Time: 05/12/2004, 23:40:18 UT; Lat: 41.0N; Long: -75.2E Distance: 300Km**

Figure 6-19: Daytime sferic showing a "cutoff" at 3100 Hz
Time: 05/12/2004, 23:09:17.8UT; Lat: 45.9N; Long: -88.2E; Distance: 1400Km
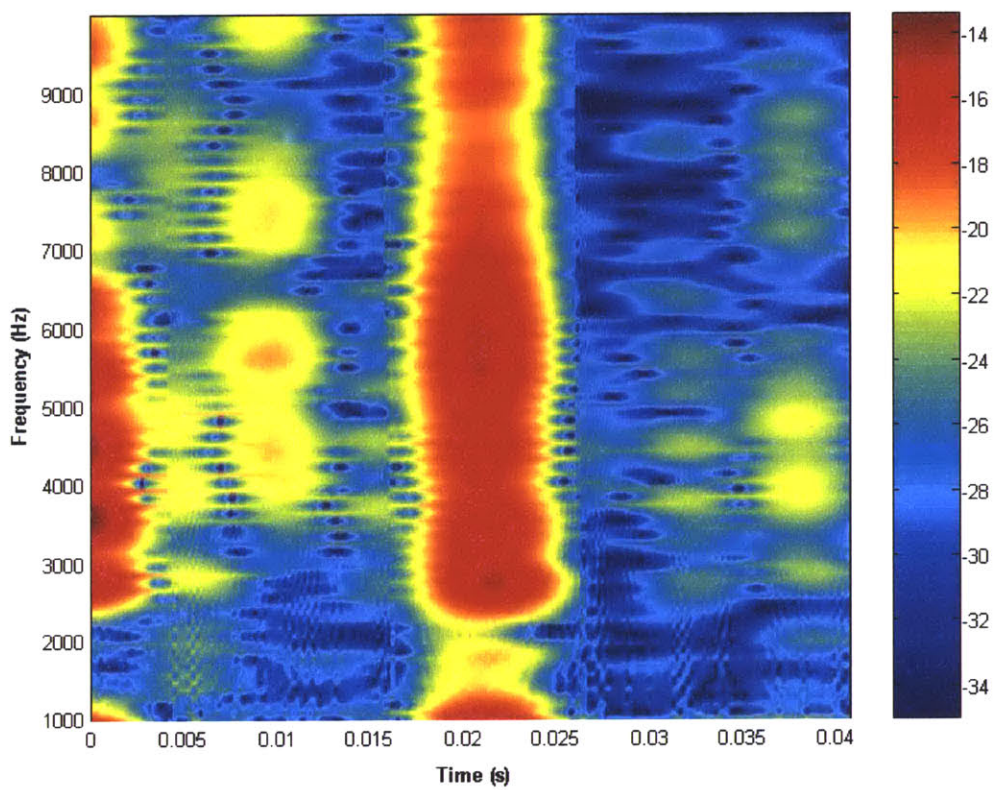
Figure 6-20: Daytime sferic showing faint dispersion at 2300 Hz
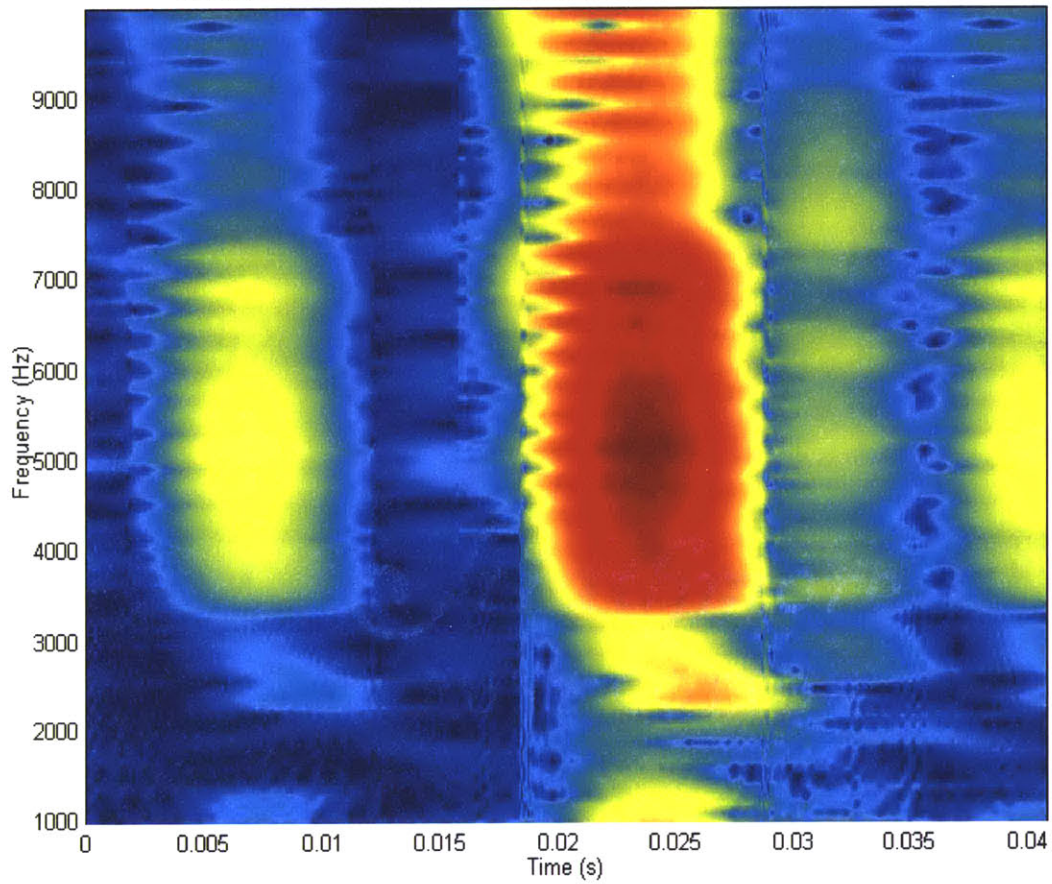
Figure 6-21: Day-time sferic showing high frequency dispersion at 2200 Hz due to a path through a transitioning ionosphere; additionally a second faint asymptote at 2000 Hz.

Time: 05/13/2004, 00:28:15.9; Lat: 32.5N; Long: -83.8E; Distance: 1500 Km
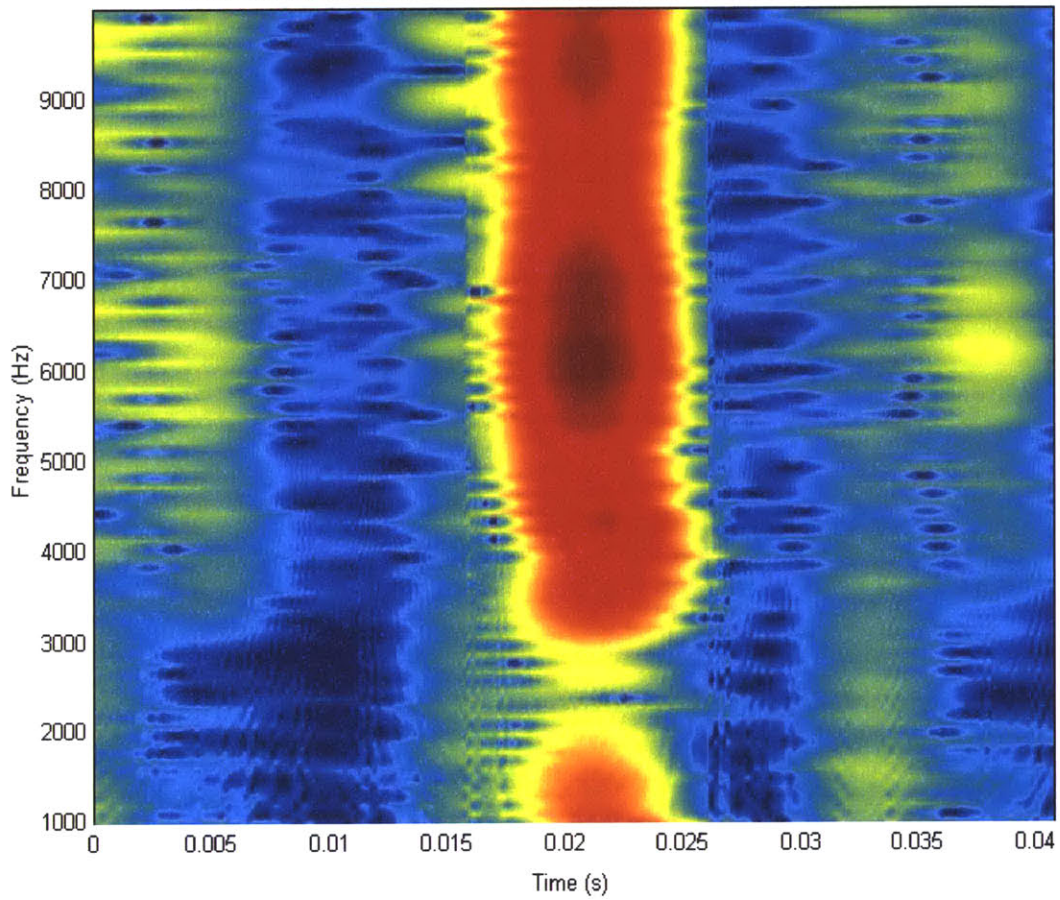
Figure 6-22: Mixed path sferic showing high frequency dispersion at 2200 Hz due to a path through a transitioning ionosphere.
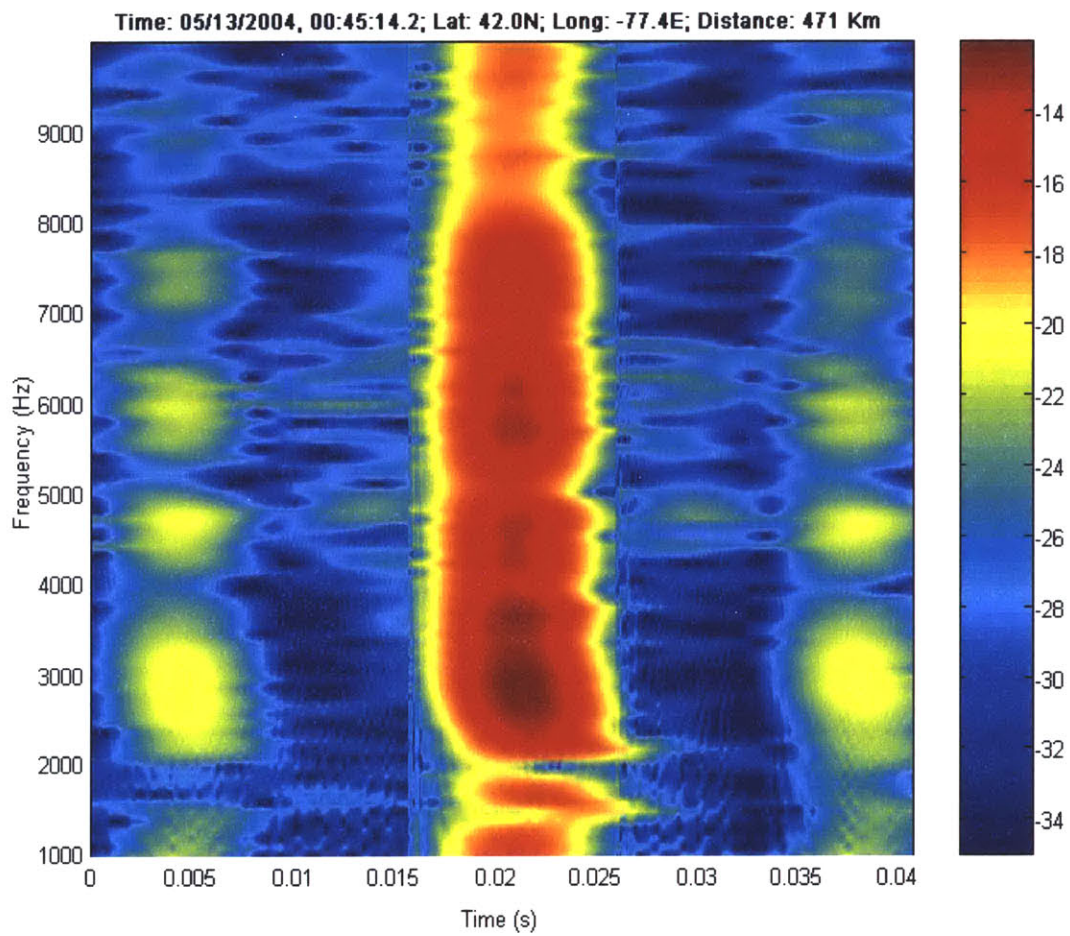
Figure 6-23: Mixed path sferic showing two asymptotes at 1600 Hz and 2000 Hz.

Time: 05/13/2004, 01:06:53.9; Lat: 30.0N; Long: -90.0E; Distance: 2100 Km

Time: 05/13/2004, 01:06:54.1; Lat: 30.0N; -90.1E; Distance: 2100Km

Figure 6-24(a) and (b): Daytime sferics showing a faint asymptote towards 1700 Hz due to a long, mixed source-receiver path.
Note that both the sferics originated from the same location within a second of each other.

81

Here,

$h_d (\approx 60Km)$ is the height of the ionosphere that is still in daytime

$h_n (\approx 90Km)$ is the height of the ionosphere that has stabilized to a nighttime height

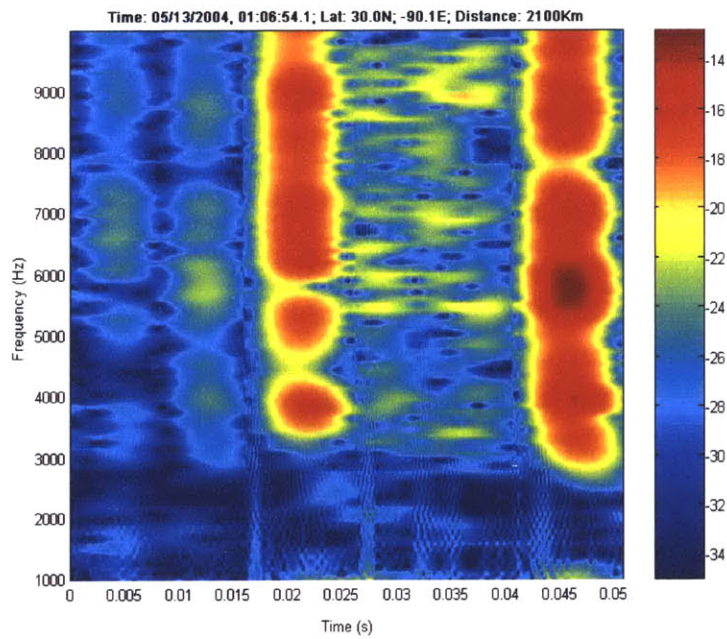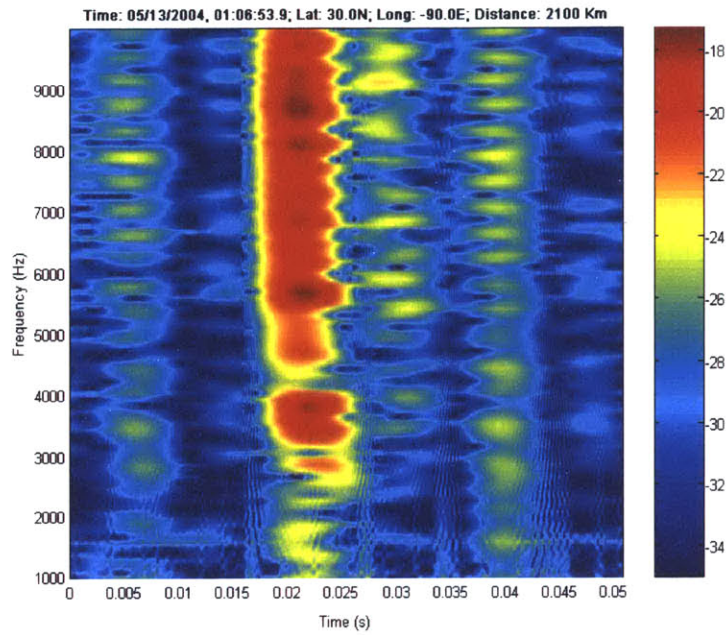Modeling lightning as an isotropic antenna (radiating energy equally everywhere), one sees that some of the energy launched from a daytime event subtend shallower angle with the horizontal than others. The above is true for all frequencies. Even if the immediate ionosphere over a source does not support a particular frequency, a part of the path itself may. It is energy in lower frequencies which manages to "sneak" into the part of the waveguide which supports lower frequencies that lead to the mixed-path behaviors tabulated earlier in this section.

Obviously, all daytime events do not show the above behavior. What is it that makes an event more likely to demonstrate the mixed path behavior described in this section?

The table in the earlier part of this section provides some clues. It is found that the right combination of the following variables determines which phenomenon is observed: Length of the source-receiver path; percentage of path-length in the ionosphere with a stable nighttime height; peak current at the source; and, proximity of the event to the nighttime ionosphere. The following rules of thumb, with at least some qualitative scientific basis, are drawn from empirical analysis. All else being the same,

1)   The closer a daytime lightning is to a nighttime ionosphere, the larger the percentage of energy that manages to "sneak in" the nighttime ionosphere, and likely, the clearer the dispersion

2)   For far away events (> 500Km away), the higher the peak current, the more the energy that reaches the observer hence, the clearer the asymptote

3)   The greater the source distance path, the longer and thus the more evident the dispersion

4)   Sferics that show two asymptotes (associated with two distinct ionosphere heights) are the norm in the day-night transition period. Sferics from a wide range

6.1.2.4 Summary

Sferic propagation from day to night, through the day-night boundary is a multi-faceted phenomenon; the sferic observations display a wide range of frequency-domain structures. These structures can be explained, at least to the first order, by means of a basic theory of rectangular waveguides.In the daytime, sferics propagate in a waveguide which has a height of about 60 Km; the nighttime sferics propagate in a waveguide which has a height of about 90 Km.
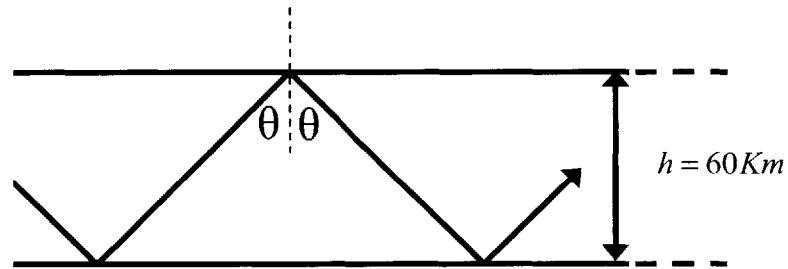

Figure 6-25: A model of daytime waveguide with h = 60 Km; the nighttime waveguide can be modeled exactly the same way with h = 90 Km

Sferic propagation in the mixed path however, is not as monotonous. At the day-night boundary, the ionosphere resembles a non-uniform waveguide that looks more like the waveguide illustrated in Figure 6-26 (over-simplified as a step in the figure), and less like the pure daytime or nighttime waveguides [Figures 6-25]. Studies by Smith et al (2004) indicate that a step-function change is not a bad approximation.
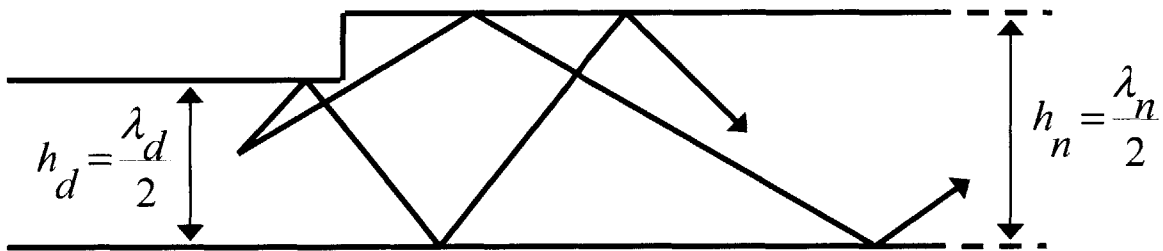

Figure 6-26: A simple model of the earth-ionosphere waveguide partially in darkness and partially in light; the source is in the daytime ionosphere while the receiver is in the nighttime ionosphere. (Source and receiver heights not to scale.)

It is the presence of this variance in height in the earth-ionosphere waveguide that leads to the observance of a wide range of observable sferic behavior, irreconcilable with either the daytime or the nighttime models simplified models.
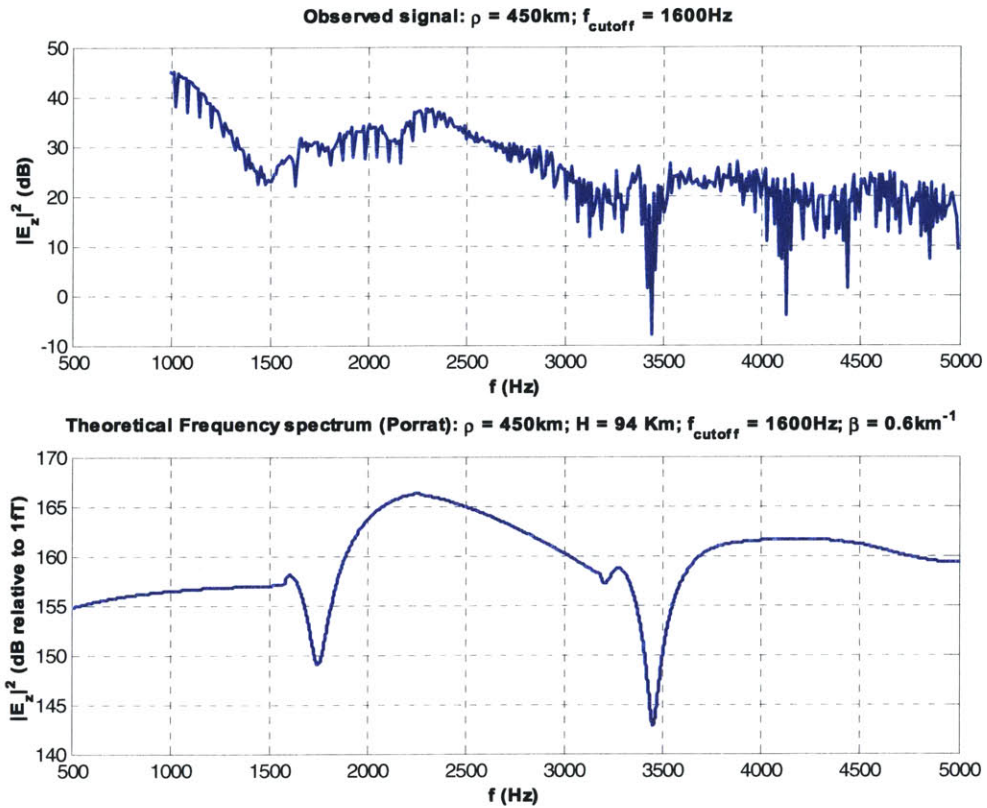
6.2   Observations versus Theoretical Predictions

This section compares a theoretical model of sferic propagation at night against empirically observed sferics on May 12, 2004, within the 500 Hz and 5000 Hz frequency range.[9] While an earlier work by Porrat (2001) forms the theoretical basis of his comparison, this comparison deviates from the one made by Porrat et al in three significant ways: Porrat et al (1) use the H_ϕ field (2) make comparisons of an averaged spectrum – averaged over many sferics – against theory and (3) make comparisons only for events greater than 1700Km away. This thesis, on the other hand, seeks to compare the frequency spectrum of the E_z fields for specific individual events whose locations are known, against that predicted by the theory. Further, this thesis seeks to make comparisons of events at various distances ranging from 400 Km to 2500 Km.[10]

Before making comparisons, it is important to note that the theoretical spectra, as shown in the following figures, have a resolution of 1 Hz. The frequency resolutions of the empirical sferic spectra, on the other hand, are limited by the size of the window. Typical window sizes of 10 ms and 25 ms have frequency resolutions of about 100 Hz and 25 Hz respectively – a more conservative estimate may consider the resolution to be as low as twice the resolution values provided above. Also worth noting is that while a longer window can improve resolution, a longer window reduces the signal-to-noise ratio. Additionally, local maxima and minima associated with power line harmonics may muddy the picture and introduce error in counting oscillations between cutoff frequencies.

---

[9] The Matlab code for making the theoretical comparison was generously provided by Dana Porrat in a personal communication.
[10] This thesis recognizes that certain second-order effects become important for distances less than 500Km which the theoretical approximations ignore; the comparisons are nevertheless useful for first order comparisons.

Observed signal: ρ = 450km; f_{cutoff} = 1600Hz

Theoretical Frequency spectrum (Porrat): ρ = 450km; H = 94 Km; f_{cutoff} = 1600Hz; β = 0.6km^{-1}

Time (UT)	Distance (Km)	Peak Current (kA)	N_{obs}	N_{th}	Theory vs Experiment
02:05:27.8	466	+80	4	3	1. Broad agreement between first and second cutoffs 2. Minor interference due to power lines noise may be the source of the discrepancy between the theoretical and observed number of oscillations

N_{obs}: Number of oscillations in the observations
N_{th}: Number of oscillations in the theoretical spectrum

Observed signal: $\rho = 2300\,\text{km}$; $f_{cutoff} = 1600\,\text{Hz}$
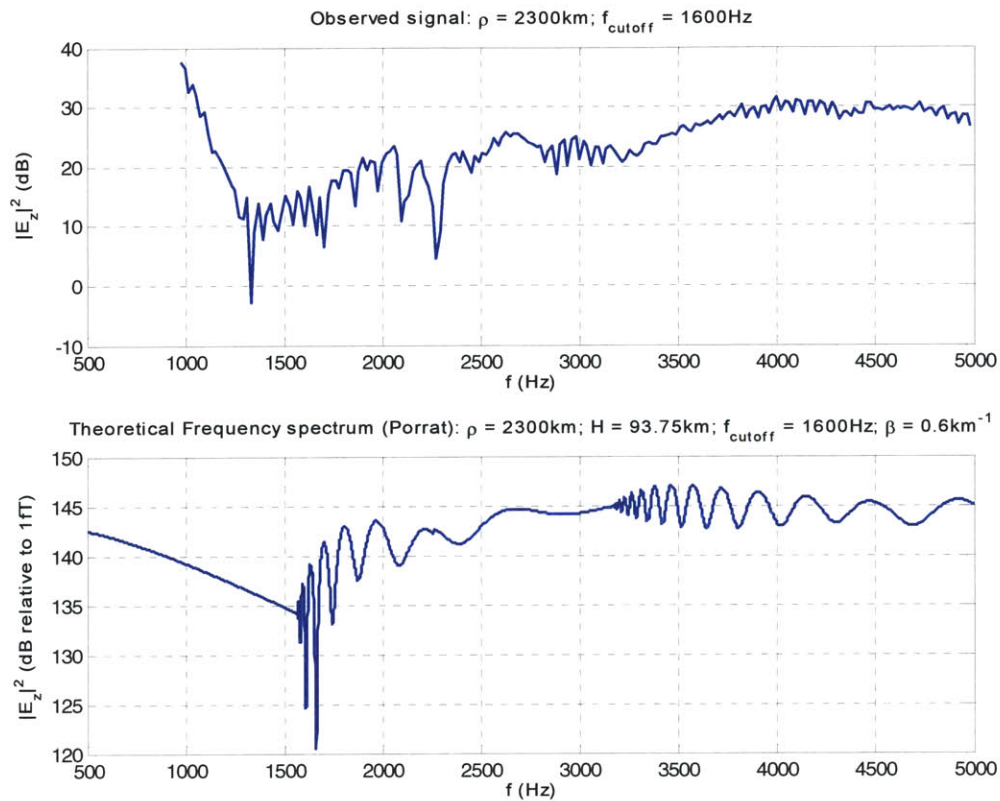
Theoretical Frequency spectrum (Porrat): $\rho = 2300\,\text{km}$; $H = 93.75\,\text{km}$; $f_{cutoff} = 1600\,\text{Hz}$; $\beta = 0.6\,\text{km}^{-1}$

Time (UT)	Distance (Km)	Peak Current (kA)	N_{obs}	N_{th}	Theory vs Experiment
02:15:50.9	2305	+87	8	8	1. Agreement in the number of oscillations between first and second cutoffs 2. Presence of a cutoff-like structure at 2600 Hz a) may be due to residual daytime effect or, b) may be attributable to a rise in energy as predicted by Porrat et al (2001) at a f = $\sqrt{2}f_c$ 3. Theoretical structure is not apparent in the observations for frequencies beyond the second mode, possibly owing to the noise-removal filter

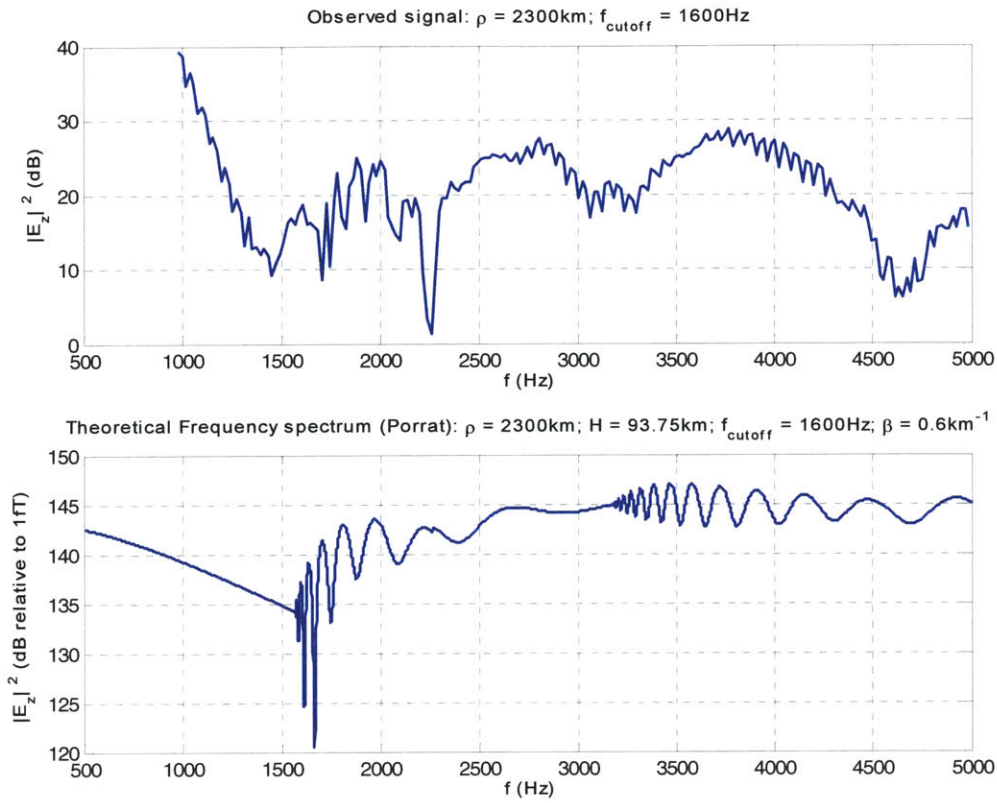N_{obs}: Number of oscillations in the observations
N_{th}: Number of oscillations in the theoretical spectrum

Observed signal: ρ = 2300km; f_{cutoff} = 1600Hz

Theoretical Frequency spectrum (Porrat): ρ = 2300km; H = 93.75km; f_{cutoff} = 1600Hz; β = 0.6km^{-1}

Time (UT)	Distance (Km)	Peak Current (kA)	N_{obs}	N_{th}	Theory vs Experiment
02:20:53.0	2303	+192	7	8	1. Broad agreement in the number of oscillations between first and second cutoffs 2. Presence of a less dramatic cutoff-like structure at 2300 Hz 3. Theoretical structure again not apparent in the observations beyond the second mode

N_{obs}: Number of oscillations in the observations
N_{th}: Number of oscillations in the theoretical spectrum

Observed signal: $\rho = 2300$km; $f_{cutoff} = 1600$Hz

Theoretical Frequency spectrum (Porrat): $\rho = 2300$km; H = 93.75km; $f_{cutoff} = 1600$Hz; $\beta = 0.6$km^{-1}

Time (UT)	Distance (Km)	Peak Current (kA)	N_{obs}	N_{th}	Theory vs Experiment
02:20:02.8	2301	+196	6	8	1. No clear agreement in the number of oscillations between first and second cutoffs of 2. Presence of a cutoff-like structure at 2600 Hz a) may be due to residual daytime effect or, b) may be attributable to a rise in energy as predicted by Porrat et al (2001) at a f = $\sqrt{2}f_c$ 3. Theoretical structure again, not apparent in the observations beyond the second mode

N_{obs}: Number of oscillations in the observations
N_{th}: Number of oscillations in the theoretical spectrum

7 Conclusions

This thesis makes novel use of accurately (~1 km) located (via the NLDN) lightning ground flashes to study the dependence of the observations on distance and lightning peak current. In the context of monitoring the behavior of the ionosphere through the day-night boundary, sferic waveforms and spectra (both 1D and FTS) for the three possible source-receiver paths of nighttime, daytime, and mixed are explored.

During the day, it is possible to measure the ionospheric height despite the lossy daytime conditions for lightning events. While measuring a clear daytime ionosphere height gets more difficult as the source-receiver distance increases, flashes with high-NLDN peak current can still provide a reasonable measure of the ionospheric height. At night, the ionosphere is less lossy making observations more favorable; clean cutoffs are relatively easier to estimate from many more events than in the daytime. The mixed path case is the most varied and often tends to show not only daytime and nighttime behaviors but also behavior that is a combination of the two with evidence for two distinct heights.

Additionally, using observations about the three distinct behaviors of sferics described above, as a function of source-receiver paths, this thesis successfully applies tweek sferics, and the waveguide cutoff and transverse resonances to expose the often abrupt transition in ionospheric height from day to night. This method, using powerful natural lightning sources, serves as a kind of ionosonde for features in the lower C and D region of the ionosphere not detectable with high power radars. From measurements of ionosphere heights through the day-night boundary for three different days, it is concluded that the typical ionosphere stabilizes to its nighttime height as early as 10 minutes past the end of civil twilight or about 40 minutes past the time of sunset at the ground. Recall, the distinction between sunset at the ground, and sunset at the ionosphere.

In addition to monitoring relatively slow changes in ionospheric height associated with the day-to-night transition, these methods are suitable for investigating fast changes in local ionospheric height. Extraordinary lightning flashes may result in nonlinear ionospheric effects, as with high peak current return strokes and elves.

The main qualifications regarding the use of these methods to examine short term changes in ionospheric height are: (1) meteorological situations with active lightning that

'pulse' the ionosphere frequently and repeatedly over the same source-receiver paths are required and (2) the best estimates will likely be observed when the ionospheric change is under nighttime conditions (when substantially greater precision is attainable on heights).

Finally, comparisons with theoretical calculations following modal theory (Porrat et al, 2001) have shown reasonably good agreements for some events characterized by extraordinarily large NLDN peak currents which presumably give a large signal-to-noise ratio. Most events, however, show a sharp daytime-like cutoff in the vicinity of 2600 Hz. This is puzzling since the events studied against the theory had entirely nighttime source-receiver paths which should have settled to nighttime levels as per Smith et al (2004). The merging of improved models with observations of the kind reported here, and specifically models which accurately treat both the daytime and the nighttime ionospheres, are expected to yield better results.

8 Future Work

This thesis studies sferic propagation in the cutoff region of the earth-ionosphere waveguide with an emphasis on comparing related current theory with observations of individual lightning flashes. It makes novel use of accurately (~1 km) located (via the NLDN) lightning ground flashes to study the dependence of the observations on distance and lightning peak current. In its study, this thesis has focused primarily on sferic propagation in the day-to-night transition.

On the empirical side, a natural extension of the study would be to explore events in other portions of the diurnal cycle, particularly to verify if wave dispersion will allow measurement of the ionosphere height near noontime so long as the lightning sources are nearby and sufficiently intense.

This thesis also emphasizes the role of tweek sferics for monitoring the nighttime earth-ionosphere waveguide. A tweek is composed of waves propagating at different angles to the boundary of the waveguide; and, the best reflection is observed for waves propagating under sliding angles (from personal communication with Alexander Shvets). This condition may provide for the largest quality factor Q of the transverse resonances of the waveguide. Therefore, another extension would be to monitor the ionosphere for long duration tweeks at around 12 UT when the Sun is over Africa and when the entire Pacific Ocean is in darkness. This condition would provide a favorable long nighttime path over conductive ocean surface for lightning events originating in the south Pacific Ocean and propagating to Rhode Island, and therefore the best opportunity for tweeks of very long duration. Another nighttime study would be to emphasize what is needed to document changes in local ionospheric height associated with the production of elves or sprites.

This study has demonstrated that strong tweeks are associated with high peak current NLDN flashes, and has also shown strong multimodal cutoff behavior for some events not identified as ground flashes by the NLDN, and hence with lightning type unidentified. Further work is needed to characterize those lightning flashes that are exceptional in producing strong multi-modal behavior, and to characterize those storms that seem to produce such events in rapid succession. These situations will be most

91

favorable for monitoring ionospheric changes on short time scales, the original motivation for this study.

On the theoretical side, an important area of exploration would be to extend the theory of waveguide propagation to daytime conditions with full exploration of the Greifinger and Greifinger 4-parameter ionospheric model, an aspect that has not been covered in the literature. Sferic studies would also benefit from a model of the background spectra and the noise associated with power lines harmonics and how best to remove them while retaining the overall structure of the observed frequency spectrum.

9 References

Bannister, P. R., *Further examples of Seasonal Variations of ELF Radio Propagation Parameters*. Radio Science, 34(1): 199-208, 1999

Bannister, P. R., *Some Notes on ELF Earth-ionosphere Waveguide Daytime Propagation Parameters*. IEEE Transactions on Antennas and Propagation, AP 27(5): 696-698, 1979

Barr, R., *The ELF and VLF Amplitude Spectrum of Atmospherics with Particular Reference to the Attenuation Band near 3 kHz*, Journal of Atmospheric and Terrestrial Physics, 32: 977-990, 1970

Barr, R., D. Llawyn Jones, C. J. Rodgers, *ELF and VLF Radio Waves*, Journal of Atmospheric and Solar-Terrestrial Physics, 62: 1689-1718, 2000

Barr, R., *Some New Features of ELF Attenuation*, Journal of Atmospheric and Terrestrial Physics, 34: 411-420, 1971

Barr, R., P. Stubbe, M. T. Rietveld, H. Kopka, *ELF and VLF Signals Radiated by the "Polar Electrojet Antenna": Experimental Results*, Journal of Geophysical Research, 91(A4): 4451-4459, 1986

Borgmann, D., *Theoretical and Experimental Coverage Analysis of a VLF Transmitter*, ELF/VLF/LF Radio Propagation and Systems Aspects AGARD-CP-529, pp. 6-1 to 6-5, 1993

Challinor, R. A., *The Phase Velocity and Attenuation Of Audio-Frequency Electromagnetic Waves from Simultaneous Observations Of Atmospherics at Two Space Stations*, Journal of Atmospheric and Terrestrial Physics, 29: 830-810, 1967

Challinor, R. A., *The Interpretation of Recently-measured Propagation Constants for Audio-frequency Electromagnetic Waves in terms of Model Ionosphere Profiles*, 29: 995-1003, 1967

Chapman, F. W., D. Llanway Jones, J. D. W. Todd, R. A. Challinor, *Observations on the Propagation Constant of the Earth-Ionosphere Waveguide in the Frequency Band 8 c/s to 16 kc/s*, Radio Science, 1(11): 1273-1282, 1966

Cummer, S. A., *Ionospheric D Region Remote Sensing using VLF Radio Atmospherics*, Radio Science, 33: 1781-1792, 1998

Cummer, S. A., *Modeling Electromagnetic Propagation in the Earth-ionosphere Waveguide*, IEEE Transactions on Antennas and Propagation, 48(9): 1420-1429, 2000

Ferguson, J. A., *Numerical Modeling of the Propagation Medium at VLF/LF*, ELF/VLF/LF Radio Propagation and Systems Aspects AGARD-CP-529, pp. 1-1 to 1-9, 1993

Fraser-Smith, A. C., R. A. Helliwell, *Overview of the Stanford University/Office of Naval Research ELF/VLF Radio Noise Survey*, Proceedings of the 1993 Ionospheric Effects Symposium, pp. 502-509, 1994

Galejs, J., *Terrestrial Propagation of Long Electromagnetic Waves*, Pergamon Press, 1st Edition, 1972

Greifinger, C., P. Greifinger, *Approximate Method for Determining ELF Eigenvalues in the Earth-ionosphere Waveguide*, Radio Science, 13(5): 831-837, 1978

Greifinger, C., P. Greifinger, *On the Ionospheric Parameters which Govern High-latitude ELF Propagation in the Earth-ionosphere Waveguide*, Radio Science, 14(5): 889-895, 1979

Hayakawa, M., K. Ohta, K. Baba, *Wave Characteristics of Tweek Atmospherics Deduced from the Direction-finding Measurement and Theoretical Interpretation*, Journal of Geophysical Research, 99(D5): 10733-10743, 1994

Huang, E., E. Williams, R. Boldi, S. Heckman, W. Lyons, M. Taylor, T. Nelson, C. Wong, *Criteria for Sprites and Elves based on Schumann Resonance Observations*, Journal of Geophysical Research, 104(D14): 16943-16946, 1999

Kong, J. A., *Electromagnetic Wave Theory*, EMW Publishing, 2000

Llanway Jones, D., D. T. Kemp, *Experimental and Theoretical Observations on the Transient Excitation of Schumann Resonances*, Journal of Atmospheric and Terrestrial Physics, 32: 1095-1108, 1970

Llanway J. D., *Propagation of ELF pulses in the Earth-ionosphere Cavity and Application to "Slow Tail" Atmospherics*, Radio Science, "5(8, 9): 1153-1162", 1970

Llanway Jones, D., *Numerical Computations of Terrestrial ELF Electromagnetic Wave Fields in the Frequency Domain*, Radio Science, 5(5): 803-809, 1970

Malan, D. J., *Physics of Lightning*, The English Universities Press, 1963

Misiti, M., Y. Misiti, G. Oppenheim, J. Poggi, *Wavelet Toolbox (For use with MATLAB) User's Guide (Version 1)*

Mushtak, V. C., E. R. Williams, *ELF Propagation Parameters for Uniform Models of the Earth-ionosphere Waveguide,* Journal of Atmospheric and Solar-Terrestrial Physics, 64: 1989-2001, 2002

94

Nickolaenko, A. P., V. A. Rafalsky, A. V. Shvets, *A Time-domain Direction Finding Technique for Locating Wideband ELF-VLF Atmospherics*, J. Atmos. Electr., 14: 97-107, 1994

Nickolaenko, A. P., M. Hayakawa, *Natural Electromagnetic pulses in the ELF range*, Geophysical Research Letters, 25(16): 3103-3106, 1998

Nickolaenko, A. P., M. Hayakawa, *Resonances in the Earth-Ionosphere Cavity*, Kluwer Academic Publishers, 2002

Ogawa, T., Y. Tanaka, T. Miura, M. Yashuhara, *Observations of Natural ELF and VLF Electromagnetic Noises by use of Ball-antennas,* Journal of Geomagnetism and Geoelectricity, 18: 443-454, 1966

Oppenheim A. V., R. W. Shafer, *Discrete Time Signal Processing*, Prentice-Hall Inc., 1989

Porrat, D., P. R. Bannister, A. C. Fraser-Smith, *Modal Phenomena in the Natural Electromagnetic Spectrum below 5 KHz*, Radio Science, 36(3): 499-506, 2001

Rafalsky, V. A., A. P. Nickolaenko, A. V. Shvets, M. Hayakawa, *Location of Lightning Discharges From a Single Station*, Journal of Geophysical Research, 100(D10): 20829-20838, 1995

Rakov, A. V., M. A. Uman, *Lightning Physics and Effects*, Cambridge University Press, 2003

Reeve, C. D., M. J. Rycroft, *The Eclipsed Lower Ionosphere as Investigated by Natural Very Low Frequency Radio Signals*, Journal of Atmospheric and Terrestrial Physics, 34: 667-672, 1972

Reising, S. C., U. S. Inan, T. F. Bell, W. A. Lyons, *Evidence for Continuing Current in Sprite-producing Cloud-to-ground Lightning*, Geophysical Research Letters, 23(24): 3639-3642, 1996

Shvets, A. V., B. V. Lazebny, A. S. Kukushkin, *Synchronous Measurement of Submarine and Atmosphere Components of VLF Atmospherics*, International Conference on Atmospheric Electricity, Osaka, Japan, pp. 448-451, 1996

Shvets, A., *On Some Aspects of Using Tweek Atmospherics for Monitoring The Lower Ionosphere*, 17th Int'l Wroclaw Symposium on Electromagnetic Compatibility, Wroclaw, June 29-July 1, 2004.

Smith, D. A., M. J. Heavner, A. R. Jacobson, X. M. Shao, R. S. Massey, R. J. Sheldon, K. C. Wiens, *A Method for Determining Intra-cloud Lightning and Ionospheric Heights from VLF/LF Electric Field Records,* Radio Science, 2004

Strang, G., T. Nguyen, *Wavelets and Filter Banks*, Ed. 2, Wellesley-Cambridge Press, 1997

Stubbe, P., H. Kopka, M. T. Rietveld, R. L. Dowden, *ELF and VLF Wave Generation by Modulated HF Heating of the Current Carrying Lower Ionosphere*, Journal of Atmospheric and Terrestrial Physics, 44(12): 1123-1135, 1982

Sukhorukov, A. I., *Approximate Solution for VLF Propagation in an Isotropic Exponential Earth-ionosphere Waveguide*, Journal of Atmospheric and Terrestrial Physics, 55(6): 919-930, 1993

Sukhorukov, A. I., *ELF-VLF Atmospheric Waveforms under Nighttime Ionospheric Conditions*, Annales Geophysicae, 14: 33-41, 1996

Sukhorukov, A. I., S. Shimakura, M. Hayakawa, *Approximate Solution for the VLF Eigenvalues near Cut-off frequencies in the Nocturnal Inhomogeneous Earth-ionosphere Waveguide*, Planetary and Space Science, 40(10): 1363-1369, 1992

Sukhorukov, A. I., S. Shimakura, M. Hayakawa, *On the Additional Dispersion of a Whistler in the Earth-ionosphere Waveguide*, Planetary and Space Science, 40(9): 1185-1191, 1992

Volland H., *Handbook of Atmospheric Electrodynamics, Volume I*, CRC Press, 1995

Wait, J. R., K. P. Spies, *Characteristics of the Earth-ionosphere Waveguide for VLF Radio Waves*, Technical Note 300, National Bureau of Standards, 1964

Wait, J. R., *Electromagnetic Waves in Stratified Media*, Pergamon Press, 1962 (Reprint IEEE Press 1996)

Wait, J. R., *On the Theory of the Slow-Tail Portion of Atmospheric Waveforms*, Journal of Geophysical Research, 65(7): 1939-1945, 1960

Watson Watt, R. A., J. F. Herd, F. E. Lutkin, *On the Nature of Atmospherics - V*, Proceedings of the Royal Society of London. Series A, Mathematical and Physical Sciences, 162(909): 267-291, 1937

Wheeler, H. A., *VLF Propagation Under the Ionosphere in the Lowest Mode of Horizontal Polarization*, Radio Science, 68D(1): 105-113, January 1964

Williams, E., K. Rothkin, D. Stevenson, D. Boccippio, *Global Lightning Variations Caused by Changes in Thunderstorm Flash Rate and by Changes in the Number of Thunderstorms*, Journal of Applied Meteorology, 2000

Williams, E., S. Stanfill, *The Physical Origin of the Land-ocean Contrast in Lightning Activity*, C. R. Physique, 3: 1277-1292, 2002

Williams, E. R., *Chapter 13: The Electrification of Severe Storms*, Meteorological Monographs, 28(50): 527-561

Yamashita, M., *Propagation of Tweek Atmospherics*, Journal of Atmospheric and Terrestrial Physics, 40: 151-156, 1978

Appendix A

Theoretical calculations based on modal theory (Wait, 1962) were taken from the work of Porrat et al (2001) for the present study. The computational framework was presented earlier in Section 3.1.2. Matlab code generously provided by Dana Porrat (personal communication, 2004) was used to compute theoretical frequency spectra in the waveguide cutoff region for nighttime conditions specified in Porrat et al (2001), for both the vertical electric (E_z) and the horizontal magnetic fields. These calculations are presented below for a number of different source-receiver separations, appropriate for making comparisons with lightning ground flash locations identified by the National Lightning Detection Network in the continental U.S.
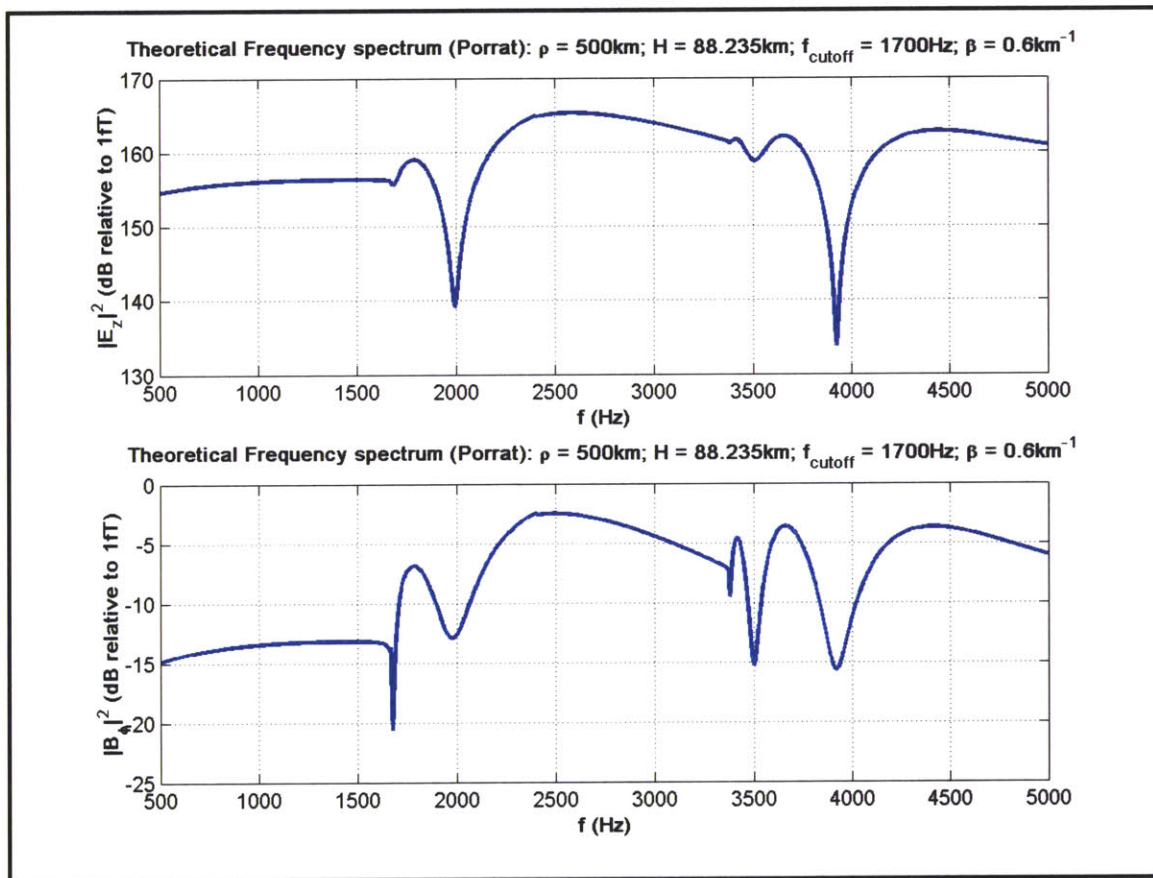
Figure A-1: E_z and H_ϕ fields; $\rho = 500 Km$
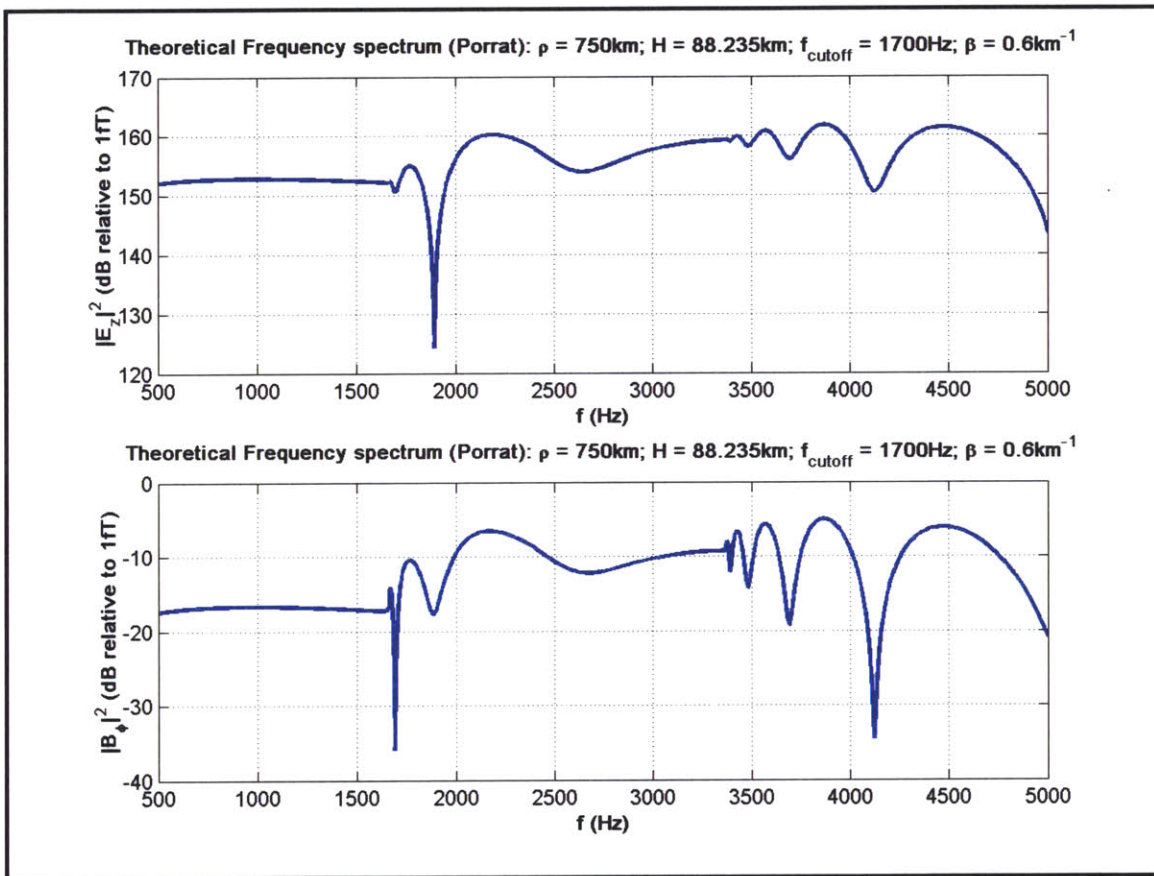
Figure A-2: E_z and H_ϕ fields; $\rho = 750 Km$
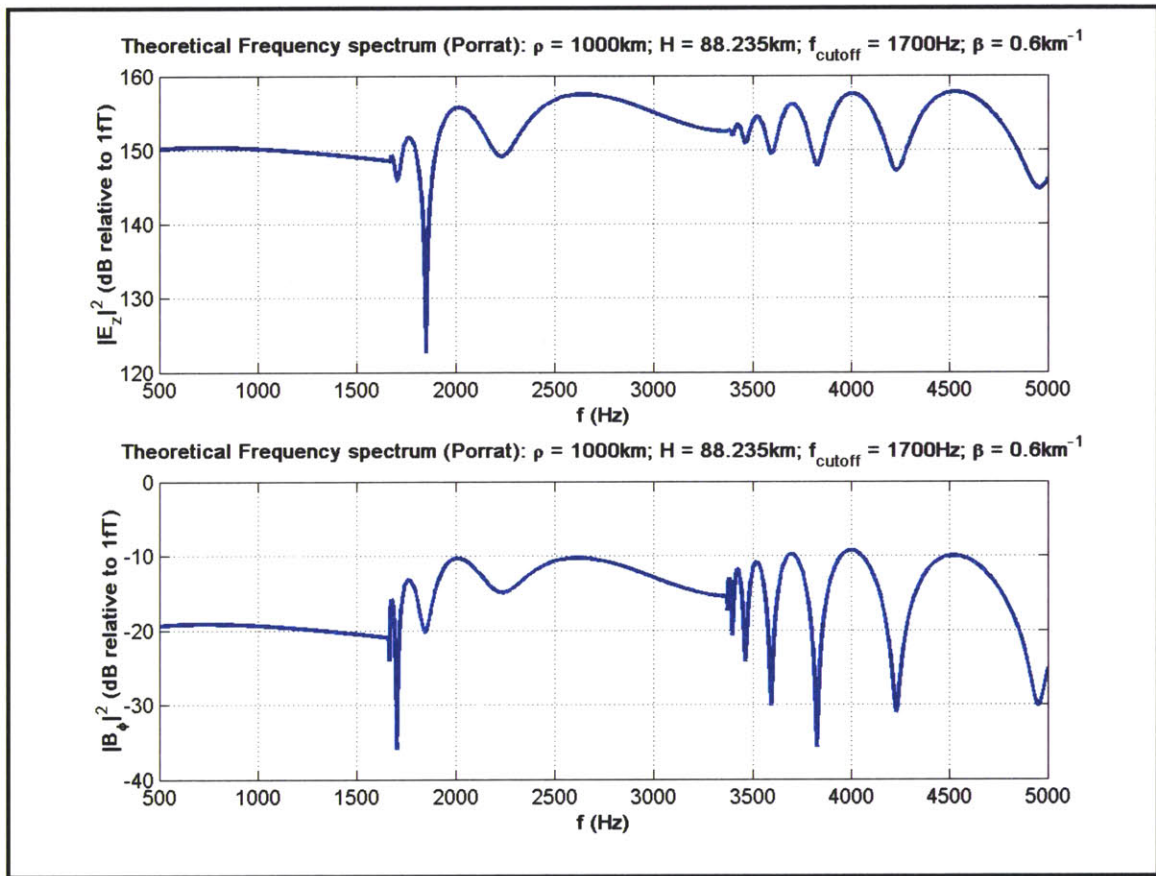
Figure A-3: E_z and H_ϕ fields; $\rho = 1000 Km$
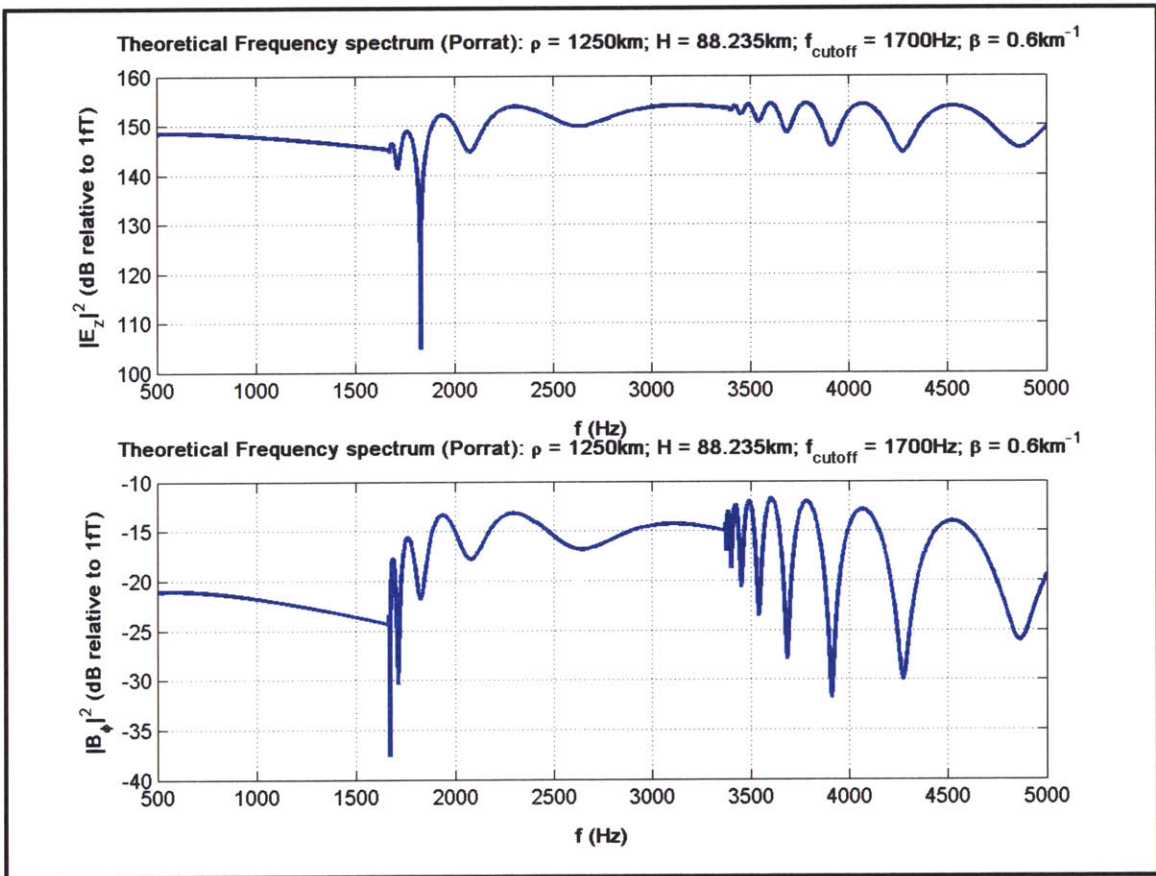
Figure A-4: E_z and H_ϕ fields; $\rho = 1250 Km$
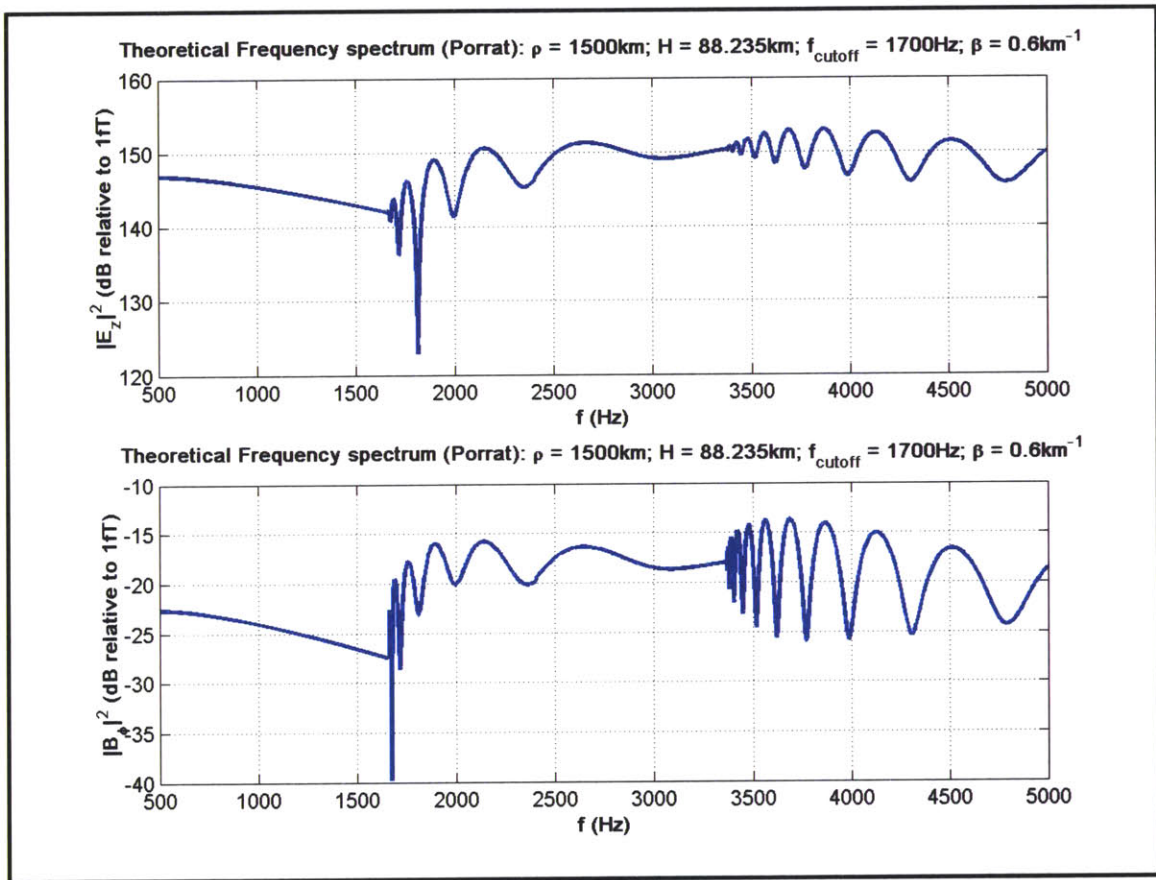
Figure A-5: E_z and H_ϕ fields; $\rho = 1500Km$
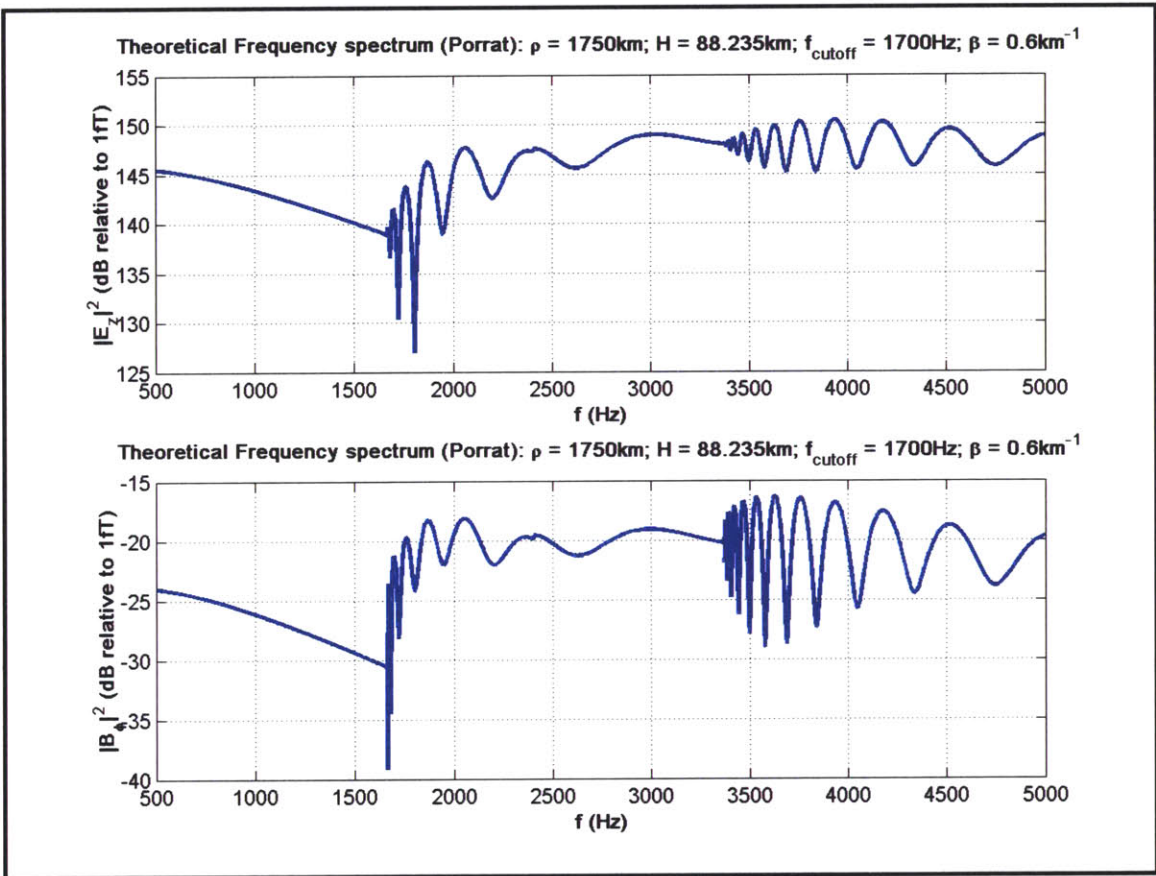
Figure A-6: E_z and H_ϕ fields; $\rho = 1750 Km$
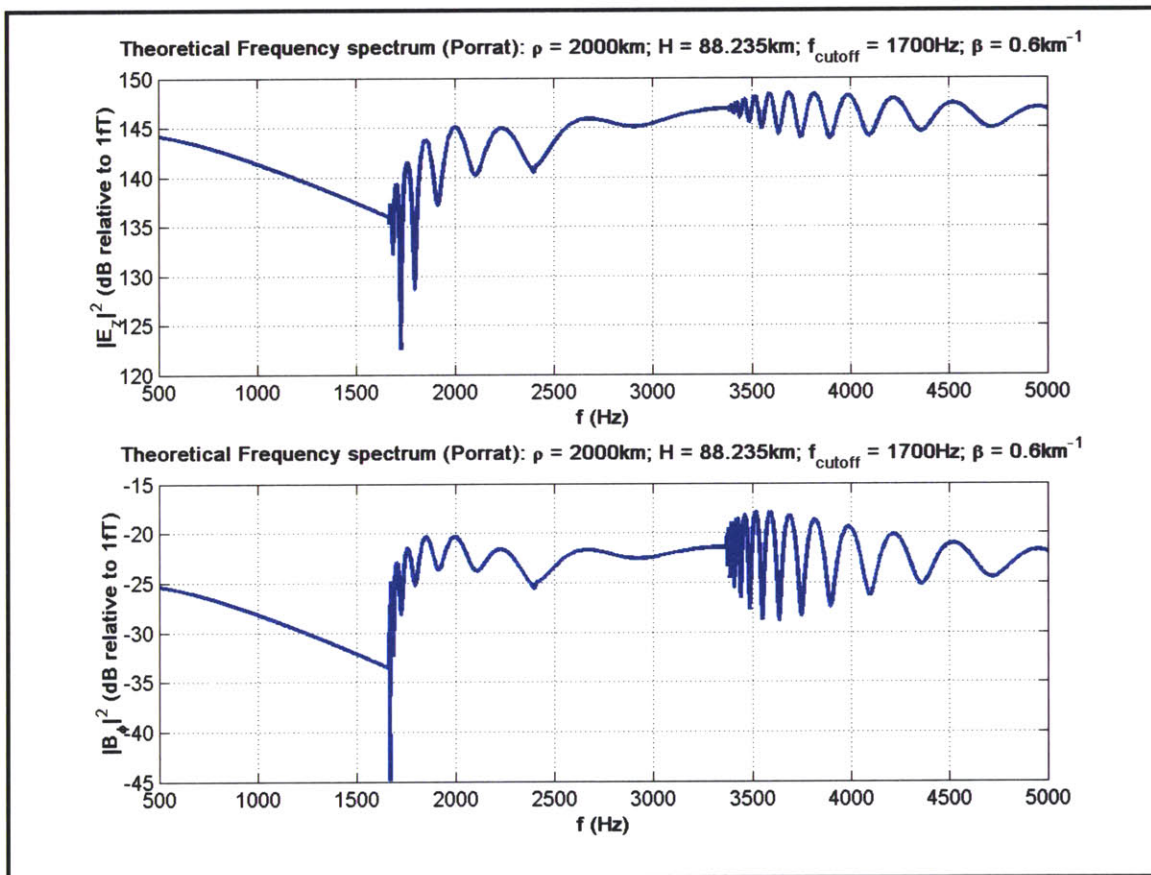
Figure A-7: E_z and H_ϕ fields; $\rho = 2000 Km$
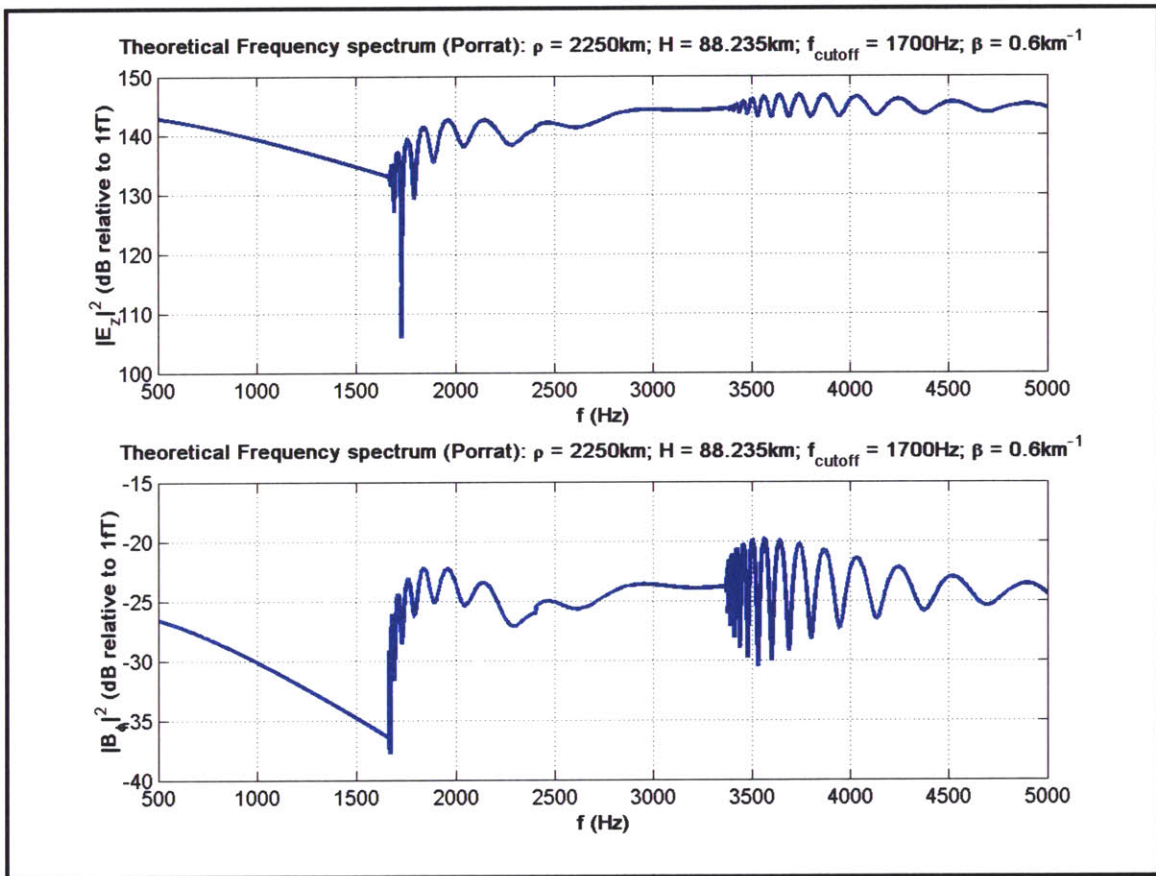
Figure A-8: E_z and H_ϕ fields; $\rho = 2250 Km$

Figure A-9: E_z and H_ϕ fields; $\rho = 2500 Km$